UNIVERSIDAD MICHOACANA DE
SAN NICOLÁS DE HIDALGO

FACULTAD DE INGENIERÍA ELÉCTRICA
DIVISIÓN DE ESTUDIOS DE POSGRADO

"Analysis of Control Interactions in Power Systems"

by
Jesús Alejandro Sotelo Martínez

A thesis submitted in fulfilment of the requirements

for the degree of

Doctor of Science in Electrical Engineering

Advisor
Dr. Claudio Rubén Fuerte Esquivel

MORELIA, MICHOACÁN August 2016

To my family for their support and incentive...

Abstract

This thesis analyses the interaction phenomena among most of the control devices in power systems, both in steady state and transient stability dynamic frames. The control devices include Flexible AC Transmission Systems (FACTS) controllers, synchronous machines' controls and variable-speed Wind Energy Generation Systems (WECS) as well as their associated power electronics-based converters. Concerning the steady-state analysis, realistic models of FACTS devices, Automatic Frequency Control (AFC) and Area power Interchange Control (AIC) are adopted. In the transient stability analysis, the dynamic models included are the synchronous machine with its controls, and the IEEE Type-4 WECS with its associated back-to-back controller. This thesis proposes practical methods to identify which control devices are interacting each other in power systems, and to quantify this interaction, both in steady state and transient stability dynamic operation frames. The proposed methods are based on the numerical analysis of a sensitivity matrix computed during the steady state and transient solution processes. Also, improved power flow models of Static VAR Compensators (SVCs) and AIC are proposed. The proposed methods and models are equally efficient but less numerically demanding than other suggested approaches. The applicability and usefulness of the proposed methods and models are tested with numerical simulations by means of a digital program developed in Matlab environment. Several real-life and benchmark power system are considered in the simulations.

Resumen

En ésta tesis se analiza el fenómeno de interacción que ocurre entre la mayoría de los dispositivos de control en los sistemas eléctricos de potencia, tanto en estado estacionario como en la dinámica de estabilidad transitoria. Los dispositivos de control incluyen dispositivos de Sistemas Flexibles de Transmisión en CA (SIFLETCA), controles de máquinas síncronas y Sistemas de Generación de Energía Eólica (SGEE) así como sus respectivos convertidores basados en electrónica de potencia. Considerando el estado estacionario, se adoptan modelos realistas de dispositivos SIFLETCA, así como Control Automático de Frecuencia (CAF) y control de potencia entre áreas. Considerando la dinámica de estabilidad transitoria, los modelos incluyen a la máquina síncrona y sus controles, así como la turbina eólica "Tipo 4" del IEEE con su respectivo controlador "back-to-back". En ésta tesis se proponen métodos prácticos para identificar los dispositivos de control que interactúan entre sí en los sistemas de potencia, y a su vez cuantificar dicha interacción, tanto en la operación de estado estacionario, como en la operación dinámica de estabilidad transitoria. Los métodos propuestos se basan en el análisis numérico de una matriz de sensibilidades calculada durante los procesos de solución de estado estacionario y transitorio. De forma adicional, se proponen modelos mejorados de Compensadores Estáticos de VARs (CEVs) y control de potencia entre áreas. Los métodos y modelos propuestos resultan igual de eficientes y menos demandantes numéricamente que otras propuestas similares. La aplicabilidad y utilidad de los métodos y modelos propuestos se prueban mediante simulaciones numéricas utilizando un programa digital desarrollado en el entorno Matlab. En las simulaciones se consideran varios sistemas de potencia, tanto reales como de referencia.

Palabras clave: Control de sistemas de potencia, interacción entre controladores, dispositivos SIFLETCA, generadores eólicos, estabilidad transitoria.

Acknowledgements

I am deeply grateful to my research advisor, PhD. Claudio Rubén Fuerte Esquivel for his guidance and support throughout these years. I also express my sincere gratitude to the faculty and teaching staff of UMSNH.

The financial support given by National Council for Science and Technology (CONACyT) during my doctoral study is deeply appreciated .

J. Alejandro Sotelo, August 2016.

Contents

List of Figures

List of Tables

Abbreviations

AC	**A**lternating **C**urrent.
AFC	**A**utomatic **F**requency **C**ontrol.
AGC	**A**utomatic **G**eneration **C**ontrol.
AIC	**A**rea **I**nterchange **C**ontrol.
BE	**B**ackward-**E**uler.
COI	**C**enter **O**f **I**nertia.
AVR	**A**utomatic **V**oltage **R**egulator.
DAE	**D**ifferential-**A**lgebraic **E**quation.
DFIG	**D**oubly-**F**ed **I**nduction **G**enerator.
EMPT	**E**lectro-**M**agnetic **T**ransient **P**rogram.
FACTS	**F**lexible **AC** **T**ransmission **S**ystems.
HVDC	**H**igh-**V**oltage **D**irect-**C**urrent.
LTC	**L**oad **T**ap **C**hanger.
MPPT	**M**aximum **P**ower **P**oint **T**racking.
NR	**N**ewton-**R**aphson.
PMSG	**P**ermanent **M**agnet **S**ynchronous **G**enerator.
PE	**P**artitioned-**E**xplicit.
PSS	**P**ower **S**ystem **S**tabilizer.
PST	**P**hase **S**hifting **T**ransformer.
ROCOF	**R**ate **O**f **C**hange **O**f **F**requency.
SI	**S**imultaneous-**I**mplicit.

SSR	**S**ub-**S**ynchronous **R**esonance.
SVC	**S**tatic **V**ar **C**ompensator.
TCSC	**T**hyristor **C**ontrolled **S**eries **C**ompensator.
TR	**T**rapezoidal **R**ule.
UPFC	**U**nified **P**ower **F**low **C**ontrollers.
WECS	**W**ind **E**nergy **C**onversion **S**ystems.

List of publications

Journal Papers

[1] **Sotelo-Martinez J. A.** and Fuerte-Esquivel C.R., *"A New Practical Area Interchange Control Model for Power Flow Studies"*, Submitted to the **IEEE Transactions in Power Systems**. (At present in third revision)

Conference Papers

[1] **Sotelo-Martinez J. A.** and Fuerte-Esquivel C.R., *"Dynamic Control Interaction Assessment in Power Systems with Wind Energy Conversion Systems"*, **PowerTech, 2015 IEEE Eindhoven**, June, 2015, DOI: (10.1109 /PTC.2015.7232287).

[2] **Sotelo-Martinez J. A.** and Fuerte-Esquivel C.R, *"Effects of Inertia Emulation on Dynamic Behavior of Bus Voltages in Power Systems"*, Accepted to be presented in the **PES Transmission and Distribution Conference and Exposition Latin America (PES T&D LA)**, September, 2016, Morelia, México.

Chapter 1

Introduction

1.1 Justification and Motivation

Power systems controls of different kinds are of vital importance for a safe and economic operation of modern power systems. In order to enhance the performance of power systems, engineers are exploiting more and more advanced and sophisticated controls, designed to accomplish various purposes. This is an inevitable development, but it must be acknowledged that there are certain drawbacks associated with this evolution [CIGRE Task Force, 2000, Acha et al., 2004].

Power systems controls are designed to perform a given task assuming certain operating conditions, and if correctly designed, the controls will fulfil their task under the considered operating scenario. The ability of a controller to perform in the desired way while various system parameters vary, is referred to as robustness of the controller [CIGRE Task Force, 2000]. The more variations in system conditions that are accepted, the more robust the controller is considered to be. Altough controllers can be designed to perform appropriately under a wide range of system conditions, they cannot cope with all operating conditions that can arise, especially under emergency events. This disadvantage will often lead to higher stresses on high-voltage equipment, and often the action of controllers could be detrimental to system performance and even system security [EPRI Report, 1998]. A basic aspect to be addressed is related to the fact that each controller may be adjusted considering

the rest of the system as solely composed by passive or slowly-varying elements. As this assumption may not be real, individual adjustments of the controller's parameters might be far away from the optimal for the best system performance and therefore the net effect of all controllers working in the same power system may be detrimental to its behaviour [CIGRE Working Group, 1999].

Throughout the years there have been several reports of adverse effects in power system caused by interactions among several types of control devices. These effects include oscillations damping problems [Mithulananthan et al., 2002, Bati, 2010], steady-state control interactions [Filho et al., 2009, EPRI Report, 1998], high-frequency interactions [Pilotto et al., 2000, Mathur and Varma, 2002], and torsional interaction phenomena [Parniani and Iravani, 1995]. In this regard, these interaction scenarios can be present among the wide variety of control devices installed in power systems: machine-related controls [Kundur et al., 1989], FACTS devices and machine controls [Mithulananthan et al., 2002], HVDC-links [Aik, 2007], substation controls [van Cutsem and Βουρνάς, 1998], FACTS devices [Kim et al., 2011], to mention a few. On the other hand, important research efforts have been conducted in order to understand and address those problems arising from adverse control interactions. An excellent discussion on controls classification and different approaches for the analysis of interactions is reported in [CIGRE Working Group, 1999, CIGRE Task Force, 2000, EPRI Report, 1998].

Based on the above-mentioned, it can be stated that the identification and analysis of interaction between controllers is paramount in the planning and designing stages of power systems, in which control schemes should be designed in such a way that effectively enhance the performance of the associated power system. In this context, this thesis proposes a new way to analyse the interaction phenomena among controls in power systems where the main contribution is the formulation and implementation of methods for calculating indices of interaction between control devices in power systems, both in the steady-state and transient stability operation frameworks. The proposed methods aim to simplify the typically-used procedures to analyse the control interaction phenomena in power systems, while, at the same time, providing useful information with the objective of identifying and quantifying the interaction among the control devices. Additionally, new mathematical models for representing the Area Interchange Control (AIC) and the operation of Static VAR Compensators (SVCs) are proposed.

1.2 Overview of Controls in Power Systems

Different kinds of controls are integrated as part of modern power systems. According to [Elgerd, 1981, CIGRE Task Force, 2000], the controls in power system can be divided in the following groups: generator controls, substation controls, FACTS controls, and system controls.

1.2.1 Generator Controls

The two main quantities that can be controlled are the turbine power and the field current. Depending on the primary energy source (hydro, fossil, nuclear, etc.) the turbine governor has different designs. On the other hand, the electrical design of the generator (round rotor or salient pole) has an impact on the design of the excitation system with its associated controls. In this section, a brief review of generator controls are described.

Turbine Controls. The turbine controls have three main tasks: First, to control the turbine rotor speed in all the possible operating conditions such as starting, parallel synchronizing, interconnected grid operation, shut-down, etc. Second, to regulate the input mechanical power in response to other controllers, e.g. frequency, stability and generation control. Third, to regulate, and if necessary trip the unit, so that the generator-turbine system is not damaged.

- *Turbine Speed Control.* This is the main control function of the speed governor which directly operates on the valve/gate opening, in such a way that an adequate dynamics of the turbine speed transients in all the operating conditions is assured.
- *Turbine Power Control.* This control function adjusts the valve/gate opening of the turbine in coordination with the speed governor, so that the desired output power from the generator is obtained.
- *Frequency Control.* The frequency control is performed by a set of generators in the system; the control function is implemented by the speed governor.

This controller is a proportional type control, P-control, and the inverse of the steady-state gain is usually called the speed droop (R), and it gives the relative speed change versus the relative power output.

Excitation Controls. The other major controls of synchronous machines are those related to the excitation system. These controls act on the physical system through the regulator and the exciter of the machine. An extensive description of this controls, as well as the recommended practices on the implementation are given in [IEEE Committee, 1981, IEEE Committee, 2006]. The major functions of these controls are given below.

- *Exciter.* The exciter provides DC power to the field winding of synchronous generators within its ceiling or saturation capabilities.
- *Automatic Voltage Regulator (AVR).* The main goal of this controller is the closed-loop automatic regulation of the generator's terminal voltage, through a suitable transfer function which assures an adequate level of dynamic performance (fast response speed and good stability).
- *Power System Stabilizer (PSS).* This control function provides an additional input signal to the regulator to increase the damping action of the generator. Common input signals are rotor speed deviation, accelerating power, and frequency deviation.
- *Limiters and Protective Circuits.* Here a wide range of control and protective functions which ensure that the capability limits of the exciter and synchronous generator are not exceeded. Examples are over-excitation limiter, terminal voltage limiter, and under-excitation limiter.

1.2.2 Substation Controls.

Within the variety of control actions that can be carried out in the power substation, the most common ones are described below.

Tap-Changer Control. Tap-changer control is very often implemented on one or several transformers from the transmission system to the distribution level. The purpose of this control is to keep a constant voltage at the consumer level, despite voltage variations at the higher system levels. Usually the control is performed based on local voltage signals.

Reactive Shunt Element Control. Reactive shunt elements are installed at various voltage levels for reactive power and voltage control. At higher voltage levels often both shunt capacitors and reactors are used, while at distribution voltage levels mainly shunt capacitors are installed. These shunt elements can often be switched in response to voltage and load changes in the system by using local signals or non-local inputs. Most often the non-local controls involve operator actions in order to achieve the desired voltage control.

Line Switching. Line switching can be performed to reduce voltage levels during light-load conditions or during a manoeuvring process.

Emergency Controls. In most power systems various controls are implemented to prevent system collapse in emergency situations. Under-frequency load shedding is the most common control. Special protection schemes are also used to prevent the system from voltage and angle instabilities. In this latter case the control actions could be generator rejection and load shedding, but also reactive shunt element switching are used.

1.2.3 Controls of Power Electronics-Based Equipment.

Power electronics-based equipment, i.e. High Voltage Direct Current (HVDC) and Flexible AC Transmission Systems (FACTS) devices, are attractive from a control point of view. The integration of these devices to the power system usually allows a continuous and easy control of a variety of quantities. Moreover, the increase in the penetration levels of renewable generation technologies, and specially of Wind Energy Generation Systems (WECS), has led to the development

of power electronics-based converters serving as an interface to the power grid and substantially increasing the control capabilities.

HVDC. The basic control loop of HVDC links is the direct current control. By controlling the current the transmitted DC power can be varied. Also, the desired DC power level can be supplemented by a signal in such a way that power oscillations can be damped. Moreover, the reactive power of a HVDC link can also be controlled. Because of their controllability, HVDC links offer higher power transfers over longer distances with lower losses than traditional transmission lines [CIGRE Task Force, 2000, Bahrman, 2006].

FACTS devices. FACTS technology has become an important alternative in order to optimally utilizing the transmission system, while, at the same time, maintaining acceptable levels of reliability and stability. FACTS controllers have the capability of either extend the power transfer capability of existing transmission lines and/or enhance the stability and security margins for given power-transmission limits [Fuerte-Esquivel and Acha, 1996, Mathur and Varma, 2002]. The FACTS devices encompass a variety of power electronics-based devices such as Thyristor-Controlled Series Compensators (TCSCs), Phase-Shifting Transformers (PSTs), Static VAR Compensators (SVCs), among others. As mentioned above, these equipments introduce a high degree of controllability and can be used for power flow control both in steady state and under dynamic conditions.

WECSs power converters. Basically, WECS can be divided in two types: fixed-speed and variable-speed. In order to overcome the limitations associated with fixed-speed and to comply with the grid-code connection requirements, the trend in modern WECS technology is to apply variable-speed concepts [Nouh and Mohamed, 2014]. The power electronics-based converters used to interface variable-speed WECSs to the power grid basically consist of back-to-back power converters that have the purpose of allowing a variable speed operation and controlling the voltage at terminals of the WECS [E. H. Camm et al., 2009].

1.2.4 System Controls.

The desired performance of the power system it is generally coordinated by local control actions on a system-wide basis. Examples of area or regional controls are given below.

Automatic Frequency Control. Automatic Frequency Control (AFC) can be carried out through the speed governor. Each generator participating in the frequency control contributes with a certain speed droop so that the system's overall speed droop is obtained. Considering a system-wide approach, the speed droop is usually expressed by its inverse in MW/Hz, and in order to achieve the desired value a system coordination must be done. Since the system operates at a single value of frequency during the steady state, local signals can be used by the speed governors.

Automatic Generation Control. Following a load disturbance and the subsequent speed-governor action (primary regulation), it results a steady state frequency error. To bring the system's frequency back to acceptable operating limits, and additional control action is needed. This is performed by the Automatic Generation Control (AGC), which is derived from the frequency deviation and power flows on selected tie-lines and which determines the power orders of the generators participating in the AGC.

1.3 State of the Art of Control Interactions in Power Systems

As described above, there are a wide variety of control devices that can be installed in power systems, going from the classical controls of synchronous generators to modern power electronics-based equipment. Also, their control actions are carried out in time scales going from milliseconds to minutes. Hence, for practical reasons, it is convenient to subdivide or classify the control interaction phenomena in order to better focus on the particular problem to be addressed. As a result of

this classification, the methods and tools used for the interaction analysis also differ from each other [Mathur and Varma, 2002, Kim et al., 2011].

1.3.1 Classification of Control Interactions

A way to classify the control interaction phenomena by the type of analysis is suggested in [Kim et al., 2011], dividing the interactions in the following categories:

- Steady-state interactions.
- Generator or machine-related oscillations.
- Interactions among FACTS controllers

Steady state interactions focus on the system response in the steady state operating space for which control dynamics are not incorporated. Generator or synchronous machine-related oscillations contain local or inter-area mode oscillations and torsional mode oscillations. Interactions among FACTS controllers may be included in control mode oscillations which also include interactions between controllers of generating units and FACTS devices. Another way of classifying interactions in power systems is based on operating frequency ranges, as reported in [CIGRE Working Group, 1999] and fully described in [Mathur and Varma, 2002, CIGRE Working Group, 1999]. In this case, the interactions are divided into the following five types:

- Steady-state interactions ($\approx$0 Hz).
- Electromechanical oscillations (0.1-2 Hz).
- Small-signal or control oscillations (2-15 Hz).
- Sub-synchronous resonance interactions (10-50/60 Hz).
- Electromagnetic transients, high-frequency or harmonic interactions (>15 Hz).

Regarding FACTS devices, a way to classify the interactions among them is also proposed in [Mathur and Varma, 2002], having the following combinations of interactions:

- FACTS controllers of a similar kind.
- FACTS controllers of a dissimilar kind.
- FACTS controllers and HVDC converter controllers.

1.3.2 Analysis of Control Interactions

Several research efforts have been conducted to address the control interactions in power systems. In this section, the methods used so far to analyse such phenomena are summarized by taking into account the classification given in [CIGRE Working Group, 1999].

Steady-state Interactions. Steady state interactions are defined to be interactions containing no dynamic behaviours. The methods to analyse this type of interactions are related to repetitive power flow-based assessment of voltage stability, adequate reactive power reserve, and transfer capability of the system. As proposed in [EPRI Report, 1998], a useful study procedure is summarized as follows:

- To determine the main modes of failure of the system and the conditions under which the failure is anticipated based on available information.
- To determine the sensitivities of various locations of shunt control devices to the voltage collapse problem using left eigenvalue formulas.
- To determine the proper locations of series controller devices for addressing line overload problems by using flow-to-flow, impedance-to-flow or voltage drop to flow sensitivity formulas.
- To perform continuation studies in order to confirm the effects predicted by linearisation (power-flow) studies.

In addition of the typical methods employed to analyse control interactions in steady-state conditions, there are few alternate proposals, such as the method reported in [Filho et al., 2009]. In any case, is very common the use of eigenvalue analysis.

Electromechanical Oscillation Interactions. Electromechanical oscillations or interactions may be most frequently studied for both small and large disturbances [EPRI Report, 1998]. In general, systems have natural modes, some of which may be critical and destabilize the system under certain disturbances. The oscillations include local mode oscillations, typically in the range of 0.8–2 Hz, and inter-area mode oscillations, typically in the range of 0.2–0.8 Hz. The local mode is contributed by synchronous generators in a plant or several generators located in close vicinity; while the inter-area mode results from the power exchange between tightly coupled generators in two areas linked by weak transmission lines [Mathur and Varma, 2002]. Eigenvalue analysis programs are typically employed for determining the frequency and damping of sensitive modes [EPRI Report, 1998, Mathur and Varma, 2002]. Examples of these methods used for addressing electromechanical-oscillation interactions can be found in [Mithulananthan et al., 2002, Bati, 2010]. However, proposals also have been made using alternate techniques such as optimization [Najafi and Kazemi, 2006] and relative gain array [Zhang et al., 2006].

Small-signal or Control Oscillations. Control interactions between individual controllers and the network or between controllers and HVDC links may lead to oscillations in the range of 2–15Hz (the range may even extend to 30Hz). These oscillations are largely dependent on the network strength and the choice of controller parameters. The emergence of these oscillations significantly influences the tuning of controller gains [Mathur and Varma, 2002]. Analysis of these relatively high frequency oscillations is made possible by frequency scanning programs, Electromagnetic-Transient Programs (EMTPs), and physical simulators (analog or digital). Eigenvalue analysis programs with certain modelling capabilities can be extended to analyse higher-frequency modes, as reported in [Pilotto et al., 1995]. Applications of these techniques to analyse control oscillations are detailed in [Parniani and Iravani, 1995, Zou et al., 2005].

Sub-synchronous Resonance Interactions. Sub-Synchronous Resonance (SSR) can be defined as an electric power system condition in which the electric network exchanges energy with the generator torsional system [IEEE Committee, 1992]. SSR oscillations may be caused by the interaction between the generator torsional system and series-compensated transmission lines, HVDC controls or generators' excitation controls, among others. These oscillations, usually in the frequency range of 10–50/60Hz, can potentially damage generator shafts. Analysis techniques and tools for investigating these control interactions are similar to those used for small-signal or control oscillations [Kundur et al., 1994, Mathur and Varma, 2002].

High-frequency Interactions. High-frequency oscillations in excess of 15 Hz are caused by large disturbances, such as the switching of capacitors, reactors, or transformers, for which reason they are classified as electromagnetic transients [Mathur and Varma, 2002]. Also, fast-acting electronic devices such as FACTS controllers, can experience interactions that produce these kinds of oscillations so that must be properly coordinated [EPRI Report, 1998]. Harmonic instabilities may also occur from synchronization of voltage-measurement systems, transformer energization, or transformer saturation [Mathur and Varma, 2002]. The study of these interactions is typically carried out by EMTPs [EPRI Report, 1998, Kim et al., 2011].

1.4 Objective

The general objective of this research work is the theoretical and computational development of a practical methodology that permits to identify and quantify the existent interaction, from the steady and dynamic point of view, among the FACTS control devices, synchronous machines controllers and the recently introduced WECS controllers.

The proposed methodology aims to identify control devices that interact with each other in an adverse manner, and to estimate the strength of this interaction, so that preventive and/or corrective actions can be carried out.

1.5 Methodology

The proposed method for the control interaction assessment, considering either the dynamic or steady-state operating frameworks, is based on the analysis of a reduced-order matrix obtained from a full Jacobian matrix, which is computed by linearising the set of differential and/or non-linear algebraic equations representing the power system. In case of the transient stability analysis, the full Jacobian matrix is obtained at the end of each integration step by following the trapezoidal rule or the backward-Euler method described in Section 3.5. In the context of the steady state assessment of interactions, the Jacobian matrix is obtained at each iteration of the Newton-based power flow solution process. On the other hand, the elements of this reduced-order matrix, referred to as *control matrix*, correspond to numerical sensitivities that directly relate the differential and/or algebraic mismatch equations associated with the control devices to their corresponding state variables.

Once the control matrix has been computed, it is analysed by applying the concepts of sensitivity theory and geometrical projections to obtain a new matrix whose elements correspond to indices of interaction. These indices permit to identify which control devices are interacting each other and to quantify how strong this interaction is.

In order to achieve the general objective of this research work and considering the above-described method, it is necessary to accomplish the following goals:

- To develop an efficient mathematical methodology to calculate the steady state operation of a large-scale power system. An equilibrium point of the system is obtained through a power flow study taking into account the transmission network, bus power injections, AFC modelling, voltage-dependent loads, AIC and the following FACTS control devices:
  - Thyristor-Controlled Series Compensator (TCSC).
  - Static VAR Compensator (SVC).
  - Phase Shifting Transformer (PST).
  - Load-Tap Changer transformer (LTC).
  - Universal Power Flow Controller (UPFC).

- To develop a methodology in order to identify and quantify the interaction level among the control devices in the steady state operating framework of the power system. In this stage, a control device interaction index is proposed.

- To develop an efficient mathematical methodology to calculate the dynamic transient-stability operation of a large-scale power system. In this stage of the project, the transient stability operation of the system is analysed using the singular perturbation theory. In this context, the power system is modelled by means of a set of Differential-Algebraic Equation (DAE) which is solved through implicit integration techniques using the power injection approach. The dynamic mathematical models of the devices considered in this stage are the most common control devices of traditional synchronous generators and the recently introduced Type-4 WECS [E. H. Camm et al., 2009], along with its respective interfacing controller. The adopted models are enlisted below.

  - Synchronous machine (4th order).
  - Automatic Voltage Regulator (AVR).
  - Turbine-governor group.
  - Power System Stabilizer (PSS).
  - IEEE Type-4 WECS including back-to-back controller.

- To develop a methodology that identifies and quantifies the interaction level among the control devices in the dynamic operating framework of the power system. In this stage, an index of interactions among control devices in the transient-stability framework is proposed.

- To integrate these methodologies along with the diverse control devices models, into digital programs.

1.6 Contributions

During the development of this research work, the following contributions have been made:

- The developing of a methodology to identify and quantify interactions among control devices embedded in the power system that is operating either on a steady or dynamic state.
- The proposal of a novel AIC model for power-flow studies.
- The proposal of two SVC models for power-flow studies.

1.7 Thesis Outline

This thesis is organised into 6 chapters; the remaining are briefly described below.

Chapter 2 presents a description of the steady-state power system modelling along with the control models considered. AFC and AIC modelling are adopted, as well as the most commonly-found FACTS devices. Also, new proposals of AIC and SVC power flow models are described.

Chapter 3 describes the transient stability dynamic modelling of power systems. The synchronous machine and its most common controls dynamic models are given, as well as the Type-4 WECS and its respective controls. Also, the general solution method and the procedure to simulate disturbances are described.

Chapter 4 presents the formulation of the proposed methods to assess control interactions in power systems, both in steady-state and dynamic frameworks.

Chapter 5 addresses the testing and demonstration of the proposals by means of numerical simulations using various power systems. Several case studies are presented, both static and dynamic.

Chapter 6 gives the general conclusions of this thesis and presents suggestions for future research work.

Chapter 2

Steady-state power system modelling

2.1 Introduction

The analysis of power systems in the steady state framework plays a fundamental role in the design, planning and operation tasks. In this context, the power flow (load flow) analysis is often considered the most popular and important computer calculation performed in power systems planing and operation because of its capability for providing reliable solutions of real life power networks [Kothari and Nagrath, 2003, Fuerte-Esquivel, 1997, Stott, 1974].

This chapter comprises the modelling approach adopted for power systems in the steady state framework. Due to its reliability and flexibility, the power flow method is used as the base for the study of the steady-state interaction phenomena among the various control devices of the power system. In order to take into account the diverse control devices and actions present in power systems, mathematical models of non conventional devices are adopted and included in the power flow formulation.

With the purpose of considering the steady state effects of the primary frequency control, an Automatic Frequency Control (AFC) model is described in order to perform a regulation of the frequency deviation produced by a load-generation

imbalance. In addition, voltage-dependent loads are also considered. Similarly, with the objective of modelling the active power transfer control among different control areas in which the system is divided, a novel Area Interchange Control (AIC) approach is proposed. Finally, various FACTS devices models are described, including those most commonly found in power systems and a proposed Static VAR Compensator (SVC) model. These proposed models have the advantage of incorporating fewer mismatch equations to the power flow formulation than the typically used so far. All the described mathematical models are also included in the general power flow formulation which is solved in a unified way by the Newton-Raphson method.

2.2 General power flow overview

In its most basic form the problem flow problem involves solving the set of non-linear algebraic equations representing the electric network under steady state conditions. The basic principle of the Newton-based power flow solution methods lies in the consideration that the set of non-linear nodal power balance equations given by

$$\mathbf{G}(\mathbf{Y}) = \mathbf{0}, \tag{2.1}$$

can be linearised around a base point determined by generation and load powers, as well as bus voltages, commonly initialised with unitary magnitudes and null angles. The N-R algorithm provides an approximate solution to the non-linear problem described by equation (2.1) by carrying out a Taylor series expansion of $\mathbf{G}(\mathbf{Y})$ around an initial guess $\mathbf{Y}^0$.

Over the years, efficient Newton-based algorithms have been developed in order to include non-conventional models in the power flow formulation. A convenient approach to incorporate FACTS controller into the power flow formulation consists of solving the non-linear equations related to the FACTS devices along with the conventional power balance non-linear equations in a unified framework, as proposed in [Fuerte-Esquivel, 1997, Fuerte-Esquivel and Acha, 1996]. This philosophy is also applied for AIC modelling in [dos Santos et al., 2004], and for AFC modelling in [Okamura et al., 1975]. This simultaneous approach has the advantage of preserving the fast convergence characteristics of Newton-based methods for all

the state variables involved in the analysis. Bearing this in mind, this modelling technique is also adopted in this research work.

In order to apply the aforementioned simultaneous modelling approach, (2.1) must be expanded with the equations relative to non-conventional devices. In addition, some non-linear equations corresponding to nodal power mismatches are modified accordingly. Considering the models associated with the AFC, AIC and FACTS controllers, the following augmented equation set is obtained:

$$\begin{aligned} \mathbf{G}_{AC}\left(\mathbf{Y}_{AC}\right) &= \mathbf{0} \\ \mathbf{G}_{F}\left(\mathbf{Y}_{F}\right) &= \mathbf{0} \\ \mathbf{G}_{AIC}\left(\mathbf{Y}_{AIC}\right) &= \mathbf{0} \end{aligned} \quad , \tag{2.2}$$

where $\mathbf{G}_{AC}$ is the set of nodal power balance equations, $\mathbf{Y}_{AC}$ are bus voltage magnitudes and angles, $\mathbf{G}_{F}$ is the set of equations relative to FACTS controllers, $\mathbf{Y}_{F}$ are the FACTS controllers' state variables, $\mathbf{G}_{AIC}$ is the set of equations of AIC, and $\mathbf{Y}_{AIC}$ are the AIC-related state variables. Note that the AFC mathematical model modifies the associated nodal power balance equations instead of augmenting the system of equations. In this context, the Jacobian matrix related to the Newton-Raphson method can be represented as shown in Figure 2.1, where nb stands for the number of buses in the system, nf is the number of embedded FACTS controllers and na is the number of control areas in the system.

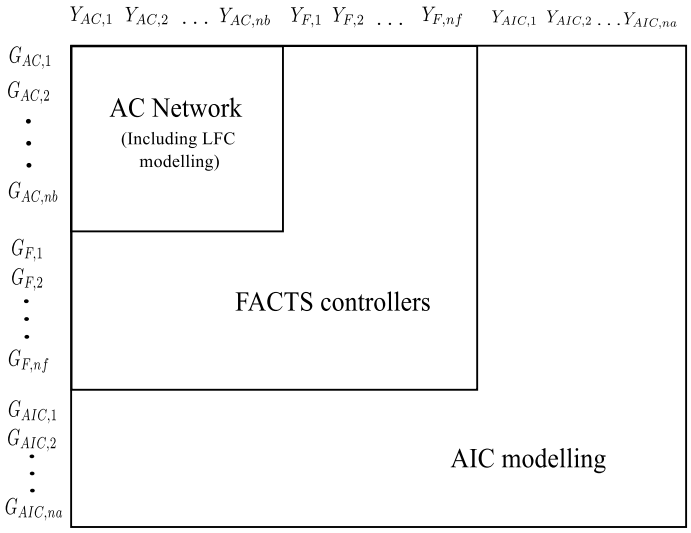

FIGURE 2.1: Representation of the Jacobian matrix.

2.3 Transmission elements modelling

Based on the transmission element depicted in Figure 2.2, the equations representing the active and reactive power (P, Q) flowing from bus k to bus m are given by

$$P_{km} = V_k^2 G_{kk} + V_k V_m \left(G_{km} \cos\left(\theta_k - \theta_m\right) + B_{km} \sin\left(\theta_k - \theta_m\right)\right), \tag{2.3}$$

$$Q_{km} = -V_k^2 B_{kk} + V_k V_m \left(G_{km} \sin\left(\theta_k - \theta_m\right) - B_{km} \cos\left(\theta_k - \theta_m\right)\right). \tag{2.4}$$

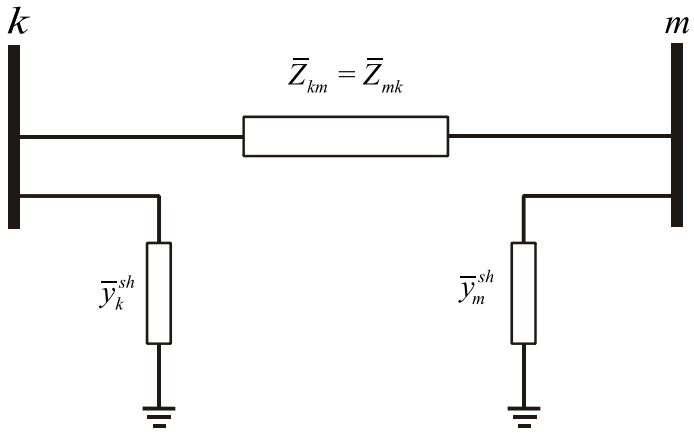

FIGURE 2.2: Equivalent circuit of a transmission element.

2.4 Automatic Frequency Control modelling

The traditional power flow analysis considers that the system's electric frequency remains at the nominal value after the occurring of a disturbance. This assumption is considered valid by making the consideration of the "slack" generator that compensates the load-generation imbalance. On the other hand, the steady state operation of a power system can be determined in a more realistic way by considering the frequency deviation resulting from a supply-demand imbalance, which in turn must be distributed among all generators in the system. In this context, voltage and frequency dependent loads cannot be neglected. All these considerations are properly granted in [Okamura et al., 1975], in which

non-conventional generator and load models are developed. These models are considered to produce the results presented in this thesis.

2.4.1 Generator modelling

When a disturbance in the power system occurs, the primary frequency control adjusts the active power output of each generator in order to restore the frequency to a value close to the nominal. This primary control is carried out in the order of seconds. The secondary frequency control is the responsible of fully restoring the frequency to the nominal value in matter of minutes. On the other hand, the voltage at the terminals of the generator is fixed at a reference value by adjusting the field of the machine and considering the limits of the exciter. For the purposes of this thesis, the generator models adopted consider the primary frequency control (also known as automatic frequency control [CIGRE Task Force, 2000]). The static behaviour of the primary frequency control can be represented by a generator that adjusts its active and reactive power output P_G and Q_G depending on the system frequency deviation, i.e. [Okamura et al., 1975]:

$$P_G = P_{G\_set} - \frac{P_R}{R}\Delta f, \tag{2.5}$$

$$P_{G\_min} \leq P_G \leq P_{G\_max}, \tag{2.6}$$

$$Q_G = Q_{G\_set} - a_Q\frac{P_R}{R} + b_Q\left(\frac{P_R}{R}\right)^2, \tag{2.7}$$

$$Q_{G\_min} \leq Q_G \leq Q_{G\_max}\ , \tag{2.8}$$

where Δf is the frequency deviation from the nominal value, P_{G_set} and Q_{G_set} are the scheduled active and reactive power outputs, respectively, P_R is the rated active power, R is the speed regulation, and a_Q, b_Q are the coefficients of reactive generation control characteristics. Lower and upper limit values are denoted by subscripts "min" and "max", respectively.

2.4.2 Load modelling

In general, loads in a power system depend on bus voltage magnitude and frequency; hence, these load characteristics must be included in the power flow formulation. In this case, active and reactive loads P_L and Q_L can be expressed by [Okamura et al., 1975]

$$P_L = P_{L\_set}\ (1 + K_p\ \Delta f)\left(p_p + p_c\left(\frac{V}{V_{LB}}\right) + p_z\left(\frac{V}{V_{LB}}\right)^2\right), \tag{2.9}$$

$$Q_L = Q_{L\_set}\,(1 + K_q\ \Delta f)\left(q_p + q_c\left(\frac{V}{V_{LB}}\right) + q_z\left(\frac{V}{V_{LB}}\right)^2\right), \tag{2.10}$$

where V_{LB} is the nominal operating voltage at load bus, P_{L_set} and Q_{L_set} are the rated active and reactive loads respectively, K_P and K_Q are frequency characteristics of active and reactive loads, while p_p, p_c, p_z, q_p, q_c and q_z are the coefficients of the load-voltage characteristic.

Both generator and load models are included in the power flow formulation and solved via the Newton-Raphson algorithm. The linearized set of equations is expressed as follows, where the frequency deviation (Δf) is treated as a state variable and computed iteratively:

$$\begin{bmatrix}\mathbf{\Delta P}\\ \mathbf{\Delta Q}\end{bmatrix} = \begin{bmatrix}\frac{\partial \mathbf{\Delta P}}{\partial \theta} & \frac{\partial \mathbf{\Delta P}}{\partial \mathbf{V}}\mathbf{V} & \frac{\partial \mathbf{\Delta P}}{\partial \Delta f}\\ \frac{\partial \mathbf{\Delta Q}}{\partial \theta} & \frac{\partial \mathbf{\Delta Q}}{\partial \mathbf{V}}\mathbf{V} & \frac{\partial \mathbf{\Delta Q}}{\partial \Delta f}\end{bmatrix}\begin{bmatrix}\mathbf{\Delta}\theta\\ \frac{\mathbf{\Delta V}}{\mathbf{V}}\\ \Delta\Delta f\end{bmatrix}. \tag{2.11}$$

In this case, $\mathbf{\Delta P}$ and $\mathbf{\Delta Q}$ are the active and reactive power mismatch vectors respectively, θ and $\mathbf{V}$ are nodal voltage angle and magnitude vectors, respectively. Opposite to the conventional power flow formulation, the slack node does not exist and only one reference bus must be chosen to set the reference voltage angle, such that the column corresponding to the reference angle must be eliminated from the Jacobian matrix that remains square. At the j-th iteration, the frequency deviation state variable is updated using the following expression:

$$\Delta f^j = \Delta f^{j-1} + \Delta\Delta f^j. \tag{2.12}$$

2.5 Proposed Area Interchange Control modelling

The regulation of inter-area active power transfers relies on the area interchange control, in which the active power flow to be exchanged through tie-lines is constrained to a specified value. A proposal for AIC modeling in power flow studies is described in [Britton, 1969] where those constraints are directly included in the system of equations to be solved by Newton's method. In this case, one slack generator is selected at each area in order to balance the corresponding area power interchange, and its corresponding active power flow mismatch equation is replaced by the mismatch equation representing the net active power interchanges in the control area. Hence, the number of variables and the number of equations are equal to those associated with the conventional formulation of the power flow problem. This proposal was expanded in [dos Santos et al., 2004] by considering multiple regulating generators in each control area. Since the active powers of these generators were considered as new state variables of the problem, the set of nodal power mismatch equations was expanded with one additional equation per each regulating generator. Unlike these proposals, and in order to maintain the numerical effectiveness, a new way of modelling the AIC is proposed in this section, where the number of equations to be included in the power flow formulation is only one per controlled area, regardless of the number of regulating generators at each area. In addition, an approach to handle the active power flow limit of individual tie-lines is proposed.

Based on the power system with n control areas shown in Figure 2.3, the AIC relies on controlling the active power output of each regulating generator embedded in a given area such that the total power interchanged with other control areas matches a specified value.

In a network with n areas, the net active power interchange can be controlled only in $n-1$ areas, because one area must be a reference area for the whole system

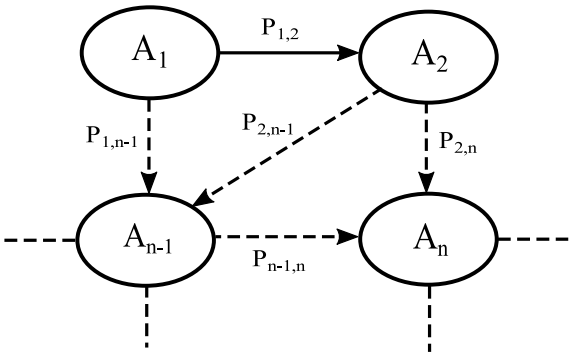

FIGURE 2.3: Power system with n areas.

in order to satisfy the Kirchhoff's currents law. With the exception of the reference area, each area must have at least one AIC regulating bus, in which the generation of active power is not specified and will be a new state variable in the power flow model. Considering the n-th control area as the reference area, the active power interchanges of the remaining areas can be expressed by (2.13), where the total active power interchange for the i-th area is defined as the algebraic sum of the active power flowing through all tie-lines interconnecting this area with the rest of the power system [dos Santos et al., 2004].

$$PI_i = \sum_{\substack{m \in \Omega_k \\ m \notin i}} P_{km} \quad , \forall i = 1, \ldots, n-1. \tag{2.13}$$

In this case, k represents a bus in the i-th area at which one or more tie-lines are connected, Ω_k is the set of buses of other areas which are directly connected to bus k, and P_{km} is the power interchange through the tie-line connecting buses k and m.

Since the net power interchanged between control areas is constrained to a scheduled value, the power interchange mismatch equation for the i-th control area is given by

$$\Delta PI_i = \left(PI_i^{sch} - PI_i\right) \leq TOL \quad , \forall i = 1, \ldots, n-1, \tag{2.14}$$

where superscript sch denotes the scheduled value and TOL denotes a specified tolerance. In order to incorporate the AIC mismatch equations to the power

flow formulation, the set of power flow mismatch equations is augmented with the inclusion of 2.14 for each control area, except the reference control area. In this proposed methodology, multiple regulating generators per area are considered to satisfy (2.14), such that the total adjustment of the active power generation in each i-th control area is considered as state variable, instead of the active power produced by each regulating generator [dos Santos et al., 2004], in the power flow formulation.

The linearised set of augmented mismatch equations, i.e. power flow mismatch equations and power interchange mismatch equations, is given by

$$\begin{bmatrix} \mathbf{\Delta P} \\ \hline \mathbf{\Delta Q} \\ \hline \mathbf{\Delta PI} \end{bmatrix} = \left[\begin{array}{ccc:c} \frac{\partial \mathbf{\Delta P}}{\partial \theta} & \frac{\partial \mathbf{\Delta P}}{\partial \mathbf{V}}\mathbf{V} & \frac{\partial \mathbf{\Delta P}}{\partial \Delta f} & \frac{\partial \mathbf{\Delta P}}{\partial \mathbf{\Delta PG}} \\ \frac{\partial \mathbf{\Delta Q}}{\partial \theta} & \frac{\partial \mathbf{\Delta Q}}{\partial \mathbf{V}}\mathbf{V} & \frac{\partial \mathbf{\Delta Q}}{\partial \Delta f} & \frac{\partial \mathbf{\Delta Q}}{\partial \mathbf{\Delta PG}} \\ \hline \frac{\partial \mathbf{\Delta PI}}{\partial \theta} & \frac{\partial \mathbf{\Delta PI}}{\partial \mathbf{V}}\mathbf{V} & \frac{\partial \mathbf{\Delta PI}}{\partial \Delta f} & \frac{\partial \mathbf{\Delta PI}}{\partial \mathbf{\Delta PG}} \end{array}\right] \begin{bmatrix} \mathbf{\Delta}\theta \\ \frac{\mathbf{\Delta V}}{\mathbf{V}} \\ \Delta\Delta f \\ \hline \mathbf{\Delta\Delta PG} \end{bmatrix}, \tag{2.15}$$

where $\Delta \mathbf{P}I$ is the vector of active power interchange mismatch equations of all areas except for the reference, and $\mathbf{\Delta PG}$ is the vector of increments in the total active power generation at each area in order to regulate to balance the power interchanges.

Lastly, assuming that AIC regulating generators also participate in the primary frequency regulation, the total generation increment ΔPG_i in the i-th control area is distributed among its n_G regulating generators by means of participation factors. Hence, the active power output of the k-th regulating generator is updated at the j-th iteration of the solution process by using the following expression:

$$P^{i,j}_{G\_set,k} = P^{i,j-1}_{G\_set,k} + \alpha^{i}_{G,k}\Delta PG^{j}_{i} \,\forall\, k \in n_G, \tag{2.16}$$

where $\alpha^{i}_{G,k}$ is the specified participation factor of the generator with a value between 0 and 1, such that $\sum_{(k\in n_G)} \alpha^{i}_{G,k} = 1$. Note that (2.16) is included in the corresponding nodal active power flow mismatch equation considering the base active power generation $P^{i,b}_{G\_set,k}$ as an initial condition for the regulating generator. When considering multiple regulating generators per area, this modelling approach offers an improvement to the method described in [dos Santos et al., 2004], which expands the system's equation set with one mismatch equation per regulating generator. In

the proposed approach, the number of equations to be included in the power flow formulation is only one per controlled area, regardless of the number of regulating generators at each area. Also, by adopting the proposed AIC modelling approach together with the AFC modelling described in Section 2.4, it is possible to control the active power generation of all generators and to place the reference generator in any area. This is not possible if using AIC modelling along with the traditional power-flow formulation, as in [dos Santos et al., 2004].

2.5.1 Revision of active power flow limits in tie-lines

The transmission system imposes a limit on the maximum amount of active power to be transferred through tie-lines, such that a suitable approach to handle the violation to this limit is proposed. In order to accomplish this limit handling, the group of regulating generators is also used to set the active power flowing through a particular overloaded tie-line at its maximum transfer capacity, while at the same time the desired AIC is achieved. That extra control action is mathematically formulated by augmenting (2.15) with one additional power flow mismatch equation per each overloaded tie-line detected during the iterative solution process. Considering the same notation as in (2.13), this additional equation is given by

$$\Delta P^{i}_{km} = P^{i}_{km,cal} - P^{i}_{km,max} = 0, \tag{2.17}$$

where subscripts *cal* and *max* refers to calculated and maximum values, respectively. An additional state variable ΔPG_{km} is also defined with the purpose of adjusting the active power output of each regulating generator $P^{i,j}_{g,k}\ \forall\, k \in n_g$ during the iterative solution process to satisfy (2.17). Hence, the active power output of the k-th regulating generator at the i-th control area is now updated at the j-th iteration of the solution process by (2.18). Note that the constraint of the power flow in the overloaded tie-line is achieved at expense of the proportion of generation specified by $\alpha^{i}_{g,k}$.

$$P^{i,j}_{g,k} = P^{i,j-1}_{g,k} + \alpha^{i}_{g,k}\Delta PG^{j}_{i} + \Delta PG^{i}_{km} \forall\, k \in n_g. \tag{2.18}$$

Based on the mentioned above, the set of linearised mismatch equations augmented with (2.17) is given by (2.19), which can be directly generalized for any number of overloaded tie-lines.

$$\begin{bmatrix} \mathbf{\Delta P} \\ \mathbf{\Delta Q} \\ \hdashline \mathbf{\Delta PI} \\ \Delta P^i_{km} \end{bmatrix} = \left[\begin{array}{ccc:cc} \frac{\partial \mathbf{\Delta P}}{\partial \theta} & \frac{\partial \mathbf{\Delta P}}{\partial \mathbf{V}}\mathbf{V} & \frac{\partial \mathbf{\Delta P}}{\partial \Delta f} & \frac{\partial \mathbf{\Delta P}}{\partial \mathbf{\Delta PG}} & \frac{\partial \Delta \mathbf{P}}{\partial \Delta PG^i_{km}} \\ \frac{\partial \mathbf{\Delta Q}}{\partial \theta} & \frac{\partial \mathbf{\Delta Q}}{\partial \mathbf{V}}\mathbf{V} & \frac{\partial \mathbf{\Delta Q}}{\partial \Delta f} & \frac{\partial \mathbf{\Delta Q}}{\partial \mathbf{\Delta PG}} & \frac{\partial \Delta \mathbf{Q}}{\partial \Delta PG^i_{km}} \\ \hdashline \frac{\partial \mathbf{\Delta PI}}{\partial \theta} & \frac{\partial \mathbf{\Delta PI}}{\partial \mathbf{V}}\mathbf{V} & \frac{\partial \mathbf{\Delta PI}}{\partial \Delta f} & \frac{\partial \mathbf{\Delta PI}}{\partial \mathbf{\Delta PG}} & \frac{\partial \Delta \mathbf{PI}}{\partial \Delta PG^i_{km}} \\ \frac{\partial \Delta P^i_{km}}{\partial \theta} & \frac{\partial \Delta P^i_{km}}{\partial \mathbf{V}}\mathbf{V} & \frac{\partial \Delta P^i_{km}}{\partial \Delta f} & \frac{\partial \Delta P^i_{km}}{\partial \mathbf{\Delta PG}} & \frac{\partial \Delta P^i_{km}}{\partial \Delta PG^i_{km}} \end{array}\right] \begin{bmatrix} \mathbf{\Delta}\theta \\ \frac{\mathbf{\Delta V}}{\mathbf{V}} \\ \Delta\Delta f \\ \hdashline \mathbf{\Delta}(\mathbf{\Delta PG}) \\ \partial\Delta(\Delta PG^i_{km}) \end{bmatrix}. \tag{2.19}$$

2.6 FACTS devices modelling

The need for modelling techniques that incorporate the FACTS devices models into power-flow methods has led to the development of several research efforts. One of these approaches has been introduced in [Fuerte-Esquivel and Acha, 1996, Acha et al., 2004] by which the state variables related to FACTS devices are handled along with the network variables in a unified framework. Hence, the non-linear equations describing the behaviour of the FACTS devices are solved together with the set of equations that model the rest of the network using a Newton-based iterative technique. This method is an efficient and realistic approach that maintains the quadratic convergence characteristic of the Newtom-Raphson method and is the one adopted in this thesis.

This section describes the models of each FACTS control devices considered in the development of this theses, which are:

- Thyristor-Controlled Series Compensator (TCSC).
- Static VAR Compensator (SVC).
- Phase Shifting Transformer (PST).
- Load-Tap Changer transformer (LTC).
- Universal Power Flow Controller (UPFC).

Also, the incorporation of these models into the conventional power-flow method along with AFC and AIC models is described.

2.6.1 Load tap changer

The function of a LTC is to regulate the voltage magnitude at either the primary (p) or secondary (s) side at a scheduled value by adjusting the tap position. The model of this device is based on the representation of the conventional two-winding power transformer, as shown in the equivalent circuit depicted in Figure 2.4.

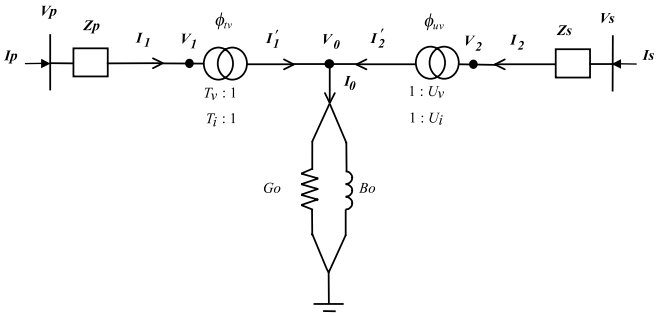

FIGURE 2.4: LTC equivalent circuit.

The power injection equations at the terminals of a two-winding transformer are giving by [Acha et al., 2004]

$$P_p = V_p^2 G_{pp} + V_p V_s \ (G_{ps}\cos(\theta_p - \theta_s) + B_{ps}\sin(\theta_p - \theta_s)) \ , \tag{2.20}$$

$$Q_p = -V_p^2 B_{pp} + V_p V_s \ (G_{ps}\sin(\theta_p - \theta_s) - B_{ps}\cos(\theta_p - \theta_s)) \ , \tag{2.21}$$

$$P_s = V_s^2 G_{ss} + V_s V_p \ (G_{sp}\cos(\theta_s - \theta_p) + B_{sp}\sin(\theta_s - \theta_p)) \ , \tag{2.22}$$

$$Q_s = -V_s^2 B_{ss} + V_s V_p \ (G_{sp}\sin(\theta_s - \theta_p) - B_{sp}\cos(\theta_s - \theta_p)) \ . \tag{2.23}$$

When the transformer is working as LTC, the tap position variable T_k is adjusted, within limits, to constrain the voltage magnitude. If controlling the voltage magnitude at the primary side is desired, T_k replaces V_p. On the other hand, if voltage magnitude at the secondary side is to be controlled, T_k replaces V_{ps}.

During the solution process, after each iteration (j) the tap controller must be updated according to the following equation:

$$T_k{}^{(j+1)} = T_k{}^{(j)} + \left(\frac{\Delta T_k}{T_k}\right)^{(j)} T_k{}^{(j)} \tag{2.24}$$

2.6.2 Phase shifting transformer

The PST allows to control the direction and magnitude of the active power flow. In similar way as the LTC, the PST model is based on the analysis of the two-winding transformer shown in Figure 2.4. The complex tap angles ϕ_{tv} and ϕ_{uv} for the primary and secondary side, respectively, are adjusted in order to control the calculated active power flow to a specified value. The control can be carried out either from the primary to the secondary side and viceversa. Note that (2.20 - 2.23) also hold for the PST. To incorporate the PST mathematical model into the power-flow model, it is necessary to augment the system's non-linear equation set with the following mismatch equation [Fuerte-Esquivel, 1997, Acha et al., 2004] :

$$\Delta P_{pst} = P_{pst}^{sch} - P_{pst}^{calc} \tag{2.25}$$

where P_{pst}^{sch} is the scheduled active power flow value through the PST and P_{pst}^{calc} is the calculated value. Note that, in order to linearise (2.25) respect to the complex tap angle, it is necessary to explicitly express P_{pst}^{calc} as a function of ϕ_{tv} or ϕ_{uv}. Which is fully detailed in [Fuerte-Esquivel, 1997]. Lastly, after each iteration (j) the complex tap angle must be updated according to the following equation:

$$\phi^{(j+1)} = \phi^{(j)} + \Delta\phi^{(j)} \tag{2.26}$$

where ϕ is the complex tap angle either for the primary or the secondary side of the PST.

2.6.3 Thyristor-controlled series controller (variable susceptance model)

The simpler TCSC model exploits the concept of a variable series reactance. The series reactance is adjusted automatically, within limits, to satisfy a specified amount of active power flows through it. The changing reactance X_{TCSC}, shown in Figures 2.5(a) and 2.5(b), represents the equivalent reactance of all the series-connected modules making up the TCSC, when operating in either the inductive or the capacitive regions [Acha et al., 2004].

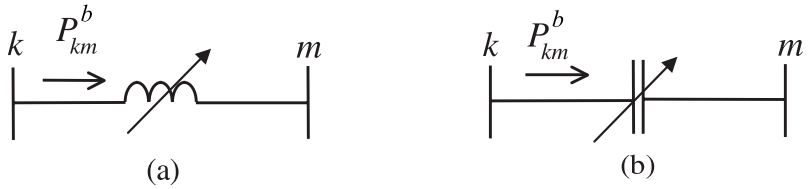

FIGURE 2.5: TCSC's equivalent circuit: (a) inductive and (b) capacitive operative regions.

The active power flowing from bus k to m is given by

$$P^b_{km} = \frac{V_k\, V_m \sin\left(\theta_k - \theta_m\right)}{X_{TCSC}} \tag{2.27}$$

The corresponding mismatch equation to be included in the power flow formulation is:

$$\Delta P^b_{km} = P^b_{km,sch} - P^b_{km,calc} \tag{2.28}$$

where subscripts *sch* and *calc* denote scheduled and calculated values, respectively. At each iteration (j), the TCSC's corresponding state variable must be updated by

$$X_{TCSC}{}^{(j+1)} = X_{TCSC}{}^{(j)} + \left(\frac{\Delta X_{TCSC}}{X_{TCSC}}\right)^{(j)} X_{TCSC}{}^{(j)} \tag{2.29}$$

2.6.4 Thyristor-controlled series controller (firing angle model)

The model presented in Section 2.6.3 uses the concept of an equivalent series reactance to represent the TCSC. The equivalent reactance, however, can also be expressed in terms of the thyristor's firing angle at fundamental frequency. This makes engineering sense only in cases when all the modules making up the TCSC have identical design characteristics and are made to operate at equal firing angles [Acha et al., 2004]. The general configuration of a TCSC at fundamental frequency is shown in Figure 2.6.

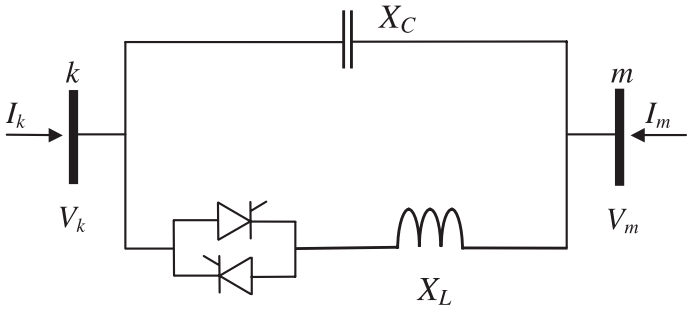

FIGURE 2.6: TCSC (firing angle) module.

The equivalent reactance as a function of the thyristor's firing angle α is given by [Fuerte-Esquivel, 1997]

$$X_{TCSC} = \frac{X_C X_L}{X_L - \frac{X_C}{\pi}\left(2\left(\pi - \alpha\right) + \sin\left(2\alpha\right)\right)}. \tag{2.30}$$

Similarly as in the variable susceptance model, the active power flowing from bus k to m is given by (2.28), and the corresponding mismatch equation to be included in the power flow formulation is:

$$\Delta P^{\alpha}_{km} = P^{\alpha}_{km,sch} - P^{\alpha}_{km,cal}, \tag{2.31}$$

where subscripts *sch* and *cal* denote scheduled and calculated values, respectively. At each iteration (j), the TCSC's corresponding state variable must be updated according to the following expression:

$$\alpha^{j+1} = \alpha^{j} - \Delta\alpha^{j} \tag{2.32}$$

2.6.5 Unified power flow controller

The UPFC is capable of simultaneously controlling active and reactive powers as well as bus voltage magnitude. Alternatively, the UPFC model can be set to control one or more of the parameters above in any combination or to control none of them. The analysis of the equivalent circuit shown in Figure 2.7 is used to derive the steady-state model [Fuerte-Esquivel, 1997].

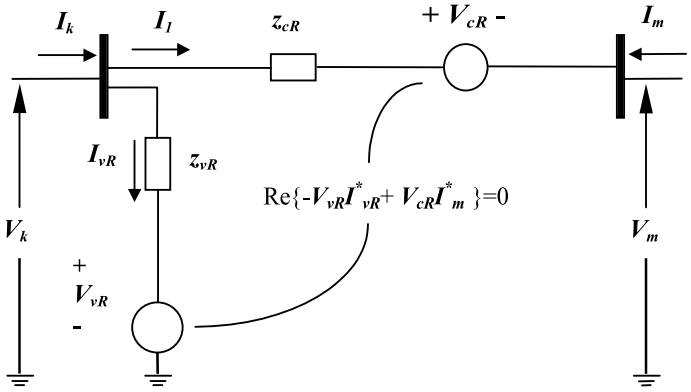

FIGURE 2.7: UPFC's equivalent circuit.

The power flow equations from bus k to bus m are:

$$\begin{aligned} P_{km}^{UPFC} &= V_k^2 G_{kk} + V_k V_m \left(G_{km}\cos\left(\theta_k - \theta_m\right) + B_{km}\sin\left(\theta_k - \theta_m\right)\right) \\ &+ V_k V_{cR} \left(G_{km}\cos\left(\theta_k - \theta_{cR}\right) + B_{km}\sin\left(\theta_k - \theta_{cR}\right)\right) \\ &+ V_k V_{vR} \left(G_{vR}\cos\left(\theta_k - \theta_{vR}\right) + B_{vR}\sin\left(\theta_k - \theta_{vR}\right)\right) \end{aligned} , \tag{2.33}$$

$$\begin{aligned} Q_{km}^{UPFC} &= -V_k^2 B_{kk} + V_k V_m \left(G_{km}\sin\left(\theta_k - \theta_m\right) - B_{km}\cos\left(\theta_k - \theta_m\right)\right) \\ &+ V_k V_{cR} \left(G_{km}\sin\left(\theta_k - \theta_{cR}\right) - B_{km}\cos\left(\theta_k - \theta_{cR}\right)\right) \\ &+ V_k V_{vR} \left(G_{vR}\sin\left(\theta_k - \theta_{vR}\right) - B_{vR}\cos\left(\theta_k - \theta_{vR}\right)\right) \end{aligned} , \tag{2.34}$$

and from bus m to bus k:

$$\begin{aligned} P_m^{UPFC} = {} & V_m^2 G_{mm} + V_m V_k \left(G_{mk}\cos\left(\theta_m - \theta_k\right) + B_{mk}\sin\left(\theta_m - \theta_k\right)\right) \\ & + V_m V_{cR} \left(G_{mm}\cos\left(\theta_m - \theta_{cR}\right) + B_{mm}\sin\left(\theta_m - \theta_{cR}\right)\right) \end{aligned}, \tag{2.35}$$

$$\begin{aligned} Q_m^{UPFC} = {} & -V_m^2\, B_{mm} + V_m\, V_k\, \left(G_{mk}\sin(\theta_m - \theta_k) - B_{mk}\cos(\theta_m - \theta_k)\right) \\ & + V_m\, V_{cR}\, \left(G_{mm}\sin(\theta_m - \theta_{cR}) - B_{mm}\cos(\theta_m - \theta_{cR})\right) \end{aligned}. \tag{2.36}$$

For the series converter the power flow equations are

$$\begin{aligned} P_{cR} = {} & V_{cR}^2\, G_{mm} + V_{cR}\, V_k\, \left(G_{km}\cos(\theta_{cR} - \theta_k) + B_{km}\sin(\theta_{cR} - \theta_k)\right) \\ & + V_{cR}\, V_m\, \left(G_{mm}\cos(\theta_{cR} - \theta_m) + B_{mm}\sin(\theta_{cR} - \theta_m)\right) \end{aligned}, \tag{2.37}$$

$$\begin{aligned} Q_{cR} = {} & -V_{cR}^2\, B_{mm} + V_{cR}\, V_k\, \left(G_{km}\sin(\theta_{cR} - \theta_k) - B_{km}\cos(\theta_{cR} - \theta_k)\right) \\ & + V_{cR}\, V_m\, \left(G_{mm}\sin(\theta_{cR} - \theta_m) - B_{mm}\cos(\theta_{cR} - \theta_m)\right) \end{aligned}, \tag{2.38}$$

and for the shunt converter:

$$P_{vR} = -V_{vR}^2\, G_{vR} + V_{vR}\, V_k\, \left(G_{vR}\cos(\theta_{vR} - \theta_k) + B_{vR}\sin(\theta_{vR} - \theta_k)\right), \tag{2.39}$$

$$Q_{vR} = V_{vR}^2\, B_{vR} + V_{vR}\, V_k\, \left(G_{vR}\sin(\theta_{vR} - \theta_k) - B_{vR}\cos(\theta_{vR} - \theta_k)\right). \tag{2.40}$$

Assuming that the active and reactive power flow are controlled from bus k to bus m, the corresponding mismatch equations to be included in the power flow model are the following:

$$\Delta P_{km}^{UPFC} = P_{km,sch}^{UPFC} - P_{km,cal}^{UPFC}, \tag{2.41}$$

$$\Delta Q_{km}^{UPFC} = Q_{km,sch}^{UPFC} - Q_{km,cal}^{UPFC}, \tag{2.42}$$

where subscripts *sch* and *cal* denote scheduled and calculated values, respectively. Also, considering a loss-free operation, the active power supplied to the shunt

converter, P_{vR} , must satisfy the active power demanded by the series converter, P_{cR} , i.e.:

$$P_{vR} + P_{cR} = 0 \tag{2.43}$$

Depending on the desired control actions to be carried out by the UPFC, at the end of each iteration the UPFC's state variables $[V_{cR}, \theta_{cR}, V_{vR}, \theta_{vR}]$ are updated accordingly by

$$V_{cR}{}^{(j+1)} = V_{cr}{}^{(j)} + \left(\frac{\Delta V_{cR}}{V_{cr}}\right)^{(j)} V_{cR}{}^{(j)}, \tag{2.44}$$

$$\theta_{cR}^{j+1} = \theta_{cR}^{j} - \Delta\theta_{cR}^{j}, \tag{2.45}$$

$$V_{vR}{}^{(j+1)} = V_{vr}{}^{(j)} + \left(\frac{\Delta V_{vR}}{V_{vr}}\right)^{(j)} V_{vR}{}^{(j)}, \tag{2.46}$$

$$\theta_{vR}^{j+1} = \theta_{vR}^{j} - \Delta\theta_{vR}^{j}. \tag{2.47}$$

2.6.6 Proposed Static VAR Compensator model (variable susceptance)

The static VAR compensator (SVC) is mainly used in power systems to maintain the voltage magnitude at the connection point within a specified range or at a specified set value. A realistic way to model this SVC's control action in the context of Newton-based power flow studies was reported in [Ambriz-Perez et al., 2000, Fuerte-Esquivel, 1997], where the SVC is considered as a variable shunt susceptance, with either firing angle limits or susceptance limits, which is adjusted to achieve the level of compensation required to set the voltage magnitude at its specified value. This model can be directly included in any power flow program by considering the bus voltage magnitude fixed at the target value and taking the SVC's susceptance or thyristor's firing angle as a state variable, as discussed in [Ambriz-Perez et al., 2000]. This model approach, however, is unsuitable for the analysis method of control interactions proposed in this thesis which requires the Jacobian to be expanded. Another way of modelling the SVC's control action in

the formulation of the Newton-based power flow problem is proposed in [Canizares and Faur, 1999] by using an expanded Jacobian approach. By implementing this modelling technique, the proposed control interaction analysis involving SVCs is possible. However, this thesis proposes an alternative expanded Jacobian method for modelling SVCs, with the advantage of having less additional mismatch equations that the method presented in [Canizares and Faur, 1999]. The variable susceptance SVC model is described in this section while the firing angle model is described in Section 2.6.7. The justification of the development of these models is detailed in Section 4.1.

Considering a SVC connected at the k-th bus with an adjustable susceptance B_{sh}, as depicted in Figure 2.8, the shunt reactive power Q_{sh}^{sch} to be provided by the SVC in order to set the voltage magnitude at the specified value $V_{k,sch}$ is given by

$$Q_{sh}^{sch} = -V_{k,sch}^2 B_{sh}. \tag{2.48}$$

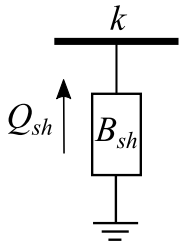

FIGURE 2.8: SVC (variable susceptance).

Similarly, the reactive power injected by the SVC as a function of the voltage magnitude $V_{k,sch}$ that is calculated at each iteration of the power flow solution process is given by

$$Q_{sh}^{cal} = -V_{k,cal}^2 B_{sh}. \tag{2.49}$$

A mismatch equation can then be mathematically formulated to represent the SVC's control action from (2.48) and (2.49), which is given by

$$\Delta Q_{SVC} = Q_{sh}^{sch} - Q_{sh}^{cal} = 0. \tag{2.50}$$

Equation (2.50) is added to the general power flow formulation, together with the reactive power flow mismatch equation at the k-th bus at which the SVC is connected in order to calculate the level of shunt compensation required to achieve the specified voltage magnitude control. Lastly, the linearisation of ΔQ_{SVC} with respect to B_{sh} is as follows:

$$\frac{d\Delta Q_{SVC}}{dB_{sh}} B_{sh} = B_{sh} \left(V_{k,cal}^2 - V_{k,sch}^2 \right) \tag{2.51}$$

At the end of each iteration (j), the SVC's corresponding state variable must be updated according to the following expression:

$$B_{sh}{}^{(j+1)} = B_{sh}{}^{(j)} + \left(\frac{\Delta V_{sh}}{B_{sh}} \right)^{(j)} B_{sh}{}^{(j)}, \tag{2.52}$$

2.6.7 Proposed Static VAR Compensator model (firing angle)

One of the most popular configurations for continuously controlled SVCs is composed by the series connection of a fixed capacitor and a thyristor-controlled reactor (FC-TCR) [Fuerte-Esquivel, 1997]. Considering the FC-TCR module shown in Figure 2.9, in the case of the SVC firing angle model, the shunt susceptance is expressed as a function of a thyristor's firing angle as [Ambriz-Perez et al., 2000, Fuerte-Esquivel, 1997]:

$$B_{sh} = -\frac{X_L - \frac{X_C}{\pi} \left(2 \left(\pi - \alpha \right) + \sin \left(2\alpha \right) \right)}{X_C X_L}. \tag{2.53}$$

The mismatch equation to be incorporated to the power flow model is given by (2.50) in the same manner that the SVC variable susceptance model. Also, at each iteration (j), the SVC's firing angle α must be updated by

$$\alpha^{j+1} = \alpha^j - \Delta\alpha^j \tag{2.54}$$

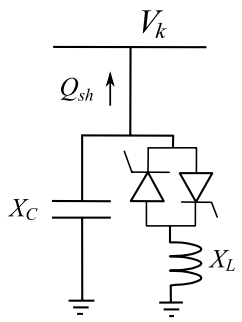

FIGURE 2.9: FC-TCR module.

2.7 Conclusions

This chapter presents the steady-state mathematical models of the power system's components considered in this work. Several steady-state models of control devices are adopted including FACTS devices, AFC and AIC. All these models are based on the power flow formulation and solved together using a Newton-based method. In addition, new mathematical models of AIC and SVCs are proposed and described.

All the above-described models and methods are implemented into a digital program developed under the Matlab environment, which is capable of solving large-scale power networks.

Chapter 3

Dynamic power system modelling

3.1 Introduction

The dynamic stability analysis of power systems plays an important role in the design, planning and operation processes. Dynamic (time-domain) numerical simulations are an important tool when monitoring of the power system and planning of preventive or corrective control action strategies suitable for mitigating the impact of several disturbances presented in the system.

Taking into consideration the complex dynamic nature of power systems, the numerical simulation of the behaviour of the power system in the presence of a disturbance implies the consideration of a large number of devices with time scales going from micro-seconds to hours. Hence, taking into account the dynamics of all devices and time scales using a unique model would be extremely impractical. Figure 3.1 shows the different time scales and related phenomena of interest in a power system [Milano, 2010]. As can be noted, the transient stability time scale encompass most of the interactions among the different controls and devices in power systems. At the same time, the generator controls are the most involved in the transient stability time scale.

Due to the above-mentioned, the transient stability time frame is considered for the assessment of the interaction among control devices in this thesis. Moreover, because of its importance in this time frame, the controls considered are those related

with conventional generators. Moreover, the controls associated with the recently introduced Type-4 Wind Energy Conversion Systems [Nouh and Mohamed, 2014] are also included in the interaction analysis.

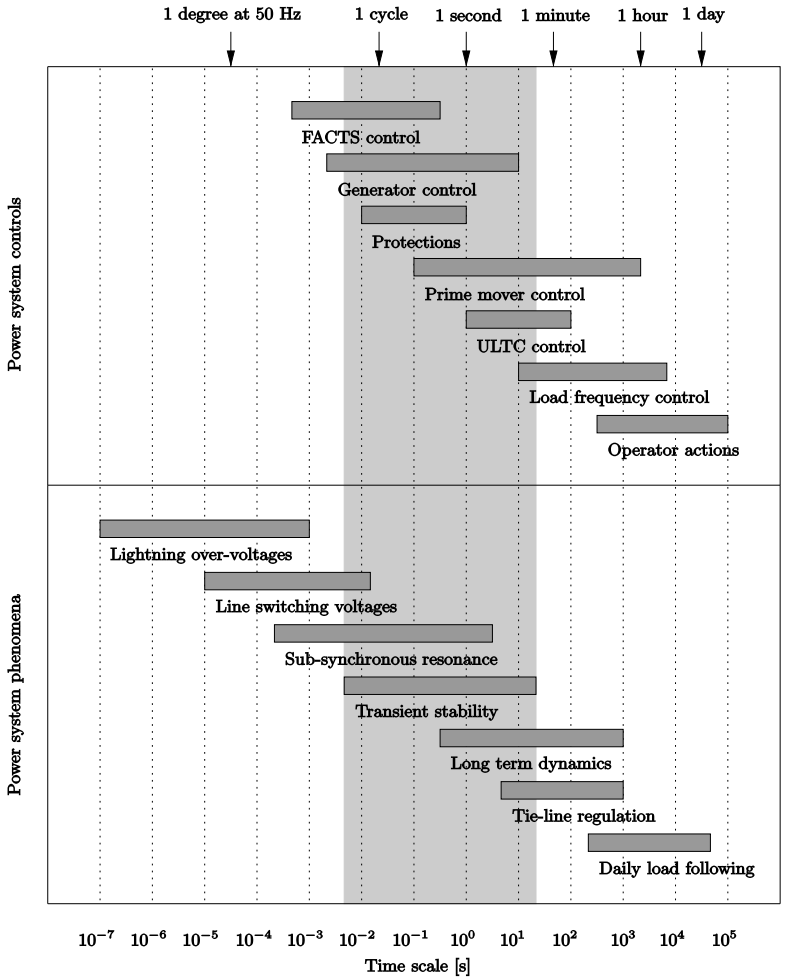

FIGURE 3.1: Time scales in power systems.

This chapter presents a description of the various device models used in the numerical simulations in order to study the existent interaction among control devices. Concerning the modelling of the conventional generators, i.e. synchronous machine, a 4th order model known as the the "two-axis model" [Sauer and Pai, 1998] is adopted in this thesis. The typical control models of the synchronous machine are also adopted and described in this chapter, i.e. Automatic Voltage Regulator (AVR), turbine-governor group and Power System Stabilizer (PSS). In addition, a dynamic model for the IEEE Type-4 WECS is described, as well as its back-to-back controller dynamic model. Based on these models, the numerical solution method

used to solve the differential-algebraic equation set associated with the entire network is then presented. Finally, the procedure employed to simulate disturbances in the power system is described.

3.2 Synchronous Generator Model

The synchronous machine scheme is shown in Figure 3.2 [Kundur et al., 1994]. This machine has a salient-pole rotor and the stator circuits consist of three-phase armature windings carrying alternating currents. Thus, the stator currents are said to be in *abc* coordinates. On the other hand, the rotor circuits consist of field and armature windings on d and q axes respectively. Hence, the rotor is said to be in *dq0* coordinates.

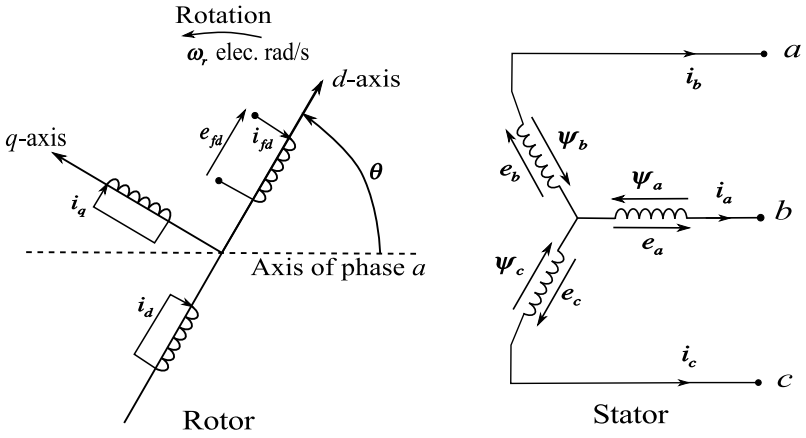

FIGURE 3.2: Synchronous machine scheme.

The stator current and voltage equations have sinusoidal time-varying inductances which increases the complexity of the machine equations. In order to overcome this problem, stator equations can be transformed into the *dq0* reference frame using the well-known "Park's Transformation" [Kundur et al., 1994, Sauer and Pai, 1998, Krause et al., 2002, Milano, 2010].

Among the many existing references that address the synchronous machine theory, several models are proposed. The differences among these models basically consist on the transfer function that relates stator fluxes with stator currents and the field voltage. Depending on the dynamic order and detail of these transfer functions,

there is a resulting change in the set of DAEs representing the dynamic behaviour of the synchronous machine.

The synchronous generator model adopted in the present work is a fourth order model obtained from a reduction of a higher order model described in [Sauer and Pai, 1998] . This reduction is made by not taking into account the sub-transient time constants. Note thet this model, often referred as the "Two-Axis Model", is the highest order model on which there is more agreement in the literature. Actually, this model is considered the most commonly used in power system stability analysis because it provides the right balance between simplicity and accuracy [Milano, 2010].

The two-axis model yields a set of four ordinary differential equations and two nonlinear algebraic equations. These equations are obtained by applying the fundamental Kirchhoff's and Faraday's laws as well as the Park's transformation [Sauer and Pai, 1998]:

$$T_{d0}^{'}\frac{dE_q^{'}}{dt} = K_1 E_q^{'} + K_3 V\cos\left(\delta-\theta\right) + E_{fd}, \tag{3.1}$$

$$T_{q0}^{'}\frac{dE_d^{'}}{dt} = K_3 E_d^{'} + K_4 V\sin\left(\delta-\theta\right), \tag{3.2}$$

$$\frac{d\delta}{dt} = \omega - \omega_0, \tag{3.3}$$

$$\frac{d\omega}{dt} = \frac{\omega_0}{2H}\left(P_m - P_g - D\left(\omega-\omega_0\right)\right), \tag{3.4}$$

$$\begin{aligned} P_g = {} & K_5 E_d^{'} V\cos\left(\delta-\theta\right) + K_6 E_q^{'} V\sin\left(\delta-\theta\right) \\ & + K_7 V^2\sin\left(2\left(\delta-\theta\right)\right) \end{aligned}, \tag{3.5}$$

$$\begin{aligned} Q_g = {} & -K_5 E_d^{'} V\sin\left(\delta-\theta\right) + K_6 E_q^{'} V\cos\left(\delta-\theta\right) \\ & + V^2\left(-K_6\cos^2\left(\delta-\theta\right) + K_5\sin^2\left(\delta-\theta\right)\right) \end{aligned}, \tag{3.6}$$

where

$$K_1 = -\frac{X_d}{X_d^{'}},\quad K_2 = -1+\frac{X_d}{X_d^{'}},\quad K_3 = -\frac{X_q}{X_q^{'}},\quad K_4 = -1+\frac{X_q}{X_q^{'}},$$
$$K_5 = -\frac{1}{X_q^{'}},\quad K_6 = \frac{1}{X_d^{'}},\quad K_7 = \frac{X_d^{'}-X_q^{'}}{2X_d^{'}X_q^{'}}.$$

Note that in the machine model described above, the armature resistance (that usually is very small) is neglected. Table 3.1 and Table 3.2 indicate the variables involved in the two-axis model equations and the related parameters and constants respectively. The synchronous machine field current is expressed as:

$$I_{fd} = -K_1 E_q^{'} - K_2 V \cos(\delta - \theta) \tag{3.7}$$

TABLE 3.1: Synchronous machine two-axis model variables

Variable	Description	Units
$E_q^{'}$	Q-axis transient voltage	p.u.
$E_d^{'}$	D-axis transient voltage	p.u.
δ	Machine's rotor angle	rad
ω	Rotor's angular speed	rad/s
P_g	Bus real power generation	p.u.
Q_g	Bus reactive power generation	p.u.
P_m	Turbine's mechanical power input	p.u.
$V\angle\theta$	Bus voltage	p.u., rad

TABLE 3.2: Synchronous machine two-axis model parameters

Variable	Description	Units
D	Damping coefficient	p.u.
H	Inertia constant	$\frac{\text{MW*s}}{\text{MVA}}$
X_d	D-axis synchronous reactance	p.u.
X_q	Q-axis synchronous reactance	p.u.
$X_d^{'}$	D-axis transient reactance	p.u.
$X_q^{'}$	Q-axis transient reactance	p.u.
$T_{d0}^{'}$	D-axis open circuit transient time constant	s
$T_{q0}^{'}$	Q-axis open circuit transient time constant	s

3.2.1 Time Reference Frame and Center of Inertia

In Equation (3.3) the machine rotor angle and speed are asumed relative to a hypothetical machine with constant speed and angle. This is the standard manner to refer the angles and speeds of machine rotors [Fabozzi and Cutsem, 2011]. A problem arising as a consequence of using this reference frame, is that after a disturbance, although the system settles at a new equilibrium point, the rotor angle variable

increases linearly with time and bus voltage phasors oscillate periodically. This behaviour requires frequent updates in the Jacobian matrix and increases the number of iterations of the Newton method used to solve the implicit equations [Kundur et al., 1994]. It also requires a small time integration step in order to track all those oscillations [Fabozzi and Cutsem, 2011]. In order to overcome this problem, it is common to use a reference transformation called the Center of Inertia (COI). This reference transformation defines the COI angle and COI speed for a system containing m machines as [Sauer and Pai, 1998, Milano, 2010]:

$$\delta_{COI} \triangleq \frac{1}{M_T} \sum_{j=1}^{m} M_j \delta_j, \tag{3.8}$$

$$\omega_{COI} \triangleq \frac{1}{M_T} \sum_{j=1}^{m} M_j \omega_j, \tag{3.9}$$

where

$$M_T \triangleq \sum_{j=1}^{m} M_j \tag{3.10}$$

and

$$M_j \triangleq \frac{2H_j}{\omega_0}. \tag{3.11}$$

Thus, equations (3.3) and (3.4) become:

$$\frac{d\delta}{dt} = \omega - \omega_{COI}, \tag{3.12}$$

$$\frac{d\omega}{dt} = \frac{\omega_0}{2H} \left(P_m - P_g - D \left(\omega - \omega_{COI} \right) \right). \tag{3.13}$$

With the use of COI reference frame, it is necessary to add (3.9) to the algebraic set of equations and to consider ω_{COI} as a state variable. On the other hand, by combining (3.8) and (3.12), it can be easily demonstrated that $\frac{d\delta_{COI}}{dt} = 0$, therefore, it is not necessary to treat δ_{COI} as a state variable.

3.2.2 Initial Condition of the Synchronous Generator

The initial condition of the synchronous generator's dynamic variables ($E_q^{'}$, $E_d^{'}$, ω, δ) is computed by the steady state synchronous machine equivalent circuit shown in Figure 3.3. This computation must be conducted after a load flow study. For a synchronous generator at the i-th bus, the initialization of machine dynamic states is described by the following steps [Sauer and Pai, 1998]:

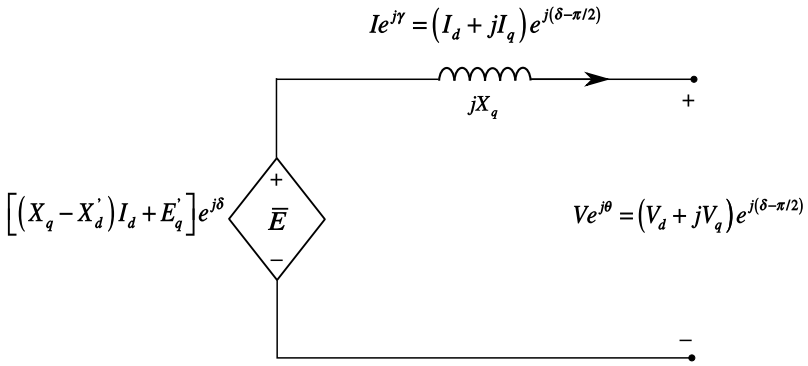

FIGURE 3.3: Synchronous machine equivalent circuit.

- Step 1. From an initial load flow, compute $I_i e^{j\gamma_i} = \frac{P_{Gi} - jQ_{Gi}}{V_i e^{-j\theta_i}}$.
- Step 2. Compute E_i, δ_i as $E_i \angle \delta_i = V_i e^{j\theta_i} + jX_{qi}^{'} I_i e^{j\gamma_i}$.
- Step 3. Compute I_{di}, I_{qi} from $(I_{di} + jI_{qi}) = I_i e^{j(\gamma_i - \delta_i + \pi/2)}$.
- Step 4. Compute $E_{di}^{'} = V_{di} - X_{qi}^{'} I_{qi}$ or $E_{di}^{'} = \left(X_{qi} - X_{qi}^{'}\right) I_{qi}$ (the latter can be used as a check on the calculations).
- Step 5. Compute $E_{qi}^{'} = V_{qi} + X_{di}^{'} I_{di}$.
- Step 6. Compute E_{fdi} from (3.1) after setting the derivative equal to zero ($E_{fdi} = -K_1 E_{qi}^{'} - K_3 V_i \cos(\delta_i - \theta_i)$).

Note that the initial conditions of the dynamic state ω_i are found from (3.3) after setting the derivative equal to zero, i.e. $\omega_i = \omega_0$. Also, if the derivative in (3.4) is set to zero, $P_{mi} = P_{gi}$. Note also that if turbine-governor models are not included, P_m is considered constant. Similarly, if exciter systems are not modelled, E_{fd} is constant. Finally, the initial value of ω_{COI} can be found with the initial values

of ω_i. As stated earlier, δ_{COI} will remain constant and it is only necessary to be computed after a dynamic simulation is conducted so that the angles of the system can be referred.

3.3 Synchronous Machine Control Models

3.3.1 Automatic Voltage Regulator

AVRs define the primary voltage regulation of synchronous machines as they provide a mechanism for controlling the synchronous machine terminal voltage magnitude. Several AVR models have been proposed in the literature [IEEE Committee, 1981, IEEE Committee, 2006]. The block diagram depicted in Figure 3.4 describes the AVR type IEEE-DC1A which is the model used in the present work. This classic model has been widely implemented by the industry [IEEE Committee, 2006].

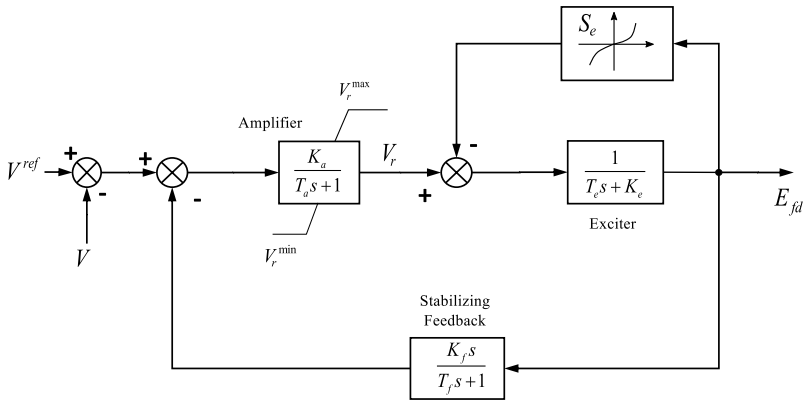

FIGURE 3.4: Block diagram of AVR type IEEE-DC1A.

As described in [IEEE Committee, 2006], an aditional lead-lag block can be included before the amplifier stage, however, the related time constants are frequently small enough to be neglected. The three corresponding differential equations of this model are:

$$\frac{dV_r}{dt} = \frac{1}{T_a}\left(K_a\left(V^{ref} - V - R_f - \frac{K_f}{T_f}E_{fd}\right) - V_r\right) \tag{3.14}$$

$$\frac{dR_f}{dt} = -\frac{1}{T_f}\left(\frac{K_f}{T_f}E_{fd} + R_f\right), \tag{3.15}$$

$$\frac{dE_{fd}}{dt} = -\frac{1}{T_e}\left(E_{fd}\left(K_e + S_e\right) - V_r\right), \tag{3.16}$$

where V_r is the exciter input, V^{ref} is the reference terminal voltage magnitude and R_f is called rate feedback [Kundur et al., 1994]. S_e is the ceiling function and it models the saturation of the AVR, typically given by:

$$S_e = A_e e^{B_e|E_{fd}|} \tag{3.17}$$

It is common to determine coefficients A_e and B_e by measuring two points of the ceiling function. Typically the values of $S_e^{\max}$ and $S_e^{0.75\cdot\max}$ are known and correspond to the field voltages $E_{fd}^{\max}$ and $0.75 \cdot E_{fd}^{\max}$, respectively. To compute A_e and B_e, the following equation system has to be solved:

$$0 = -\left(1 + S_e^{\max}\right)E_{fd}^{\max} + V_r^{\max}, \tag{3.18}$$

$$S_e^{\max} = A_e e^{B_e E_{fd}^{\max}}, \tag{3.19}$$

$$S_e^{0.75\cdot\max} = A_e e^{B_e \cdot 0.75 \cdot E_{fd}^{\max}}, \tag{3.20}$$

where $S_e^{\max}$, $S_e^{0.75\cdot\max}$ and $V_r^{\max}$ are given values. Table 3.3 describes the AVR model parameters and constants. It is important to note that typically the value of K_e must be selected so that $V_r = 0$, as described in [IEEE Committee, 1981].

TABLE 3.3: AVR type IEEE-DC1A parameters.

Parameter	Description	Units
A_e	1st ceiling coefficient	-
B_e	2nd ceiling coefficient	1/p.u.
K_a	Amplifier gain	-
K_e	Field circuit integral deviation	-
K_f	Stabilizer gain	-
T_a	Amplifier time constant	s
T_f	Stabilizer time constant	s
T_e	Field circuit time constant	s
T_r	Measurement time constant	s
$V_r^{\max}$	Maximum regulator voltage	p.u.
$V_r^{\min}$	Minimum regulator voltage	p.u.

3.3.2 Turbine-Governor

The speed governors define the primary frequency control of the synchronous machines, it adjusts the steam input to the turbine through the valve position. There are several speed governor models available in the literature, as described in [IEEE Committee, 1973]. The model implemented in the present work is shown in the block diagram of Figure 3.5 This is a simple (yet practical) model that actually correspond to a General Electric EH system [Sauer and Pai, 1998, IEEE Committee, 1973].

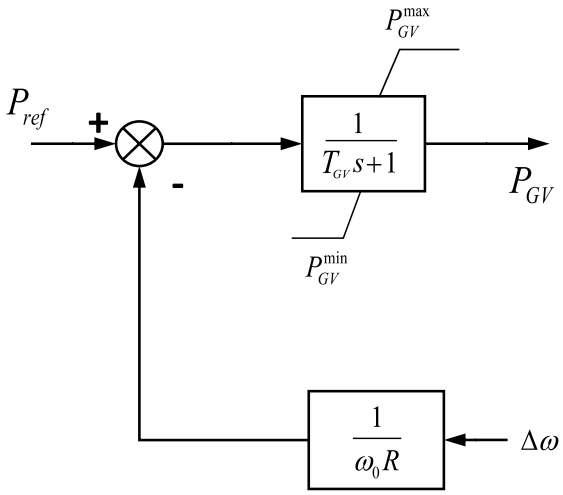

FIGURE 3.5: Block diagram of the speed governor.

The differential equation that describes the functioning of the speed governor is given by

$$T_{GV}\frac{dP_{GV}}{dt} = -P_{GV} + P_{ref} - \frac{1}{R}\left(\frac{\omega - \omega_0}{\omega_0}\right) \tag{3.21}$$

where T_{GV} is the governor time constant in s and R is the regulation droop, defined as a measure of the participation of each machine to the system power and frequency variations. Note that (3.21) is valid for values of ω in rad/s. For values of ω in p.u., the gain block following the angular speed deviation should not be divided by ω_0 [Rafian et al., 1987]. Also, according to [Kundur et al., 1994, IEEE Committee, 1973], the value of P_{GV} and its derivative should be constrained so that:

$$0 \leq P_{GV} \leq P_{GV}^{\max}, \tag{3.22}$$

$$\frac{dP_{GV}^{\min}}{dt} \leq \frac{dP_{GV}}{dt} \leq \frac{dP_{GV}^{\max}}{dt}. \tag{3.23}$$

The meaning of (3.22) is that there is a certain limit in the position of the valves, i.e. wide open valves. On the other hand, (3.23) restricts the rate of changes for large, rapid speed variations.

The valve position P_{GV} is the input of the turbine which in turn adjusts the mechanical power P_m applied to the generator's shaft. This can be seen in Figure 3.6 (a) that depicts a tandem-compound, single-reheat steam turbine [IEEE Committee, 1973]. This configuration is in general appropriate to model today's steam turbines commonly used in generator units [Kundur et al., 1994], and can be used to represent hydro turbines by means of a proper selection of parameters [IEEE Committee, 1973]. Hence, this turbine model is implemented in the present work.

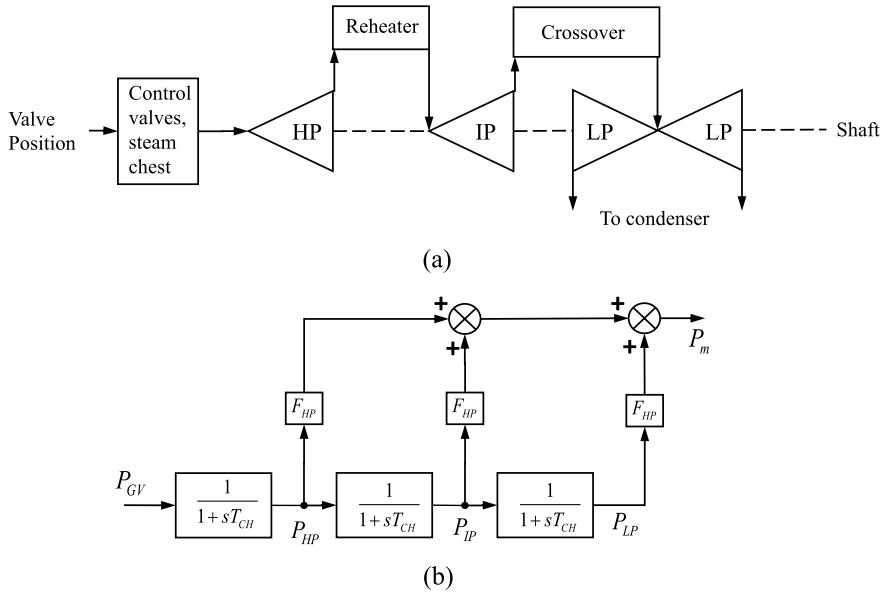

FIGURE 3.6: a) Steam turbine Configuration b) Steam turbine block diagram.

The following differential equation set describes the behaviour of the steam turbine:

$$\frac{dP_{HP}}{dt} = \frac{P_{GV} - P_{HP}}{T_{CH}}, \tag{3.24}$$

$$\frac{dP_{IP}}{dt} = \frac{P_{HP} - P_{IP}}{T_{RH}}, \tag{3.25}$$

$$\frac{dP_{LP}}{dt} = \frac{P_{IP} - P_{LP}}{T_{CO}}, \tag{3.26}$$

and the mechanical power injected to the generator is:

$$P_m = P_{HP}F_{HP} + P_{IP}F_{IP} + P_{LP}F_{LP}, \tag{3.27}$$

where P_{HP}, P_{IP} and P_{LP} are the high, intermediate and low-pressure section powers, respectively. Table 3.4 describes the tandem-compound, single-reheat turbine parameters.

TABLE 3.4: Tandem-compound, single-reheat turbine parameters.

Parameter	Description	Units
R	Speed Regulation	p.u.
T_{GV}	Governor time constant	s
F_{HP}	High-pressure turbine power fraction	-
F_{IP}	Intermediate-pressure turbine power fraction	-
F_{LP}	Low-pressure section turbine power fraction	-
T_{CH}	Steam chest time constant	s
T_{RH}	Re-heater time constant	s
T_{CO}	Cross-over time constant	s
P_{GV}^{max}	Input power maximum limit	p.u.
P_{GV}^{min}	Input power minimum limit	p.u.

3.3.3 Power System Stabilizer

The basic function of a PSS is to add damping to the generator rotor oscillations by controlling its excitation using auxiliary stabilizing signals [Kundur et al., 1994]. The functioning of a PSS can be illustrated by the block diagram shown in Figure 3.7. This type of PSS is consistent with type IEEE-PSS1A model [IEEE Committee, 2006, Xu et al., 1998].

Typical PSS inputs are proportional to rotor speed, active power and bus voltage [IEEE Committee, 2006, van Cutsem and Βουρνάς, 1998]. PSS gain is set by K_S and signal washout is set by the time constant T_w. The next two blocks allow two stages of lead-lag compensation, as set by time constants T_1 to T_4. Finally,

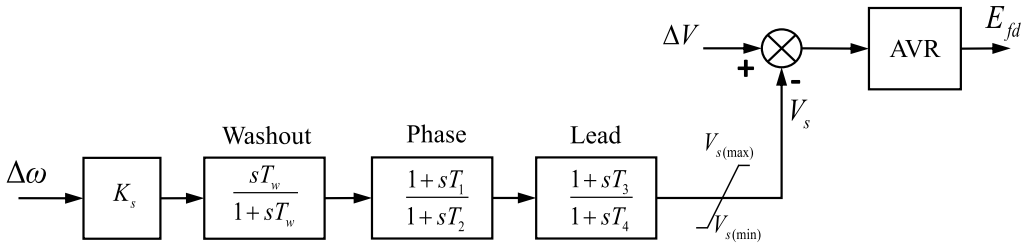

FIGURE 3.7: Block diagram of the PSS.

V_S output signal modifies the reference voltage of the AVR. The PSS parameters are summarized in Table 3.5.

TABLE 3.5: PSS parameters.

Parameter	Description	Units
K_S	PSS gain	-
T_w	Washout time constant	s
T_1, T_2	Phase section time constants	s
T_3, T_4	Lead section time constants	s
$V_{S\,\max}$	Max. PSS output signal	p.u.
$V_{S\,\min}$	Min. PSS output signal	p.u.

The PSS mathematical model is described by the following equations [Milano, 2010]:

$$\frac{dx_1}{dt} = -\frac{1}{T_w}\left(K_S\Delta\omega + x_1\right), \tag{3.28}$$

$$\frac{dx_2}{dt} = \frac{1}{T_2}\left(\ c_1\left(K_S\Delta\omega + x_1\right)\ -\ \ x_2\ \right), \tag{3.29}$$

$$\frac{dx_3}{dt} = \frac{1}{T_4}\left(\ c_2\left(x_2 +\ c_3\left(K_S\Delta\omega + x_1\right)\right)\ \ - x_3\ \right), \tag{3.30}$$

where x_1, x_2 and x_3 are the state variables associated with the washout, phase and lead blocks respectively, while the PSS output V_s is given by

$$V_S = c_2x_3 + c_4\left(\ c_1x_2 + c_3\left(K_S\Delta\omega + x_1\right)\ \right)\ . \tag{3.31}$$

Constants c_1-c_4 are given by

$$c_1 = 1 - \frac{T_1}{T_2}, \quad c_2 = 1 - \frac{T_3}{T_4}, \quad c_3 = \frac{T_1}{T_2}, \quad c_4 = \frac{T_3}{T_4}. \tag{3.32}$$

The initial conditions for the state variables x_1, x_2 and x_3 are determined by setting (3.28)-(3.30) and $\Delta\omega$ equal to zero. In other words, the PSS compensation is zero under steady state operating conditions.

3.4 Wind Generator Model

In recent years, wind turbines have become an important alternative to the conventional fossil fuel power generation plants, because of the environmental and economic benefits. With the increase of the wind energy penetration level in several regions around the world, the need of more flexible and adaptable wind generation systems has become evident in order to meet the power grid requirements and codes.

3.4.1 Overview

Wind Energy Conversion Systems (WECS) produce electricity by using the kinetic power of the wind to move a rotor by means of aerodynamically designed blades. The rotor drives an electrical generator and a gearbox can be used to make the coupling. In addition to a step-up transformer, power converters can be used to couple the generator with a power grid [Nouh and Mohamed, 2014].

From the standpoint of the velocity control, WECS can be simply divided into two types: fixed-speed and variable-speed [Nouh and Mohamed, 2014, E. H. Camm et al., 2009]. From these, there is a clear trend towards the utilization of variable-speed WECS because of their substantial degree of flexibility in terms of active and reactive power generation as well as the rotational speeds of operation. This adaptability of variable-speed WECS has been possible largely because of the development of power electronics technology and control systems in order to interface the WECS with the power grid. A full description and classification of WECS is given in [Nouh and Mohamed, 2014, E. H. Camm et al., 2009, Tiegna et al., 2012]. Due to its relatively complex control system and variable speed operation, the WECS

model adopted in this work comprises a direct-drive Permanent Magnet Synchronous Generator (PMSG) and a full back-to-back power converter as interface to the grid. This WECS technology, often referred as "Type-4" [E. H. Camm et al., 2009], has the flexibility and adaptability needed by modern grid requirements.

The typical topology of a Type-4 WECS is shown in Figure 3.8, where a full range power converter is used to connect the generator to the grid. Furthermore, because of this type of generator may not be driven by a gearbox, it is also called direct-drive wind turbine.

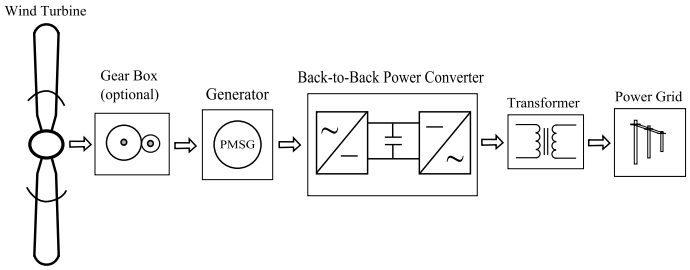

FIGURE 3.8: Typical Type-4 WECS topology.

3.4.2 PMSG model

The differential equations that describe the dynamic electrical behaviour of the PMSG are given by [Krause et al., 2002]

$$L_d \frac{di_d}{dt} = \left(-R_d i_d + L_q p \omega_r i_q - v_d\right), \tag{3.33}$$

$$L_q \frac{di_q}{dt} = \left(-R_q i_q - L_d p \omega_r i_d + p \omega_r \psi - v_q\right), \tag{3.34}$$

where the subscripts d and q denote the direct and quadrature axes respectively, i and v are the machine's current and voltage, respectively, ω_r is the mechanical rotating speed, L and R are the inductance and resistance of the machine's rotor, respectively, p is the number of pole pairs, and ψ is the magnetic flux induced by the permanent magnets.

3.4.3 Wind turbine mechanical model

The mechanical behaviour of the wind turbine's shaft system can be simply described by [Wu et al., 2008]

$$H_C \frac{d\omega_r}{dt} = (T_e - B\omega_r - T_m)\,, \tag{3.35}$$

where B is the viscous frictional coefficient, H_C is the combined mechanical system and generator's total inertia, while T_e and T_m are the electrical and mechanical torques, respectively, given by

$$T_m = \frac{\rho \pi r^2 C_p v_w^3}{2\omega_r}, \tag{3.36}$$

$$T_e = \frac{3}{2} p \left(\psi i_q + (L_d - L_q)\, i_q i_d\right), \tag{3.37}$$

where ρ is the air density, r is the turbine blade radius, v_w is the air speed and

$$C_p = \frac{1}{2}\left(\frac{rC_f}{\lambda} - 0.022\beta - 2\right) e^{-0.255\left(rC_f/\lambda\right)}, \tag{3.38}$$

where C_f is the turbine design coefficient, β is the blade pitch angle, and λ is the blade tip speed ratio, $\lambda = \omega_r r / v_w$.

3.4.4 Back-to-Back converter model

The back-to-back converter is an AC-DC-AC link. The active power entering and exiting the converter is balanced through a DC-link, as described by [Wu et al., 2008]:

$$v_{dc} C \frac{dv_{dc}}{dt} = \frac{3}{2}\left(v_d i_d + v_q i_q + v_{dg} i_{dg} + v_{qg} i_{qg}\right), \tag{3.39}$$

where the subscript g denotes voltages and currents on the grid side of the converter, v_{dc} is the DC-link voltage, and C is the DC-link capacitance. As shown in 3.8,

the back-to-back controller divides into a generator-side converter and a grid-side converter. The controller models for the converters have been proposed in [Wu et al., 2008, Xin et al., 2013], with their corresponding block diagrams shown in Figures 3.9 and 3.10 for the converter connected at the generator side and grid side, respectively.

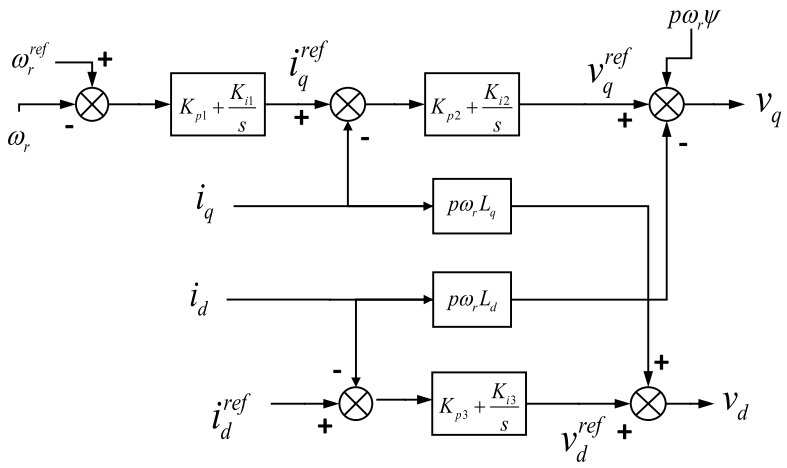

FIGURE 3.9: Block diagram of the WECS's generator side controller.

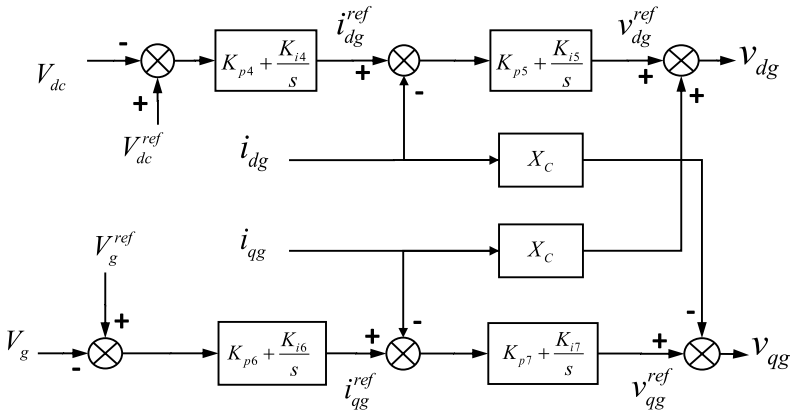

FIGURE 3.10: Block diagram of the WECS's grid side controller.

The objective of the generator side controller is to control the output active power of the PMSG to achieve the Maximum Power Point Tracking (MPPT) depending on the wind speed. The set of equations corresponding to the generator side controller are:

$$\frac{dx_1}{dt} = \omega_r^{ref} - \omega_r, \tag{3.40}$$

$$\frac{dx_2}{dt} = K_{i1}x_1 + K_{p1}\left(\omega_r^{ref} - \omega_r\right) - i_q, \tag{3.41}$$

$$\frac{dx_3}{dt} = i_d^{ref} - i_d, \tag{3.42}$$

$$\begin{aligned} v_q = {} & K_{i2}x_2 + K_{p2}\left(K_{i1}x_1 + K_{p1}\left(\omega_r^{ref} - \omega_r\right) - iq\right) \\ & - p\omega_r L_d i_d + p\omega_r \psi \end{aligned}, \tag{3.43}$$

$$v_d = K_{i3}x_3 + K_{p3}\left(i_d^{ref} - i_d\right) + p\omega_r L_q i_q, \tag{3.44}$$

where the superscript "*ref*" denotes reference values, while x_1 , x_2 and x_3 are internal differential variables of the controller. In addition, note that i_d^{ref} is normally set to zero in order to minimize generator power losses [Wu et al., 2008]. On the other hand, the grid side controller aims to maintain the DC-link voltage and the AC terminal voltage magnitude at corresponding specified values [Xin et al., 2013]. The set of equations corresponding to the grid side controller are:

$$\frac{dx_4}{dt} = V_{dc}^{ref} - V_{dc}, \tag{3.45}$$

$$\frac{dx_5}{dt} = K_{i4}x_4 + K_{p4}\left(V_{dc}^{ref} - V_{dc}\right) - i_{dg}, \tag{3.46}$$

$$\frac{dx_6}{dt} = V_g^{ref} - V_g, \tag{3.47}$$

$$\frac{dx_7}{dt} = K_{i6}x_6 + K_{p6}\left(V_g^{ref} - V_g\right) - i_{qg}, \tag{3.48}$$

$$v_{dg} = K_{i5}x_5 + K_{p5}\left(K_{i4}x_4 + K_{p4}\left(V_{dc}^{ref} - V_{dc}\right) - i_{dg}\right) + X_C i_{qg}, \tag{3.49}$$

$$v_{qg} = K_{i7}x_7 + K_{p7}\left(K_{i6}x_6 + K_{p6}\left(V_g^{ref} - V_g\right) - i_{qg}\right) - X_C i_{dg}, \tag{3.50}$$

where x_4 , x_5, x_6 and x_7 are internal differential variables of the controller, V_g is the terminal voltage magnitude and X_c is the converter smoothing reactance.

3.4.5 Inertia emulation

In a power system, the balance between active power generation and load determines the value of frequency at which the power system is operating. If

a sudden change in the total load or generation occurs, the value of frequency varies at a rate initially determined by the inertia of the spinning masses of the generators, which all together comprise the total system inertia. A few seconds after the disturbance, the primary control of synchronous generators increases their active power output in order to decrease the frequency deviation [Kundur et al., 1994]. On the other hand, the Type-4 WECS do not contribute to the natural inertial response of the system because they are decoupled from the grid by a power converter; however, these generators also have spinning masses with kinetic energy that can be released by means of a controller that releases the spinning masses' kinetic energy. This released "hiding" inertia is often referred as *emulated inertia* or *synthetic inertia* [Gonzalez-Longatt, 2012, Morren et al., 2006, Rahmann et al., 2015].

Inertia constant. The constant of inertia of a rotating mass associated with the k-th WECS embedded in the power system is given by [Kundur et al., 1994]

$$H_C^k = \frac{1}{2}\frac{J_C^k(\omega_0)^2}{S_{base}^k}, \tag{3.51}$$

where J_C^k is the combined moment of inertia of the generator and turbine prime mover in $kg \cdot m^2$, ω_0 is the synchronous angular speed in rad/s, and S_{base}^k is the rated base apparent power output of the generator in VA. The constant of inertia H_C^k represents the time in seconds that it would take the rotating mass to provide the rated power by only using its kinetic energy, and is a constant given by the wind generator manufacturer.

Center of inertia and system's frequency. Considering the commonly used COI reference transformation described in Section 3.2.1 and neglecting the damping effect, (3.4) and (3.9) can be combined in order to demonstrate that

$$\frac{d\omega_{COI}}{dt} = \frac{\omega_0}{2H_T}\left(\sum_{j=1}^{ng}(P_{mj} - P_{gj})\right) \tag{3.52}$$

By observing the similarity of (3.52) and (3.4) (without damping effects), $f_{COI} = \omega_{COI}/2\pi$ can be defined as the electric frequency of a theoretical equivalent generator that supplies the power system demand, i.e. an equivalent frequency of the system or simply *system's frequency.*

Inertia Emulation Controller. The concept behind the inertia emulation in WECSs is the extraction of kinetic energy from its rotating mass by means of a controller that increases its power output during the first stage of a power imbalance event. To achieve this, the power output of the k-th WECS increases proportionally to the Rate of Change of Frequency (ROCOF) of the power system by adding a power signal P^k_{syn}, which is defined as [Gonzalez-Longatt, 2012, Morren et al., 2006]

$$P^k_{syn} = 2H^k_C \, f_{sys} \frac{df_{sys}}{dt} \tag{3.53}$$

where f_{sys} is the frequency of the system. Note that the ROCOF (df_{sys}/dt) can be simply determined by two consecutive frequency readings at the terminals of each generator [Gonzalez-Longatt, 2012], however, based on the concepts of system frequency and COI described above, in this research f_{COI} is considered to be the frequency of the system ($f_{sys} = f_{COI}$). By this consideration, the ROCOF of the system can be determined with readily available data from the dynamic numerical simulation of the power system.

Figure 3.11 shows the block diagram of the synthetic inertia controller and its connection scheme [Gonzalez-Longatt, 2012, Rahmann et al., 2015]. Note that P_{gen} is the power output from the PMSG and P_{out} is the power injected into the grid.

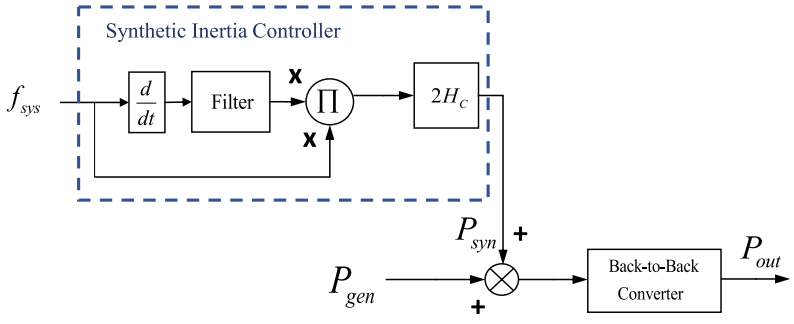

FIGURE 3.11: Scheme of the synthetic inertia controller.

It is adequate to highlight that the consideration of f_{COI} as the system's frequency in the numerical implementation of an inertia controller, is a proposal of the research work described in this thesis.

3.5 Numerical Solution

In general, the power system dynamic behaviour in general is simulated by solving a set of DAE in the following form:

$$\dot{x} = f(x, y), \tag{3.54}$$

$$0 = g(x, y), \tag{3.55}$$

where x represents the set of dynamic state variables and y represents the set of algebraic state variables. Dynamic variables correspond to time-varying modelling devices e.g. synchronous machines. On the other hand, algebraic variables correspond to the nodal power balance equations, i.e. voltage magnitudes and angles. The DAE set can be solved using mainly two approaches [Milano, 2010]:

- "Partitioned-Explicit" (PE) method. Variables x and y are updated sequentially.
- "Simultaneous-Implicit" (SI) method. Variables x and y are solved together in a unified frame of reference.

From a computational solution approach, both methods have advantages and drawbacks. The partitioned approach can be considered faster but less numerically stable than the simultaneous approach [Milano, 2010]. SI method has the advantage of handling stiff equations with no numerical problems and is widely used in commercial grade programs [Sauer and Pai, 1998, van Cutsem and Βουρνάς, 1998]. Due to this convenience, SI method is adopted in this work.

The numerical solution of the DAE set via SI method comprises the following steps:

1. Discretization of the differential equations, commonly using either the Backward-Euler (BE) method or the Trapezoidal Rule (TR).

2. The discretized set of equations is augmented with the set of algebraic equations and solved using the Newton-Raphson (NR) method.

These steps are repeated for each time instant in the simulation interval. The time interval of the simulation is defined by $T \in [t_0, t_f]$. The mathematical expressions that describe the SI method are the following:

$$F_1(\cdot) = x^{k+1} - x^k - h\left(\beta_0 f^{k+1} + \beta_1 f^k\right) = 0, \tag{3.56}$$

$$F_2(\cdot) = g^{k+1} = 0, \tag{3.57}$$

$$\underbrace{\begin{bmatrix} I - h\beta_0 f_x^{k+1} & -h\beta_0 f_y^{k+1} \\ g_x^{k+1} & g_y^{k+1} \end{bmatrix}}_{J} \begin{bmatrix} \Delta x^k \\ \Delta y^k \end{bmatrix} = - \begin{bmatrix} F_1(\cdot) \\ F_2(\cdot) \end{bmatrix}, \tag{3.58}$$

where k indicates the time instant and h is the time step. Equation (3.56) represents the discretization of the dynamic equations, and constants β_0 and β_1 vary according to the following:

- $\beta_0 = 1, \quad \beta_1 = 0$ if discretization is made using the BE method.
- $\beta_0 = \beta_1 = 0.5$ if discretization is carried out via the TR.

Equation (3.57) represents the set of algebraic equations, and (3.58) corresponds to the linearised system of equations to be solved iteratively at each time instant using the NR method, where J is called the Jacobian matrix, with sub-matrices given by

$$\begin{aligned} f_x^{k+1} &= \frac{\partial F_1}{\partial x^{k+1}}, & f_y^{k+1} &= \frac{\partial F_1}{\partial y^{k+1}} \\ g_x^{k+1} &= \frac{\partial F_2}{\partial x^{k+1}}, & g_y^{k+1} &= \frac{\partial F_2}{\partial y^{k+1}} \end{aligned}. \tag{3.59}$$

At each NR iteration the set of variables are updated by

$$\begin{bmatrix} x^{k+1} \\ y^{k+1} \end{bmatrix} = \begin{bmatrix} x^{k} \\ y^{k} \end{bmatrix} + \begin{bmatrix} \Delta x^{k} \\ \Delta y^{k} \end{bmatrix}, \tag{3.60}$$

and at each time instant the NR method starts with the assumption that

$$\begin{bmatrix} x^{k+1} \\ y^{k+1} \end{bmatrix} = \begin{bmatrix} x^{k} \\ y^{k} \end{bmatrix}. \tag{3.61}$$

3.6 Disturbances Simulation

3.6.1 Numerical Considerations

In order to perform a dynamic simulation, the digital program has to be able to compute the disturbance and post-disturbance condition of the system variables. An important aspect to consider is that at the instant of either application or clearing of a disturbance, the dynamic variables cannot change instantaneously. Therefore, at these two instances of time such variables keep constant and their correspondent variations respect to time are considered zero while the algebraic variables suddenly change dynamically. This behaviour can be properly represented by setting the step size to zero ($h = 0$), such that only the set of algebraic equations are solved considering the dynamic variables as fixed inputs at the instant of a disturbance. Thus, at the instant of a disturbance application or clearing, the equation system to be solved is equivalent to a power flow study.

3.6.2 Fault Simulation

An important part of time domain simulations, from a transient stability analysis viewpoint, is the assessment of the electro-mechanical response of power system networks following a large disturbance, such as short circuits [Kundur et al., 1994, Milano, 2010]. Three-phase short circuits can be properly simulated by setting a shunt impedance close to zero at the faulted bus or by setting the corresponding voltage magnitude and angle to zero [Milano, 2010]. In order to avoid convergence

issues, at the instant of application of a fault, NR method has to start with the algebraic variables set to the corresponding fault values. This fault values can be found prior to the dynamic analysis through the following steps [Kothari and Nagrath, 2003]:

1. Perform a load-flow study and obtain the pre-fault bus voltages: $V^0 = |V^0| \angle \theta^0$.
2. Loads are neglected during the fault (Voltages dip very low so that currents drawn by loads can be neglected in comparison to fault currents).
3. The synchronous generators' steady state reactances are substituted by transient reactances. Y^{fault} is obtained by adding generators transient admittances to diagonal elements of original Y_{BUS}. Then make $Z^{fault} = \left(Y^{fault}\right)^{-1}$.
4. For the *i-th* bus, and considering a fault at the *r-th* bus, compute the voltage during the fault by

$$V_i^{fault} = V_i^0 - \left(\frac{Z_{i,r}^{fault}}{Z_{r,r}^{fault}}\right) V_r^0. \tag{3.62}$$

The set of algebraic variables must be then initialized by (3.62) at the instant of application of the fault. As mentioned above, loads are considered zero during the fault application period. At the instant of clearing of the fault, voltage magnitude and angles must be restored to the pre-fault values.

3.7 Conclusions

The dynamic mathematical models of the power system components to be considered in this thesis have been described in this chapter. These models are integrated in a single frame of reference by means of a set of differential-algebraic equations, in order to carry out transient stability analyses. Furthermore, the corresponding numerical solution method for this kind of studies was also described. Lastly, the adopted procedure to perform simulation of disturbances in the power system is described.

Chapter 4

Control devices interaction assessment

During the development of the research work presented in this thesis, novel proposals for the assessment of control interactions in power systems have been implemented. Concerning the steady-state framework, the proposed interaction assessment method is based on the concepts of sensitivity theory and geometrical projections. Regarding the dynamic analysis, two methods are proposed: the first is also based on sensitivity theory and geometrical projections, while the other relies on dynamic sensitivity theory. The proposed interaction assessment approaches have the advantage of requiring fewer steps for the computing of the related indices than those based on the eigenvalue theory, i.e. mode shapes and participation factors. In addition, due to the nature of the computing of the indices based on geometrical projections, the computational burden of the proposals is lower than the typical approaches.

4.1 Steady state interaction assessment

The proposed steady-state interaction assessment method is based on a sensitivity matrix that relates the mismatch equations related to control devices and its associated state variables. In order to obtain this sensitivity matrix is convenient to subdivide the linearised equation system (2.2) as follows:

$$\begin{bmatrix} \mathbf{\Delta S} \\ \mathbf{\Delta Y} \end{bmatrix} = [\mathbf{J}] \begin{bmatrix} \mathbf{\Delta U} \\ \mathbf{\Delta X} \end{bmatrix} = \begin{bmatrix} \mathbf{J_{AC}} & \mathbf{J_{SX}} \\ \mathbf{J_{YU}} & \mathbf{J_{YX}} \end{bmatrix} \begin{bmatrix} \mathbf{\Delta U} \\ \mathbf{\Delta X} \end{bmatrix} \tag{4.1}$$

where:

- $\mathbf{J}$ Full expanded Jacobian matrix.
- $\mathbf{J_{AC}}$ Derivatives of the active and reactive power mismatch equations and AIC mismatch equations with respect to voltage angles, voltage magnitudes, frequency deviation and area power shifts.
- $\mathbf{J_{SX}}$ Derivatives of the active and reactive power mismatch equations and AIC mismatch equations with respect to control devices' state variables.
- $\mathbf{J_{YU}}$ Derivatives of the control mismatch equations with respect to voltage angles, voltage magnitudes, frequency deviation and area power generation shifts.
- $\mathbf{J_{YX}}$ Derivatives of the control mismatch equations with respect to control devices' state variables.

In order to obtain the control sensitivity matrix, which is required for the assessment of the interaction among controllers, let $\mathbf{\Delta S} = 0$, then,

$$\mathbf{\Delta Y} = \left(\mathbf{J_{YX}} - \mathbf{J_{YU}} \mathbf{J_{AC}^{-1}} \mathbf{J_{SX}}\right) \mathbf{\Delta X}, \tag{4.2}$$

$$\mathbf{\Delta Y} = \mathbf{J_C}\ \mathbf{\Delta X}, \tag{4.3}$$

where

$$\mathbf{J_C} = \mathbf{J_{YX}} - \mathbf{J_{YU}} \mathbf{J_{AC}^{-1}} \mathbf{J_{SX}}. \tag{4.4}$$

$\mathbf{J_C}$ is called the power flow control sensitivity matrix or simply control matrix [Filho et al., 2009]. This is a matrix that directly relates the control mismatch equations to the control state variables. In this context, the assumption of $\mathbf{\Delta S} = 0$ permits a better focus on control devices and the reduction of the computational effort [Gao et al., 1992, Filho et al., 2009]. Note that $\mathbf{J_C}$ is not a direct sensitivity matrix: it cannot be used to predict values of variables in another operation point.

As mentioned in Section 2.6.6, the use of typical SVC models do not permit to obtain $\mathbf{J_C}$. This problem arises because the set of linearised mismatch equations (2.2) is not augmented, which in turn causes the corresponding mismatch control equations ($\mathbf{\Delta Y}$) to be null. On the other hand, if the reactive power mismatch equation at the controlled bus is considered as the control mismatch equation, the corresponding sub-matrix $\mathbf{J_{SX}}$ becomes null and the existing relationship among state variables associated with different SVCs cannot be mathematically established. This drawback is overcome by the proposed modelling approach for the SVC in which the linearised set of equations is expanded, such that $\mathbf{\Delta Y}$ is explicitly defined and $\mathbf{J_{SX}}$ is not null.

4.1.1 Steady-state control interaction index

Regarding the steady state operation framework, the main contribution of the research work presented in this thesis is the development of a method for computing an index that identifies, if any, the control devices that present an adverse interaction. This analysis is performed focusing on the matrix $\mathbf{J_C}$.

As reported in [Filho et al., 2009], the singularity of $\mathbf{J_C}$ denotes that two or more rows or columns are linearly dependent, and this situation can occur due to poor control coordination or infeasible control configurations. In this regard, it is important to understand how the control matrix can show coupling or linear dependence scenarios directly related to the control devices variables. For illustration purposes, (4.5) and (4.6) represent trivial cases where control state variables are completely decoupled and coupled, respectively. The column vectors of these matrices are plotted in Figure 4.1. Note that the coupling of the vectors is given by the angle between them. In the completely decoupled case (a) the angle between the vectors is 90°. On the other hand, in the completely coupled case (b) the vectors are collinear and the angle between them is 0°.

$$\mathbf{\Delta Y} = \begin{bmatrix} 1 & 0 & 0 \\ 0 & 2 & 0 \\ 0 & 0 & 1 \end{bmatrix} \mathbf{\Delta X} \tag{4.5}$$

$$\mathbf{\Delta Y} = \begin{bmatrix} 1 & 2 & 1 \\ 1 & 2 & 1 \\ 1 & 2 & 1 \end{bmatrix} \mathbf{\Delta X} \tag{4.6}$$

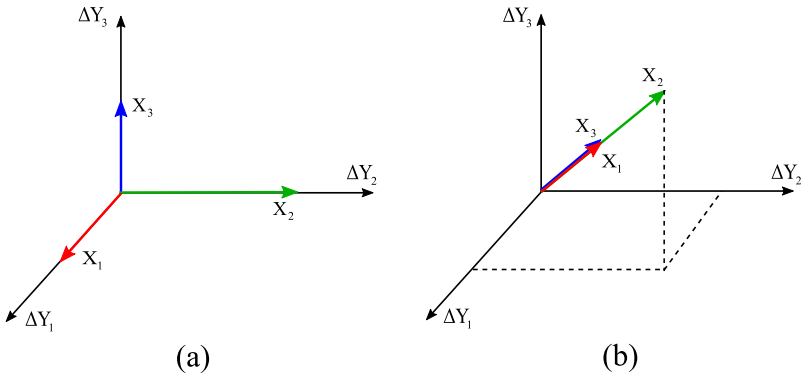

FIGURE 4.1: Coupling scenarios among variables: (a) Completely decoupled control variables. (b) Completely coupled control variables.

Note also that when the vectors are collinear but pointing in opposite directions, the angle between them is 180° and they are still completely coupled. Hence, a measure of coupling between variable vectors can be determined by computing the cosine between them. Based on the mentioned above, a matrix $\mathbf{r}$ can be defined with its elements given by the cosine of the angle between the i-th and j-th column vectors ($\mathbf{X}_i$, $\mathbf{X}_j$) of $\mathbf{J_C}$ as:

$$\mathbf{r}_{ij} = \cos\theta_{\mathbf{X}_i,\mathbf{X}_j} = \frac{\mathbf{X}_i \bullet \mathbf{X}_j}{\|\mathbf{X}_i\| \ \|\mathbf{X}_j\|} \tag{4.7}$$

Note that $\mathbf{r}$ is symmetric and its order, as well as the order of $\mathbf{J_C}$, is given by the number of state variables associated with the control devices. Hence, each element of $\mathbf{r}$ gives a measure of the coupling level between the related state variables and, therefore, their corresponding control devices. Following this line of reasoning, the element (i, j) of $\mathbf{r}$ is a coupling index between the i-th and j-th control state variables.

It has also been documented that coefficients based on geometric measures can provide a relative degree of the linear dependence or coupling among variables [Hamdan and Elabdalla, 1988, Rogers and Overbye, 2009, Rodgers et al., 1984, Freund et al., 2004]. In this regard,the control coupling index matrix $\mathbf{r}$ is symmetrical

with values between -1 and 1 and provides a relative measure of the linear dependence between state variables of the control devices. From this viewpoint, if the index has an absolute value of 1, there is a complete coupling between the two control variables and independent control actions in the devices are not possible. On the other hand, a coupling index with an absolute value of 0 means that control actions of the associated control devices can be performed in a totally independent way.

Another useful information contained in $\mathbf{r}$ is the sign of each of its elements. If a pair of coupled variables respond each other in the same direction, the sign of the associated element of $\mathbf{r}$ is positive. On the other hand, the sign is negative if the associated variables respond each other in opposite directions. Note, however, that $\mathbf{J_C}$ is the input for the computing of $\mathbf{r}$ and the former is not a direct sensitivity matrix, thus, the practical information that can be interpreted from the sign of each element of $\mathbf{r}$ is not accurate unless there are an important coupling amount between the associated control devices. This feature is tested in Section 5.2.2.

4.2 Dynamic interaction assessment

4.2.1 Geometry-based method

Regarding the dynamic operation framework, one of the two proposed approaches to estimate the interaction level among controllers in power systems is based, in similar way as the method described in Section 4.1.1, on the geometrical projections of a control sensitivity matrix. However, in the transient stability frame the formulation is adapted to the DAE set that models the entire power system.

The proposed method for the control interaction assessment is based on the analysis of a reduced matrix obtained from the Jacobian matrix once an operating condition is found for the time t by following the trapezoidal rule or the backward-euler method described in Section 3.5. For this purpose, it is convenient to expand the DAE system given by (3.54) and (3.55) as follows:

$$\dot{x}_\alpha = f_\alpha(x_\alpha, y_\alpha, x_\beta, y_\beta, \rho, \lambda), \tag{4.8}$$

$$\dot{x}_\beta = f_\beta(x_\alpha, y_\alpha, x_\beta, y_\beta, \rho, \lambda), \tag{4.9}$$

$$0 = g_\alpha(x_\alpha, y_\alpha, x_\beta, y_\beta, \rho, \lambda), \tag{4.10}$$

$$0 = g_\beta(x_\alpha, y_\alpha, x_\beta, y_\beta, \rho, \lambda), \tag{4.11}$$

where x_β and y_β are the differential and algebraic state variables, respectively, among which the interaction level is to be assessed, while f_β and g_β are their corresponding differential and algebraic functions. On the other hand, x_α and y_α are the remaining differential and algebraic state variables with their corresponding differential and algebraic functions given by f_α and g_α, respectively. Note that $x = [x_\alpha, x_\beta]$, and $y = [y_\alpha, y_\beta]$. Hence, the difference-algebraic linearised system associated with (4.8-4.11) becomes

$$\underbrace{\begin{bmatrix} J^t_{\alpha\alpha} & J^t_{\alpha\beta} \\ J^t_{\beta\alpha} & J^t_{\beta\beta} \end{bmatrix}^k}_{J^k} \underbrace{\begin{bmatrix} \Delta x_{\alpha,t} \\ \Delta y_{\alpha,t} \\ \Delta x_{\beta,t} \\ \Delta y_{\beta,t} \end{bmatrix}^k}_{\Delta\xi^k} = -\underbrace{\begin{bmatrix} F^t_\alpha(\cdot) + F^{t-\Delta t}_\alpha(\cdot) \\ g^t_\alpha(\cdot) \\ F^t_\beta(\cdot) + F^{t-\Delta t}_\beta(\cdot) \\ g^t_\beta(\cdot) \end{bmatrix}^k}_{\Gamma(\cdot)^k}, \tag{4.12}$$

where

$$J^t_{\alpha\alpha} = \begin{bmatrix} I - \frac{\Delta t}{2} f^{\,t}_{\alpha x_\alpha} & -\frac{\Delta t}{2} f^{\,t}_{\alpha y_\alpha} \\ g^{\,t}_{\alpha x_\alpha} & g^{\,t}_{\alpha y_\alpha} \end{bmatrix}, \tag{4.13}$$

$$J^t_{\alpha\beta} = \begin{bmatrix} I - \frac{\Delta t}{2} f^{\,t}_{\alpha x_\beta} & -\frac{\Delta t}{2} f^{\,t}_{\alpha y_\beta} \\ g^{\,t}_{\alpha x_\beta} & g^{\,t}_{\alpha y_\beta} \end{bmatrix}, \tag{4.14}$$

$$J^t_{\beta\alpha} = \begin{bmatrix} I - \frac{\Delta t}{2} f^{\,t}_{\beta x_\alpha} & -\frac{\Delta t}{2} f^{\,t}_{\beta y_\alpha} \\ g^{\,t}_{\beta x_\alpha} & g^{\,t}_{\beta y_\alpha} \end{bmatrix}, \tag{4.15}$$

$$J^t_{\beta\beta} = \begin{bmatrix} I - \frac{\Delta t}{2} f^{\,t}_{\beta x_\beta} & -\frac{\Delta t}{2} f^{\,t}_{\beta y_\beta} \\ g^{\,t}_{\beta x_\beta} & g^{\,t}_{\beta y_\beta} \end{bmatrix}, \tag{4.16}$$

and

$$
\begin{aligned}
f_{\alpha x_\alpha}^{\ t} &= \left.\frac{\partial f_\alpha(\cdot)}{\partial x_\alpha}\right|_{(x_t,y_t)} & f_{\alpha y_\alpha}^{\ t} &= \left.\frac{\partial f_\alpha(\cdot)}{\partial y_\alpha}\right|_{(x_t,y_t)} \\
g_{\alpha x_\alpha}^{\ t} &= \left.\frac{\partial g_\alpha(\cdot)}{\partial x_\alpha}\right|_{(x_t,y_t)} & g_{\alpha y_\alpha}^{\ t} &= \left.\frac{\partial g_\alpha(\cdot)}{\partial y_\alpha}\right|_{(x_t,y_t)}
\end{aligned}, \tag{4.17}
$$

$$
\begin{aligned}
f_{\alpha x_\beta}^{\ t} &= \left.\frac{\partial f_\alpha(\cdot)}{\partial x_\beta}\right|_{(x_t,y_t)} & f_{\alpha y_\beta}^{\ t} &= \left.\frac{\partial f_\alpha(\cdot)}{\partial y_\beta}\right|_{(x_t,y_t)} \\
g_{\alpha x_\beta}^{\ t} &= \left.\frac{\partial g_\alpha(\cdot)}{\partial x_\beta}\right|_{(x_t,y_t)} & g_{\alpha y_\beta}^{\ t} &= \left.\frac{\partial g_\alpha(\cdot)}{\partial y_\beta}\right|_{(x_t,y_t)}
\end{aligned}, \tag{4.18}
$$

$$
\begin{aligned}
f_{\beta x_\alpha}^{\ t} &= \left.\frac{\partial f_\beta(\cdot)}{\partial x_\alpha}\right|_{(x_t,y_t)} & f_{\beta y_\alpha}^{\ t} &= \left.\frac{\partial f_\beta(\cdot)}{\partial y_\alpha}\right|_{(x_t,y_t)} \\
g_{\beta x_\alpha}^{\ t} &= \left.\frac{\partial g_\beta(\cdot)}{\partial x_\alpha}\right|_{(x_t,y_t)} & g_{\beta y_\alpha}^{\ t} &= \left.\frac{\partial g_\beta(\cdot)}{\partial y_\alpha}\right|_{(x_t,y_t)}
\end{aligned}, \tag{4.19}
$$

$$
\begin{aligned}
f_{\beta x_\beta}^{\ t} &= \left.\frac{\partial f_\beta(\cdot)}{\partial x_\beta}\right|_{(x_t,y_t)} & f_{\beta y_\beta}^{\ t} &= \left.\frac{\partial f_\beta(\cdot)}{\partial y_\beta}\right|_{(x_t,y_t)} \\
g_{\beta x_\beta}^{\ t} &= \left.\frac{\partial g_\beta(\cdot)}{\partial x_\beta}\right|_{(x_t,y_t)} & g_{\beta y_\beta}^{\ t} &= \left.\frac{\partial g_\beta(\cdot)}{\partial y_\beta}\right|_{(x_t,y_t)}
\end{aligned}. \tag{4.20}
$$

Considering that an operating condition has been obtained by means of iteratively solving (4.12) for a time t, i.e. $k = nk$ where nk is the NR iteration at which the convergence criterion is satisfied, the *dynamic control matrix* J_{cs} is derived by considering $F_\alpha^t(\cdot) + F_\alpha^{t-\Delta t}(\cdot) = g_\alpha^t(\cdot) = 0$. Thus, the following holds:

$$
\Gamma_\beta(\cdot)^{nk} = \left(J_{\beta\beta}^t - J_{\beta\alpha}^t \cdot \left(J_{\alpha\alpha}^t\right)^{-1} \cdot J_{\alpha\beta}^t\right) \cdot \Delta\xi_\beta^{nk}, \tag{4.21}
$$

where

$$
J_{cs} = J_{\beta\beta}^t - J_{\beta\alpha}^t \cdot \left(J_{\alpha\alpha}^t\right)^{-1} \cdot J_{\alpha\beta}^t, \tag{4.22}
$$

and

$$
\Gamma_\beta(\cdot)^{nk} = \begin{bmatrix} F_\beta^t(\cdot) + F_\beta^{t-\Delta t}(\cdot) & g_\beta^t(\cdot) \end{bmatrix}^T, \tag{4.23}
$$

$$
\Delta\xi_\beta^{nk} = \begin{bmatrix} \Delta x_{\beta,t} & \Delta y_{\beta,t} \end{bmatrix}^T. \tag{4.24}
$$

The concept behind the computing of the J_{cs} was originally introduced in [Gao et al., 1992] and has been previously used for steady-state applications [Gao et al., 1992, Filho et al., 2009]. For purposes of this research work, however, this reduction

concept is also applied in the dynamic operation framework. The reduced-order matrix J_{cs} directly relates the DAE functions corresponding to control devices to their corresponding state variables, which allows to better focus on the variables of interest.

Dynamic control interaction index. In similar manner as described in Section 4.1.1, an index based on geometric projections of column vectors of matrix J_{cs} can be computed in order to assess the interaction level among control devices from the dynamic point of view. Considering also the exemplification depicted in Figure 4.1, a dynamic control interaction matrix $\mathbf{r}^s$ is formed by the cosine of the angle between the i-th and j-th column vectors $\mathbf{v}_i, \mathbf{v}_j$ of J_{cs}, with its elements given by

$$\mathbf{r}^s_{ij} = \cos\theta^s_{ij} = \frac{\mathbf{v}_i \cdot \mathbf{v}_j}{\|\mathbf{v}_i\| \, \|\mathbf{v}_j\|}. \tag{4.25}$$

The matrix $\mathbf{r}^s$ is obtained once an operating condition is found for a time t. In a dynamic numerical simulation of a period given by $t_0 < T < t_f$, this matrix is obtained at each time step given by the step size h. Note that $\mathbf{r}^s$ is symmetric and its order, as well as the order of J_{cs}, is given by the number of state variables corresponding to the control devices to be analysed. Also, it provides a relative measure of the linear dependence between state variables associated with the control devices; if the index has an absolute value of 1, there is a complete coupling between the dynamic response of two control devices. On the other hand, a null index means that the dynamic response is totally independent. Likewise the sign of the index tells if the coupled variables respond to each other in the same direction (positive) or in opposite directions (negative). This index can provide important information about which controllers can be operated independently and the level of dynamic interaction (negative or positive) among the control devices.

4.2.2 Sensitivity-based method

The proposed sensitivity-based method intents to assess the interaction level between any two state variables in the power system dynamic simulation. These variables can be either explicitly time-dependant or algebraic. A practical numerical

index is obtained and yields a quantification of the interaction level over the entire simulation period. For a time step $h = t_2 - t_1$, and considering the i-th and j-th state variables z_i, z_j, their respective finite difference equations are given by [Boole, 2009]

$$\frac{\Delta z_i}{\Delta t} = \frac{z_i(t_2) - z_i(t_1)}{t_2 - t_1}, \tag{4.26}$$

$$\frac{\Delta z_j}{\Delta t} = \frac{z_j(t_2) - z_j(t_1)}{t_2 - t_1}, \tag{4.27}$$

which correspond to the discrete time derivatives of z_i, z_j. Now, according to the implicit function theorem [Stewart, 2011]

$$\frac{dz_i}{dt} + \frac{dz_i}{dz_j}\ \frac{dz_j}{dt} = 0 \tag{4.28}$$

and considering that $\frac{\Delta z_i}{\Delta t}, \frac{\Delta z_j}{\Delta t}$ represent true numerical fractions, the sensitivity of the i-th state variable with respect to the j-th state variable is given by

$$\frac{dz_i}{dz_j} \approx \frac{z_i(t_1) - z_i(t_2)}{z_j(t_2) - z_j(t_1)}. \tag{4.29}$$

Note that the sensitivity given by (4.29) can be computed by using values of the considered state variables for each consecutive time instant such that this sensitivity is time-dependent or *dynamic*. Now, for a dynamic simulation period $t_0 \leq T \leq t_f$ consisting of nh simulation steps, the average of the absolute values of the sensitivity of the i-th state variable respect to the j-th state variable is given by

$$I_{i,j} = \frac{\sum_{m=t_0}^{t_f} \left|\frac{dz_i}{dz_j}\right|_m}{nh}, \tag{4.30}$$

where $I_{i,j}$ is called the *dynamic sensitivity index*. This sensitivity can be numerically interpreted as the mean amount of variation, along a simulation period, of the i-th state variable respect to the j-th state variable. By using this index it is possible to link any pair of variables during the power system dynamic simulation. Hence, it is

possible to assess the dynamic impact that a certain state variable has on any other. Moreover, since the data used to obtain the proposed index is readily available in each step of the simulation, the required additional computational burden is not considerable.

4.3 Conclusions

In this chapter the proposed approaches for assessing the interaction among control devices are described. Both steady-state and transient stability operation frameworks are considered. Regarding the steady-state framework, a method based on the analysis of the Jacobian matrix is proposed having its theoretical basis on the concepts of sensitivity theory and geometrical projections.

Concerning the dynamic analysis, two approaches are proposed. Having the same conceptual basis as the steady-state proposal, the first of these approaches also relies on the analysis of the Jacobian matrix obtained at each simulation step of a transient stability study. On the other hand, the second proposed method is based on the computing of dynamic numerical sensitivities directly from the state variables' values at each simulation step. Numerical indices are obtained in order to quantify the interaction level among control devices both in the steady-state and dynamic frameworks.

Chapter 5

Case studies and results

5.1 Introduction

In this chapter, numerical simulations and studies are carried out in order to demonstrate the usefulness and applicability of the proposals presented in this thesis. All the static and dynamic mathematical models described in chapters 2 and 3 were implemented on the steady-state and transient stability programs, respectively, which were developed under the Matlab environment. Moreover, the mathematical formulation of the proposals are included in the code implementation in order to perform numerical simulations of large-scale power systems.

At first instance, the proposed method to obtain the interaction levels among control devices in the steady-state framework is tested by means of power flow numerical simulations on various tutorial, benchmark and real-life power systems. The AIC modelling proposed approach and developed models of SVCs are then tested using power flow studies. Finally, the suitability of the dynamic interaction assessment proposals are demonstrated through dynamic simulations on several real-life and benchmark systems.

5.2 Steady-state interaction assessment

In regard to the demonstration of the usefulness and applicability of the steady-state proposals, all the power flow simulations reported in this section are carried on taking into consideration the AFC modelling described in Section 2.4. The maximum mismatch tolerance specified for all simulations are defined as $\varepsilon = 1 \times 10^{-12}$. Lastly, all data related to the systems used in power flow studies are given in Appendix A.

5.2.1 5-bus system test cases

A small 5-bus test system [Stagg and El-Abiad, 1968] is used to demonstrate the applicability of the proposed interaction assessment method under a steady-state operation framework. For this purpose, Figure 5.1 shows the base power flow results of the original network and Table 5.1 shows the bus voltages.

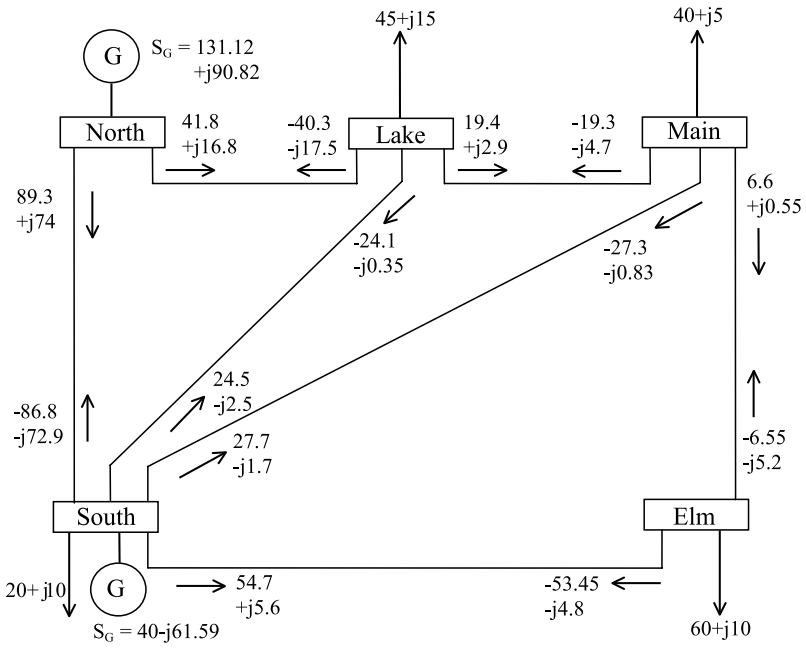

FIGURE 5.1: Base power flows of the 5-bus test system.

Example 1. The original 5-bus system is modified by including a PST and a TCSC (variable susceptance) connected in series, as shown in Figure 5.2. The

TABLE 5.1: Base bus results for the 5-bus test system.

Bus	V(p.u.)	$\theta(^\circ)$
North	1.6	0.00
South	1.000	-2.06
Lake	0.987	-4.64
Main	0.984	-4.96
Elm	0.972	-5.77

generator embedded at bus North is participating in the frequency regulation while bus South is considered a typical PV bus. The parameters of the control devices and their initial conditions are shown in Table 5.2. Furthermore, the control devices were set to control different power flows, from which results evident that both control devices will conflict each other since the Kirchhoff's current law in bus "Lake 1" cannot be satisfied.

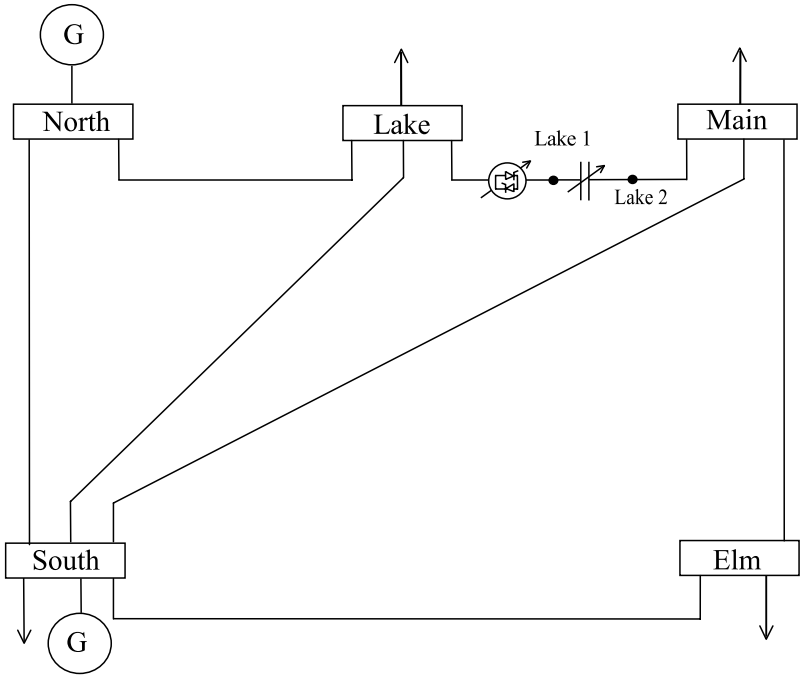

FIGURE 5.2: 5-bus system with power flow controllers connected in series.

TABLE 5.2: FACTS devices' parameters for Example 1.

Device	**Parameters**	**Initial conditions**
PST	$R_p = R_s = 0$, $X_p = X_s = 0.5$, $G_{s0} = B_{s0} = 0$	$T_v = U_v = 1$, $\phi_{Tv} = \phi_{Uv} = 0$
TCSCb	(variable susceptance)	$X = 0.015$ p.u.

The Newton-Raphson algorithm diverges for these conditions, nevertheless, the coupling behaviour of the control devices variables is present from the beginning

of the iterative process. Table 5.3 shows the resulting control and control coupling matrices at the first two iterations of the algorithm. The first and second rows and columns in $\mathbf{J_C}$ and $\mathbf{r}$ correspond to TCSCb and PST respectively.

TABLE 5.3: Control and coupling matrices for Example 1 at the first two iterations.

Iteration	$\mathbf{J_C}$	$\mathbf{r}$
1	$\mathbf{J_C} = \begin{bmatrix} 1.0 & 0.0 \\ 0.0 & -2.53 \end{bmatrix}$	$\mathbf{r} = \begin{bmatrix} 1.0 & 0.0 \\ 0.0 & 1.0 \end{bmatrix}$
2	$\mathbf{J_C} = \begin{bmatrix} -0.08 & -2.46 \\ -0.08 & -2.46 \end{bmatrix}$	$\mathbf{r} = \begin{bmatrix} 1.0 & 1.0 \\ 1.0 & 1.0 \end{bmatrix}$

Note that apparently in the first iteration there is no coupling between the control devices. This is due to the modelling technique used for the TCSCb, in which the mismatch equations are included in the power flow equations after the first iteration [Fuerte-Esquivel, 1997]. In the second iteration is evident that the control matrix columns are linearly dependent and $\mathbf{r}$ shows a complete coupling between the devices. Note that completely coupled control variables can be identified by the proposed index from the beginning of the Newton-Raphson iterative process. Thus, the convergence problems of the power flow algorithm due to existing conflicts in control settings can be spotted independently if the method converges or not.

Example 2. Another case based on the 5-bus system is shown in Figure 5.3, where SVCs are connected at buses "Main" and "Elm". The SVCs are set to control the voltage magnitudes at nodes Main and Elm at 1 p.u. and 0.99 p.u., respectively. In order to perform these control actions, the variable susceptance of both SVCs is initialized at $B = 0.15$ p.u..

The Newton-Raphson method converges in 4 iterations, to an operation point that presents a frequency deviation $\Delta f = -1.89 \times 10^{-3}$ Hz, and the final values of matrices $\mathbf{J_C}$ and $\mathbf{r}$ are presented in Table 5.4. The first and second rows and columns in $\mathbf{J_C}$ and $\mathbf{r}$ correspond to SVCb1 and SVCb2 respectively. Note that matrix $\mathbf{r}$ shows some coupling between the control devices, which does not affect the convergence of the method. In order to demonstrate how the control devices can interact each other in an adverse manner, the reactance and resistance of the transmission line "Main-Elm" are reduced in 80% such that both SVCs are trying to control different voltage magnitudes at buses which are electrically very close. The algorithm still

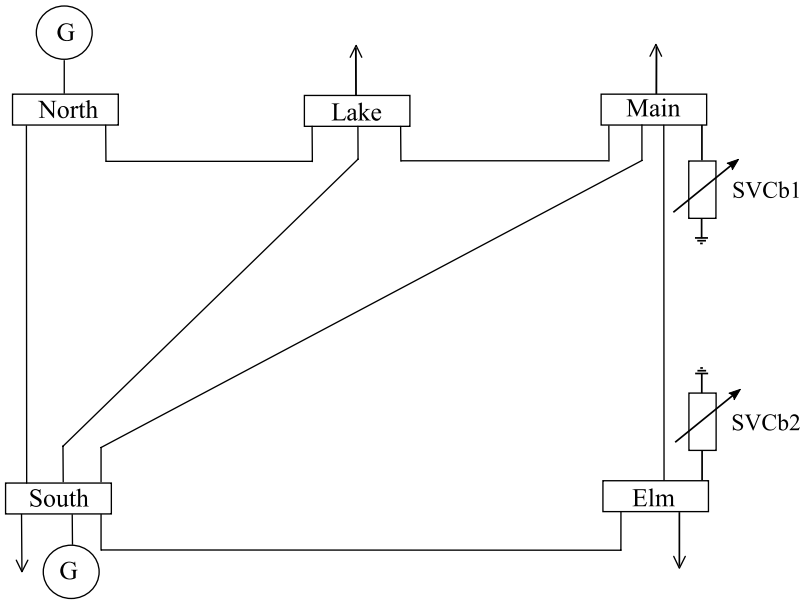

FIGURE 5.3: 5-bus system with a pair of SVCs.

converges for this case with controlled voltage magnitudes at buses Main and Elm, but matrices $\mathbf{J_C}$ and $\mathbf{r}$ result quite different, as shown in Table 5.5.

TABLE 5.4: Control and coupling matrices for Example 2 at the final iteration.

Iteration	$\mathbf{J_C}$	$\mathbf{r}$
1	$\mathbf{J_C} = \begin{bmatrix} 0.005 & 0.001 \\ 0.001 & 0.005 \end{bmatrix}$	$\mathbf{r} = \begin{bmatrix} 1.0 & 0.55 \\ 0.55 & 1.0 \end{bmatrix}$

TABLE 5.5: Control and coupling matrices for Example 2 at the final iteration showing adverse interaction.

Iteration	$\mathbf{J_C}$	$\mathbf{r}$
1	$\mathbf{J_C} = \begin{bmatrix} 0.0142 & -0.0003 \\ -0.0003 & 0.0 \end{bmatrix}$	$\mathbf{r} = \begin{bmatrix} 1.0 & -0.99 \\ -0.99 & 1.0 \end{bmatrix}$

Note that singularity of matrix $\mathbf{J_C}$ is due to the loss of control of SVCb2. This can be seen in the zero value of the diagonal element of $\mathbf{J_C}$ corresponding to SVCb2, meaning that the controlled variable (bus voltage magnitude) of such control device is insensitive to changes in the corresponding control variable. The coupling matrix shows practically a complete coupling between the control devices.

In order to compare the obtained results with an eigenvalue-based method to identify control conflicts [Filho et al., 2009], an eigenvalue analysis is performed for the last case. The eigenvalue vector $\mathbf{\Lambda}$ of $\mathbf{J_C}$ shown in Table 5.5 is the following:

$$\mathbf{\Lambda} = \begin{bmatrix} 0.0142 \\ 9.8 \times 10^{-6} \end{bmatrix}. \tag{5.1}$$

In addition, the modal participation factor matrix $\mathbf{P}$ results as follows:

$$\mathbf{P} = \begin{bmatrix} 0.99 & 0.0006 \\ 0.0006 & 0.99 \end{bmatrix}. \tag{5.2}$$

From (5.1) and (5.2) can be noted that the near-zero eigenvalue denotes a mode close to be unstable [Gao et al., 1992, Filho et al., 2009], and that this mode is associated 99% with SVCb2 and 0.06% with SVCb1. It is important to point out that the proposed matrix $\mathbf{r}$ delivers very good practical results identifying which control devices are causing conflicts. Also, considering the nature of the computing of (5.2), the numerical effort of our proposal is significantly reduced in comparison with the eigen-analysis.

5.2.2 118-bus system test cases

Example 1. With the objective of testing the proposed steady-state interaction assessment methodology in a larger system, a modified 118-bus IEEE test case is analysed in this section.

This system is divided in 9 control areas according to [Zhu et al., 2006], where Area 6 is defined as the reference. Tables 5.6 and 5.7 show the location of FACTS series and shunt controllers, respectively, while the one-line diagram shown in Figure 5.4 schematically indicates the location of the embedded FACTS controllers. Note that FACTS devices controlling power flows are placed as inter-area tie elements with the idea that they interact with the AIC. Furthermore, some FACTS devices are located close each other in order to test the proposed interaction index. Lastly, Table 5.8 shows the data corresponding to the FACTS devices embedded in the network.

For this example, where none of the area interchange powers are being controlled, convergence is achieved in 6 iterations with a frequency deviation $\Delta f = 9.0405 \times 10^{-1}$ Hz.

TABLE 5.6: Series FACTS devices included in the 118-bus system.

From Bus	To Bus	From Area	To Area	FACTS controller
22	23	2	4	TCSCb
30	38	2	3	TCSCfa
70	75	4	5	PST
21	22	2	2	LTC

TABLE 5.7: Shunt FACTS devices included in the 118-bus system.

Bus	FACTS controller
22	SVCb1
70b	SVCb2
30	SVCfa1
48	SVCfa2

TABLE 5.8: Data for FACTS devices included in the 118-bus system (Example 1).

Device	Parameters	Initial conditions	Target values
TCSCb	-	$X_0 = -0.02$ p.u.	$P_{targ} = -45$ MW
TCSCfa	$\alpha_{TCSC} = 145°$	$X_C = 9.365 \times 10^{-3}$ p.u., $X_L = 1.60 \times 10^{-3}$ p.u.	$P_{targ} = 80$ MW
PST	$R_p = R_s = 0$, $X_p = X_s = 0.05$, $G_{s0} = B_{s0} = 0$ p.u.	$T_v = U_v = 1$, $\phi_{Tv} = \phi_{Uv} = 0°$	$P_{targ} = 20$ MW
LTC	$R_p = R_s = 0$, $X_p = X_s = 0.1$, $G_{s0} = B_{s0} = 0$ p.u.	$T_v = U_v = 1$, $\phi_{Tv} = \phi_{Uv} = 0°$	$V_{targ} = 1.02$ p.u.
SVCb1	-	$X_0 = 0.02$ p.u.	$V_{targ} = 1.0$ p.u.
SVCb2	-	$X_0 = 0.02$ p.u.	$V_{targ} = 1.0$ p.u.
SVCfa1	$X_C = 9.365 \times 10^{-3}$ p.u., $X_L = 1.60 \times 10^{-3}$ p.u.	$\alpha_{SVC} = 140°$	$V_{targ} = 1.02$ p.u.
SVCfa2	$X_C = 9.365 \times 10^{-3}$ p.u., $X_L = 1.60 \times 10^{-3}$ p.u.	$\alpha_{SVC} = 140°$	$V_{targ} = 1.02$ p.u.

The resulting coupling matrix **r** is shown in Table 5.9, along with the order of correspondence of the rows and columns with respect to the FACTS devices.

The FACTS controllers have been located with the idea that if the devices are placed topologically close, the coupling among them will be somehow noticeable. Bearing this idea in mind, it is noted from Table 5.9 that some closely installed devices show moderate coupling, this is the case of PST and SVCb2 that are connected to the same bus. A more severe coupling is identified for LTC and SVCb1 that are both connected to Bus 22. This is a way to confirm some expected results from the coupling matrix.

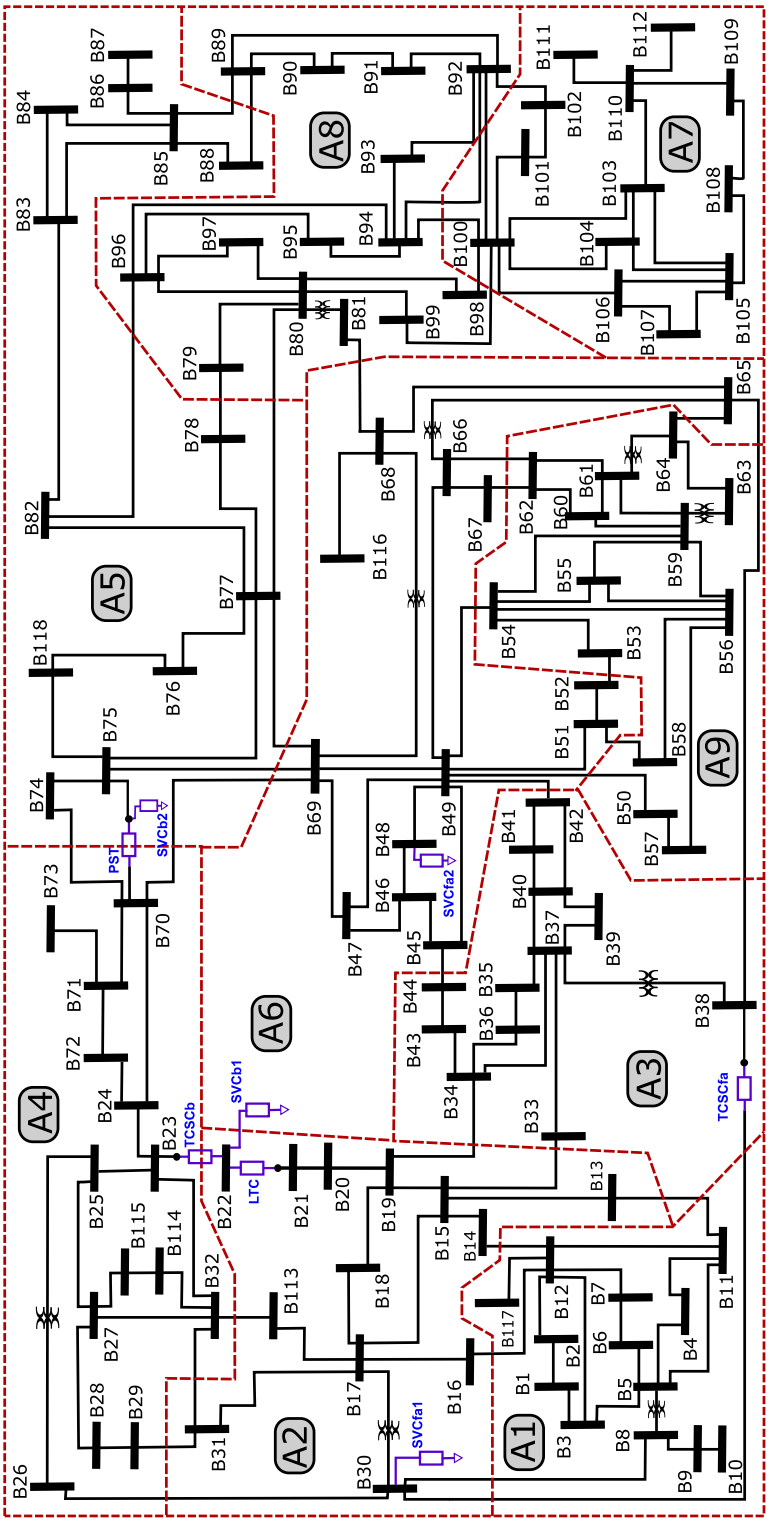

FIGURE 5.4: One-line diagram of the modified 118-bus power system.

TABLE 5.9: Coupling matrix for Example 1 (118-bus system).

Control Device	TCSCb	TCSCfa	PST	SVCb1	SVCb2	SVCfa1	SVCfa2	LTC
TCSCb	1.0000	0.0411	0.0505	-0.2032	-0.0427	-0.0933	-0.0017	0.1711
TCSCfa		1.0000	-0.1366	-0.0026	0.0964	-0.0166	-0.0287	0.0259
PST			1.0000	-0.0040	**-0.8706**	0.0290	0.0025	-0.0012
SVCb1				1.0000	0.0035	0.3069	0.0020	**-0.9101**
SVCb2					1.0000	-0.0193	-0.0015	0.0004
SVCfa1						1.0000	0.0088	-0.3129
SVCfa2							1.0000	-0.0027
LTC								1.0000

Example 2. The same system of Example 1 is considered, but now the power interchanges for Area 3 and 8 are controlled to -395 MW and 470 MW, respectively. Considering these modifications, another power flow study is carried out obtaining convergence after 8 iterations. Frequency deviation results in $\Delta f = 4.7576 \times 10^{-1}$ Hz.

Variables corresponding to power generation shifts of Area 3 and 8 are included in the computing of matrices $\mathbf{J_C}$ and $\mathbf{r}$. Table 5.10 shows the coupling matrix with the new control devices' variables included.

TABLE 5.10: Coupling matrix for Example 2.

Control Device	TCSCb	TCSCfa	PST	SVCb1	SVCb2	SVCfa1	SVCfa2	Area3	Area8	LTC
TCSCb	1.0000	0.0720	0.0537	-0.2457	-0.0467	-0.1080	-0.0020	0.0633	0.0689	0.2075
TCSCfa		1.0000	-0.1002	-0.0092	0.0673	0.0082	-0.0201	**0.4850**	**0.2188**	0.0281
PST			1.0000	-0.0055	-0.8702	0.0714	0.0019	-0.0472	**0.1258**	-0.0010
SVCb1				1.0000	0.0045	0.2237	0.0013	-0.0009	-0.0223	-0.9325
SVCb2					1.0000	-0.0437	-0.0001	0.0304	**-0.1492**	0.0005
SVCfa1						1.0000	0.0184	**-0.4550**	**-0.2382**	-0.2383
SVCfa2							1.0000	-0.0003	-0.0295	-0.0022
Area3								1.0000	0.0545	0.0087
Area8									1.0000	0.0273
LTC										1.0000

This example shows the advantage of the proposed coupling analysis in terms of its application to any state variable of the system. In this context, note that there there exists a noticeable coupling among the control of Area 3, TCSCfa and

SVCfa1, which are the topologically closest devices to the buses belonging to Area 3. Regarding the control of Area 8, there exists a noticeable coupling with PST, SVCb2, TCSCfa and SVCfa1. The application of the proposed coupling index considering control devices and area power interchange can be very useful since directly relates the effect that an adjustment in a controller's parameter would have in the power generation of a certain area and vice-versa.

It should be also noted that the results of coupling indices of matrix **r** do not provide an absolute measure of how close the system is to become unstable due to control devices adverse interactions. As presented in Example 2 for the 5-bus system, there is a direct relationship of a complete coupling behavior among control devices and a near-unstable mode, however, in order to determine the proximity of the system to instability, the controlled variables of control devices should be brought closer or farther away in order to obtain a coupling index with an absolute value near to 1, this is how close the control matrix would be to become singular due to the corresponding interaction. This concept is similar to that reported in [Gao et al., 1992].

Example 3. The same 118-bus system of Example 1 is considered again with the purpose of numerically showing the meaning of the proposed interaction index sign. In order to cause more evident interaction levels among the controllers, the voltage target values of LTC and SVCb1 have been changed to 0.99 p.u. and 1.05 p.u., respectively. The coupling (or interaction) index matrix **r** resulting from the numerical simulation with this conditions is shown in Table 5.11. Note that, according to the highlighted values, there is an important coupling or interaction level among some variables associated with FACTS devices

As mentioned in Section 4.1.1, the sign of an element of **r** indicates if the associated variables respond each other in the same or opposites directions. In order to validate this statement, a series of numerical simulations are carried out for different values of the active power demanded at Bus 106 with the purpose of showing how the variable associated with each control device changes. In this case, PL_{106} is varied from 30MW to 60MW with an increase of 10MW in each simulation. The values corresponding to the state variables of each FACTS control device are shown in Table 5.12.

TABLE 5.11: Coupling matrix for Example 3.

Control Device	TCSCb	TCSCfa	PST	SVCb1	SVCb2	SVCfa1	SVCfa2	LTC
TCSCb	1.0000	0.0445	0.0200	**-0.9498**	-0.0175	-0.2822	-0.0031	**0.7824**
TCSCfa		1.0000	-0.1366	0.0192	0.0964	-0.0047	-0.0287	0.0379
PST			1.0000	-0.0058	**-0.8706**	0.0289	0.0026	-0.0010
SVCb1				1.0000	0.0043	0.2802	0.0013	**-0.8482**
SVCb2					1.0000	-0.0192	-0.0015	-0.0001
SVCfa1						1.0000	0.0087	-0.3018
SVCfa2							1.0000	-0.0030
LTC								1.0000

TABLE 5.12: FACTS devices' variables values for variations in PL_{106} (Example 3).

Device	Variable	PL_{106} (MW)			
		30	40	50	60
TCSCb	B (p.u.)	-0.0521	-0.0536	-0.0551	-0.0567
TCSCfa	α (°)	144.7642	144.8812	145.0213	145.1910
PST	ϕ (°)	-4.1354	-4.0504	-3.9643	-3.8769
SVCb1	B (p.u.)	0.5897	0.5940	0.5986	0.6032
SVCb2	B (p.u.)	0.3009	0.3005	0.3000	0.2995
SVCfa1	α (°)	136.3887	136.3763	136.3649	136.3544
SVCfa2	α (°)	136.0130	136.0130	136.0130	136.0130
LTC	T_U	1.0141	1.0139	1.0138	1.0137

Figure 5.5 shows the resulting values of the state variables associated with TCSCb (a) and SVCb1(b) with respect to each increase in PL_{106}. As can be observed, as one variable increases, the other decreases. This opposite relation is indicated by the sign of the corresponding interaction index relating these control devices shown in Table 5.11 (-0.9498). The same relation holds in case of the interaction between PST and SVCb2, whose state variables values are plotted in Figure 5.6 and have an index value of -0.8706. A negative interaction index with a value of -0.8482 also occurs in the case of LTC and SVCb1, whose state variables' values are plotted in Figure 5.7. On the other hand, in case of the interaction between LTC and TCSb, the positive index value of 0.7824 denotes that the corresponding variable's values change in the same direction as shown in Figure 5.8.

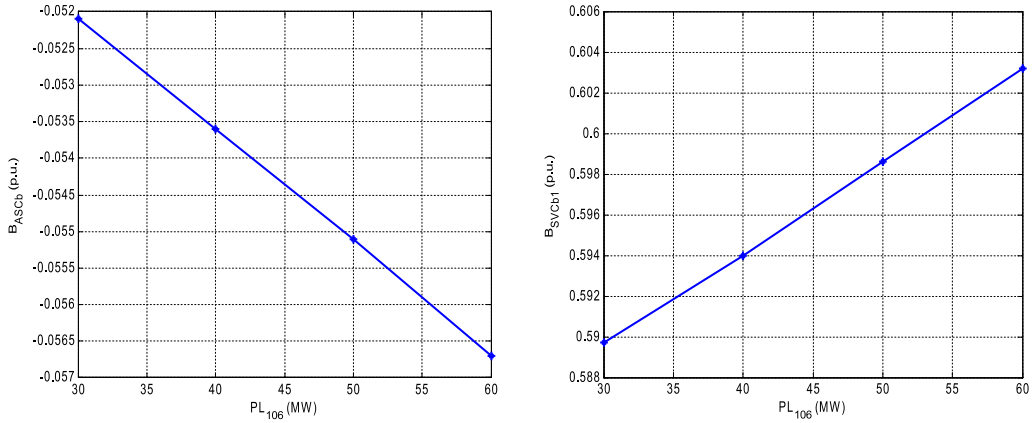

FIGURE 5.5: Resulting values of state variables corresponding to TCSCb (a) and SVCb1(b) for each load increase in PL_{106}.

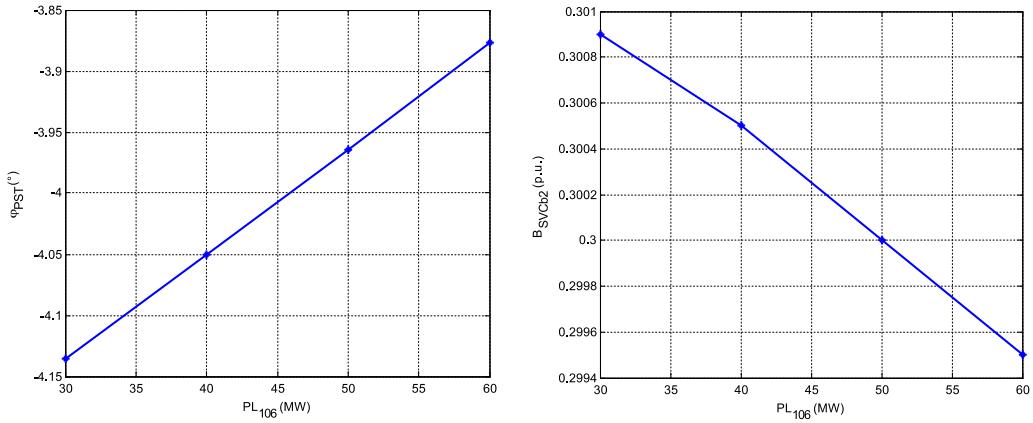

FIGURE 5.6: Resulting values of state variables corresponding to PST (a) and SVCb2(b) for each load increase in PL_{106}.

Note that, for small interaction indices' values is not possible to establish a relationship between devices' variables given by the sign of the corresponding index. An example of this limitation is given by observing the values of the the variables associated with TCSCb and PST, and the related interaction index. This is because $\mathbf{J_C}$ is not a "direct" sensitivity matrix, as mentioned in Section 4.1.

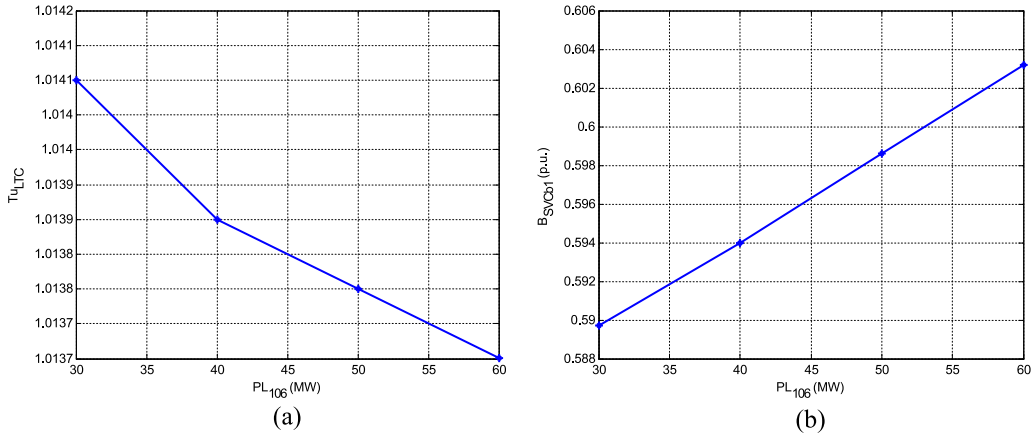

FIGURE 5.7: Resulting values of state variables corresponding to LTC (a) and SVCb1(b) for each load increase in PL_{106}.

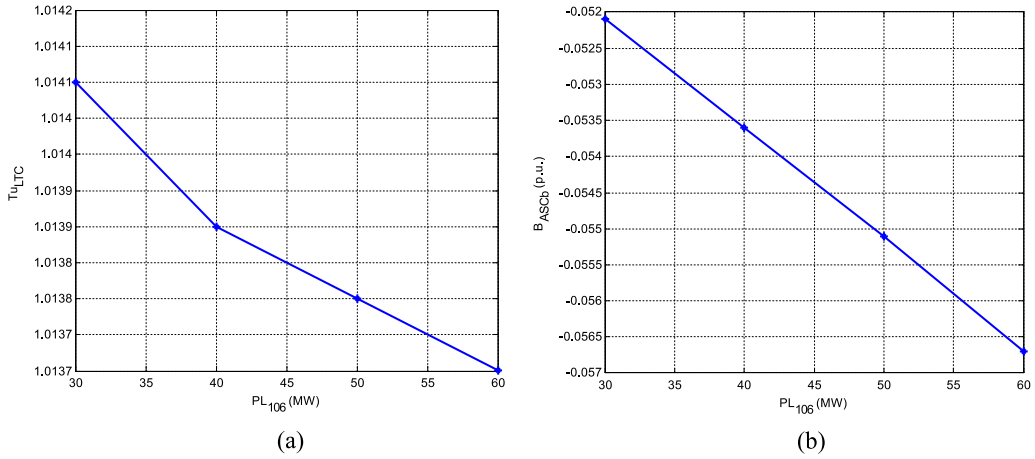

FIGURE 5.8: Resulting values of state variables corresponding to LTC (a) and TCSCb(b) for each load increase in PL_{106}.

5.3 Proposed control models

5.3.1 AIC model

The proposed AIC model presented in Section 2.5 has been incorporated into a power flow program and its suitability has been tested in a modified IEEE 118 bus test case. This system has been sub-divided in 9 control areas, as described in [Zhu et al., 2006], where Area 6 is defined as the reference. Table 5.13 shows the base and target power interchanges for each area, where the former were obtained from a base power flow study and the latter correspond to a random ±10% area power

interchange deviation from the base case. For each controlled area, all its active generators have been considered as regulators with equal participation factors.

Numerical simulations have been performed for the base case and considering the AIC with target values listed in Table 5.13. The maximum mismatches resulting at each iteration are reported in Table 5.14 for a mismatch tolerance of 10^{-12}. Note that the quadratic convergence characteristic is maintained in both simulations and all target interchange values were met.

TABLE 5.13: Base and target area power interchanges.

Area	**Base power interchange** PI_i^{base} (MW)	**Target power interchange** PI_i^{sch} (MW)
1	135.0376	121.53
2	-375.0197	-337.52
3	-401.0762	(not controlled)
4	215.1893	236.71
5	-528.9522	-476.06
6	994.2497	(reference)
7	-50.7137	-55.79
8	448.6535	493.52
9	-399.0883	-359.18

TABLE 5.14: Maximum mismatch values.

Iteration	**Base Case**	**AIC Case**
1	8.25E-01	7.82E-01
2	1.35E-02	3.51E-02
3	4.18E-03	8.73E-05
4	3.89E-07	6.42E-10
5	1.14E-13	1.14E-13

Table 5.15 shows active power output of each generator at Area 9 for both study cases. Note that each regulating generator increases its active power generation in the same proportion in order to meet the AIC target value.

Lastly, and in order to show the suitability of the proposed approach for handling active power flow limits in tie-lines, another numerical simulation is carried out considering the maximum power transfers on tie-lines connecting buses 26-30 and

TABLE 5.15: Active power generation of Area 9 for Base and AIC cases.

Generator at Bus #	**Base case Pg_k^b (MW)**	**AIC case Pg_k (MW)**	$Pg_k - Pg_k^b$ **(MW)**
54	48	61.2077	13.2077
59	155	168.2077	13.2077
61	160	173.2077	13.2077
TOTAL	**363**	**402.6231**	**39.6231**

81-68 at 235 MW and 77 MW, respectively. Tables 5.16 and 5.17 report the active power flows through all tie-lines associated with areas 4 and 8, respectively, for the AIC case with and without considering the tie-line power flow limits. The active power outputs of regulating generators in control areas 4 and 8 are shown in Table 5.18 for these study cases. These results clearly show that the AIC targets are also accomplished in the case of considering tie-line limits. Also note that the tie-lines power flow constraining causes that the proportions of generator outputs specified by equal AIC participation factors are no longer met.

TABLE 5.16: Power flows of tie-lines of Area 4.

From bus	**To bus**	**From Area**	**To Area**	**AIC (MW)**	**AIC (with line limits, MW)**
23	22	4	2	55.7306	56.7178
29	31	4	2	-15.7104	-14.8876
26	30	4	2	239.9333	**235**
32	31	4	2	13.4671	14.632
32	113	4	2	11.2863	12.6057
70	74	4	5	17.1251	17.1008
70	75	4	5	1.009	0.9793
70	69	4	6	-86.1328	-85.4398
Total PI from area 4 (MWs)				**236.7082**	**236.7082**

TABLE 5.17: Power flows of tie-lines of Area 8.

From bus	To bus	From Area	To Area	AIC (MW)	AIC (with line limits, MW)
79	78	8	5	31.8062	26.2306
89	85	8	5	63.7555	78.5733
89	88	8	5	91.7378	106.3178
80	77	8	5	162.5851	144.9486
96	82	8	5	3.9707	0.7813
81	68	8	6	81.5832	**77**
98	100	8	7	-13.6146	-28.1107
99	100	8	7	-30.9452	-45.4174
94	100	8	7	10.4772	16.2042
92	100	8	7	39.5293	51.9891
92	102	8	7	52.6337	65.0021
Total PI from area 8 (MWs)				**493.5189**	**493.5189**

TABLE 5.18: Active power generations of Areas 4 and 8.

Generator at Bus #	Area #	Base Pg_k^b (MW)	AIC Pg_k (MW)	AIC (with line limits) Pg_k (MW)
25	4	220	231.0685	279.4232
26	4	314	325.0685	277.2312
80	8	477	501.0935	421.4755
89	8	607	631.0935	716.9605

5.3.2 SVC models

In order to demonstrate the suitability of the proposed SVC models presented in Sections 2.6.6 and 2.6.7, numerical simulations are performed in a real-life power network consisting of 166 buses, 108 transmission lines and 128 transformers [Aboytes and Arroyo, 1986]. In order to improve the voltage magnitude profile along the network, three SVCs are embedded in key locations of the network aiming to control bus voltage magnitudes at 1 p.u. The SVCs parameters are

given in [Ambriz-Perez et al., 2000]. Two power flow studies are performed for each one of the two cases defined in this section. The first case considers the typical SVCs' models described in [Ambriz-Perez et al., 2000]: the SVC total susceptance model and the SVC firing angle model, where the SVCs' state variables directly replace the associated controlled voltage magnitudes in the formulation of the power flow problem without using control mismatch equations. The second study case considers the proposed SVC power flow models. Table 5.19 shows the maximum mismatch values obtained during the iterative solution process for each study case considering a maximum tolerance of 10^{-12} for all mismatch equations. On the other hand, the same final values of SVCs' equivalent reactance required to achieve the specified voltage control were obtained for all SVC models, i.e. those proposed in [Ambriz-Perez et al., 2000] and the ones proposed in the theses, as reported in Table 5.20.

TABLE 5.19: Maximum mismatch values.

Iteration	**Study case I (SVC models [Ambriz-Perez et al., 2000])**	**Study case II (Proposed models)**
1	3.22E-01	3.18E-01
2	2.41E-02	2.39E-02
3	4.32E-05	4.30E-05
4	1.24E-10	1.25E-10
5	1.71E-13	1.14E-13

TABLE 5.20: Final SVCs' susceptance values.

SVC	**Study Cases I and II**		
	Variable Susceptance Model	**Firing Angle Model**	
	$B_{sh}(p.u.)$	$\alpha(^\circ)$	$B_{sh}(p.u.)$
SVC1	0.2378	136.038	0.2378
SVC2	0.0848	136.016	0.0848
SVC3	0.1709	136.028	0.1709

These results show that the formulated approach retains Newton's quadratic convergence while producing exactly the same results when compared with the typical models.

5.4 Dynamic interaction assessment

In order to validate the proposed approach for the dynamic interaction assessment, several dynamic simulations are performed considering a base operating point provided by a power flow solution. The steady-state data of each power system are given in Appendix A, while the dynamic data of each analysed system are given in Appendix B. The ω_{COI} reference frame has been adopted in all dynamic simulations, which are performed with an integration step size of $h = 0.001$ s and a base frequency of $f_0 = 60$ Hz.

5.4.1 Geometry-based approach

14-bus system, Example 1. The proposed control interaction assessment approach in the dynamic framework is numerically illustrated on a modified IEEE 5-machine, 14-bus system as shown in Figure 5.9. The active power in this system is generated by machines embedded at Buses 1 and 2; the other machines are synchronous condensers. All conventional synchronous generators have AVRs type IEEE-DC1A [IEEE Committee, 2006], and the generator connected to Bus 1 has also a steam driven turbine with tandem compound, single reheat configuration [IEEE Committee, 1973]. The synchronous generator originally embedded at bus 2 has been replaced by an equivalent 40 MW Type-4 WECS. The period of the time-domain simulation is defined by $t_{end} = 25$ s with an integration step time of 0.001 s.

The proposed approach is applied to assess the level of dynamic interaction between the terminal voltage controllers when a disconnection of the transmission line connecting buses 2-4 occurs at time $t = 1$ s. The topological proximity of generators embedded at buses 1 and 2 implies that a high interaction level is expected between the voltage controllers of these machines, i.e. the AVR of the synchronous generator and the grid side controller of the Type-4 WECS. Table 5.21 shows the dynamic interaction indices given by the elements of matrix $\mathbf{r}^s$ at the end of the first step size of the simulation. The state variables considered for the computing of $\mathbf{r}^s$ are those associated with the AVR of Bus 1 as well as the grid-side controller of the WECS connected to Bus 2. The order of correspondence of rows and columns of $\mathbf{r}^s$ is also shown in this Table.

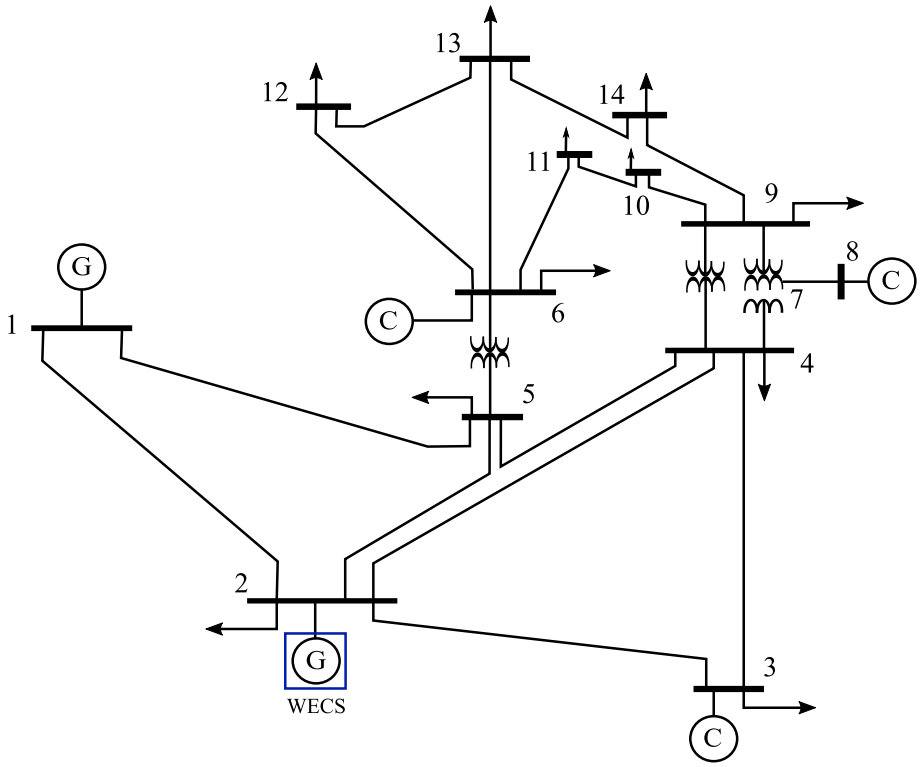

FIGURE 5.9: Modified IEEE 14-bus system .

TABLE 5.21: Dynamic interaction indices at time $t = 0.001$ s, 14-bus system, Example 1.

	V_r	R_f	E_{fd}	X_1	X_2	X_3	X_4	X_5	X_6	X_7	v_{cd}
V_r	1.0000	0.9993	0.3010	0.0000	0.0000	0.0000	-0.9527	-0.9539	**0.9948**	0.9948	0.5154
R_f		1.0000	0.3342	0.0000	0.0000	0.0000	-0.9532	-0.9544	0.9954	0.9954	0.5156
E_{fd}			1.0000	-0.0021	0.0000	0.0000	-0.3249	-0.3254	0.3348	0.3348	
X_1				1.0000	0.0151	0.0000	0.0292	0.0292	-0.0093	-0.0093	-0.0840
X_2					1.0000	0.0000	0.0002	0.0002	-0.0001	-0.0001	-0.0005
X_3						1.0000	0.0000	0.0000	0.0000	0.0000	0.0000
X_4							1.0000	0.9987	-0.9773	-0.9773	-0.7463
X_5								1.0000	-0.9785	-0.9785	-0.7477
X_6									1.0000	1.0000	0.5949
X_7										1.0000	0.5949
v_{cd}											1.0000

As can be noted from Table 5.21, the largest value of $\mathbf{r}^s$ relating both control devices, correspond to state variables V_r and X_6, which are directly associated with the first blocks of the AVR and the WECS' grid-side voltage controller, respectively. As mentioned above, this large interaction index value is due to the electrical

proximity between Buses 1 ans 2. Figure 5.10 shows the plot of the dynamic interaction index relating V_r and X_6 along the entire simulation period. Note that the value presents a minor variation during the period and this is the same case for the other indices contained in $\mathbf{r}^s$.

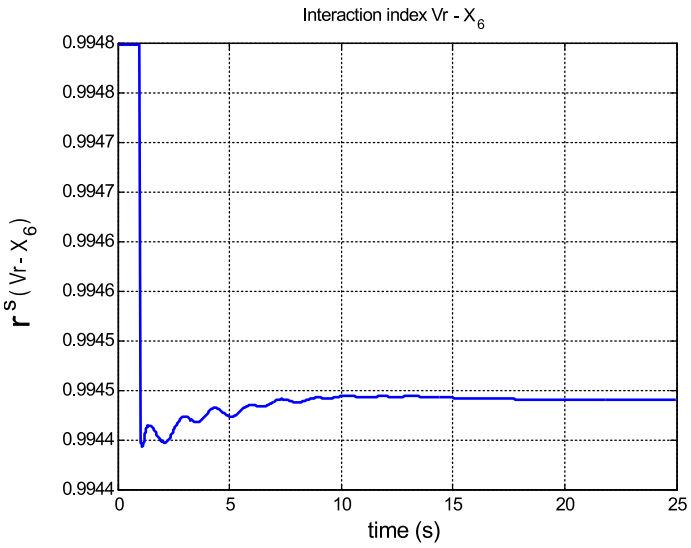

FIGURE 5.10: Dynamic interaction index for V_r-X_6, 14-bus system, Example 1.

Figure 5.11 shows the voltage magnitude profiles for Bus 1 (a) and 2 (b) during the simulation period. It becomes apparent that the oscillation frequency in both signals is very similar, so as the duration of the oscillation.

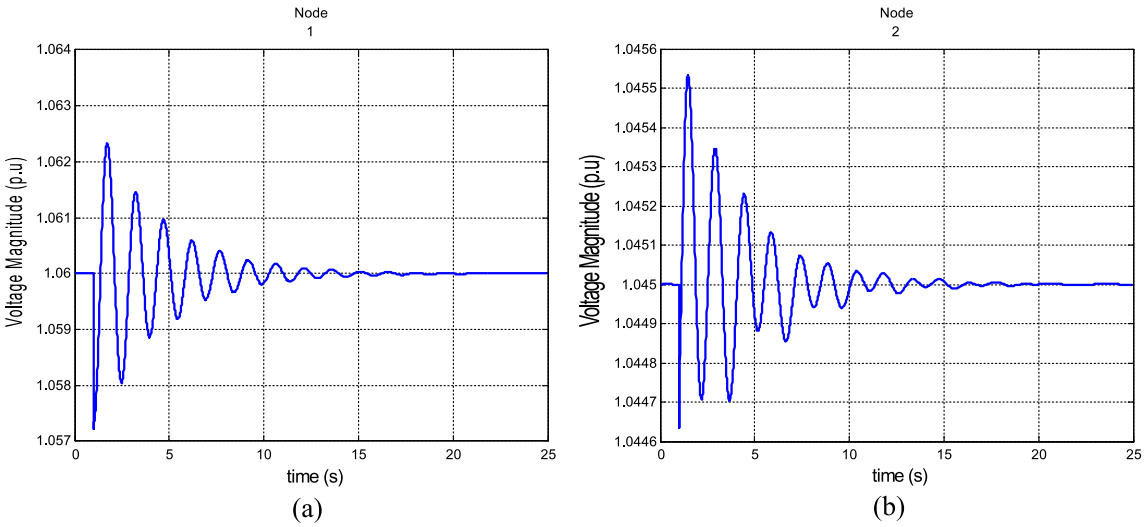

FIGURE 5.11: Voltage profiles for Buses 1 and 2, 14-bus system, Example 1.

14-bus system, Example 2. This example is identical to Example 1, except that the gain parameter of AVR of the machine is changed to a lower value (from $K_a = 200$ to $K_a = 5$, see Section 3.3.1). Table 5.22 shows the dynamic interaction indices given by the elements of matrix $\mathbf{r}^s$ at the end of the first step size of the simulation. The dynamic interaction index that relates the same variables as in Example 1 is plotted in Figure 5.12. The voltage profiles of Buses 1 and 2 are also shown in Figure 5.13.

TABLE 5.22: Dynamic interaction indices at time $t = 0.001$ s, 14-bus system, Example 2.

	V_r	R_f	E_{fd}	X_1	X_2	X_3	X_4	X_5	X_6	X_7	v_{cd}
V_r	1.0000	0.9276	-0.0256	0.0000	0.0000	0.0000	-0.0786	-0.0797	**0.2528**	0.2528	0.0150
R_f		1.0000	0.0088	0.0000	0.0000	0.0000	-0.0730	-0.0740	0.2348	0.2348	0.0140
E_{fd}	-		1.0000	-0.0022	0.0000	0.0000	-0.0228	-0.0231	0.0241	0.0241	0.0226
X_1				1.0000	0.0151	0.0000	0.0963	0.0977	-0.0948	-0.0948	-0.0980
X_2					1.0000	0.0000	0.0006	0.0006	-0.0006	-0.0006	-0.0006
X_3						1.0000	0.0000	0.0000	0.0000	0.0000	0.0000
X_4							1.0000	0.9854	-0.9703	-0.9702	-0.9820
X_5								1.0000	-0.9845	-0.9845	-0.9977
X_6									1.0000	1.0000	0.9711
X_7										1.0000	0.9710
v_{cd}											1.0000

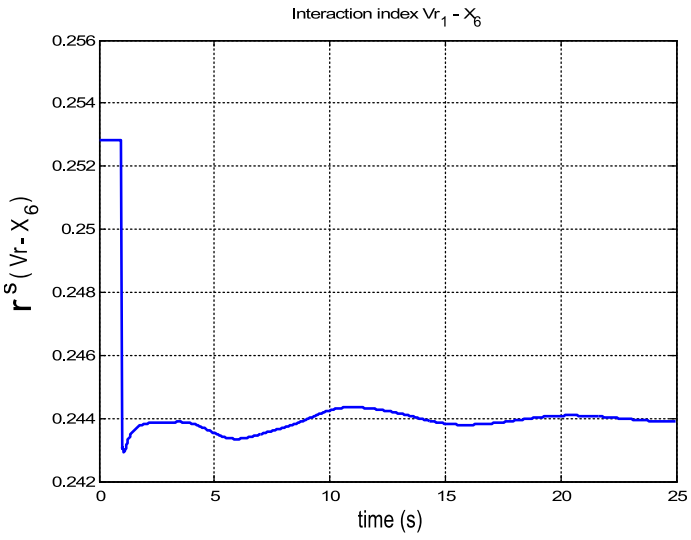

FIGURE 5.12: Dynamic interaction index for V_r-X_6, 14-bus system, Example 2.

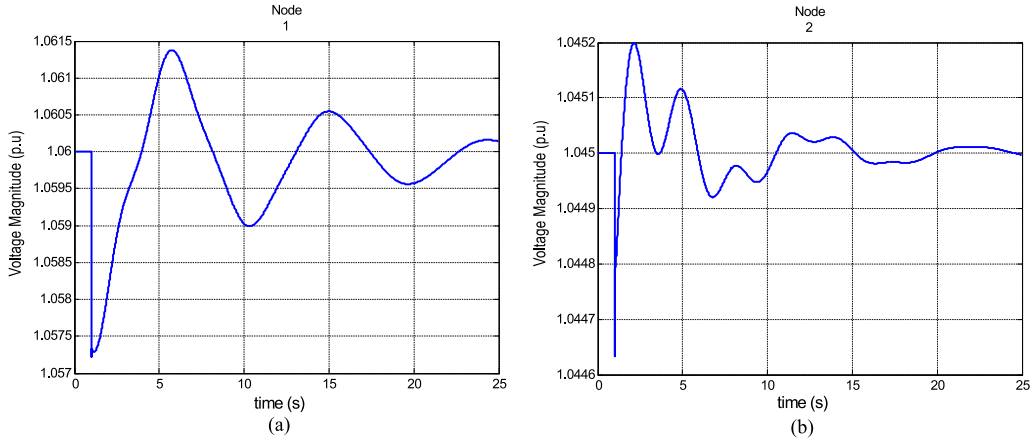

FIGURE 5.13: Voltage profiles for Buses 1 and 2, 14-bus system, Example 2.

Note that, opposite from Example 1, the voltage profiles of Bus 1 and 2 are rather different from each other in terms of frequency and duration of the oscillations. This coincide with a noticeably lower interaction index between the voltage controllers' variables. Hence, the more similar the dynamic response is, the closer the index value is to 1. This can give a guide of the interaction or coupling level of state variables and therefore of the associated control devices. Also, it can be noted that the coupling indices present little variation along the simulation period, hence, the interaction behaviour involving topological or control tuning issues can be spotted from the first simulation steps.

190-bus system, Example 1. The proposed dynamic interaction assessment methodology is also demonstrated on a 46-machine, 190-bus reduced-order model of the Mexican interconnected system described in [Messina et al., 2002]. The experiment is similar to Example 1: an equivalent WECS replaces the synchronous machine originally embedded at Bus 38. A dynamic simulation is carried out considering the time period $0 < T < 12$ s and the outage of the line connecting Buses 115 and 120 at time $t = 1$ s. The interaction index is computed for AVRs of synchronous machines connected at Buses 1, 4, 18, 39 and 42, and for the generator side and grid-side controller of the WECS. Figure 5.14 shows an one-line diagram of the 190-bus system highlighting the analysed buses.

Table 5.23 reports the computed matrix of dynamic interaction indices at the first simulation step considering the above-mentioned control devices. The order of

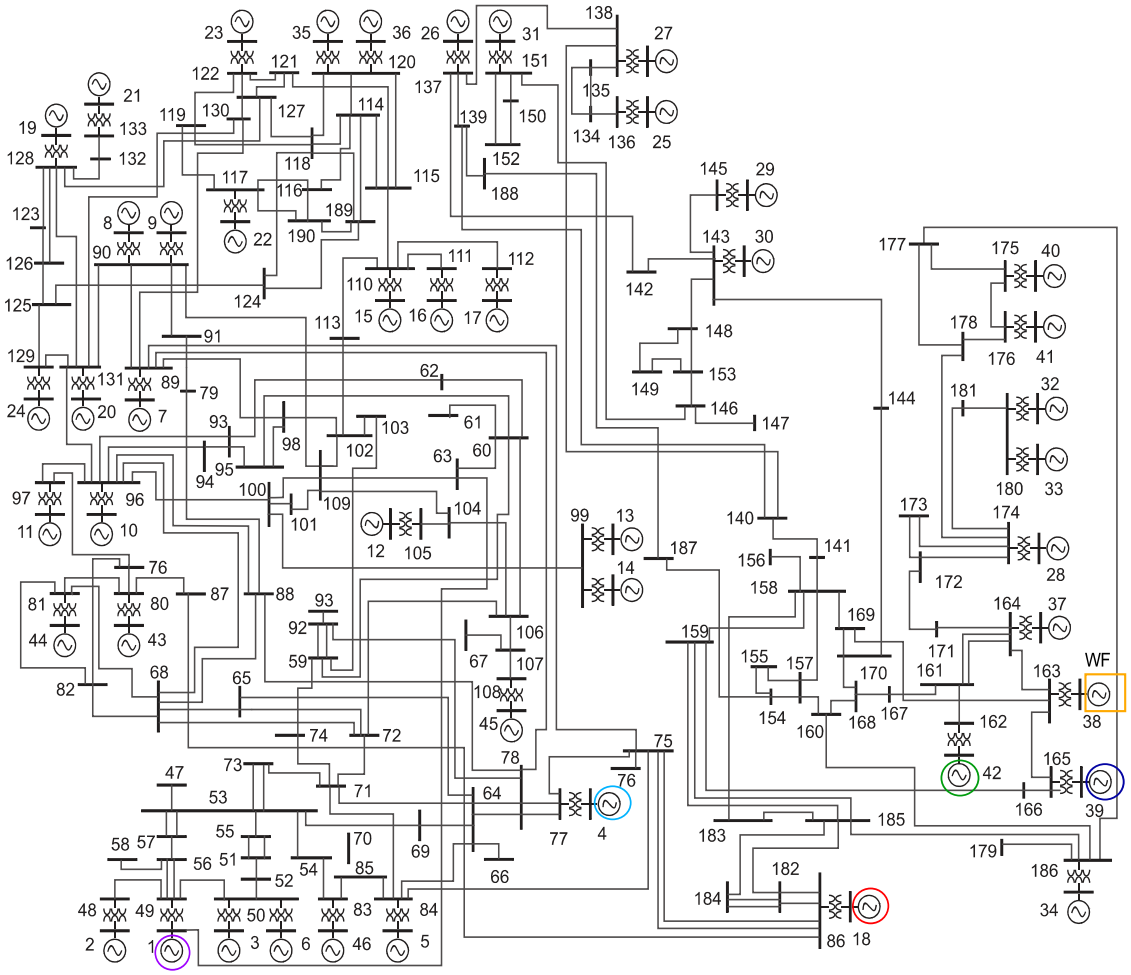

FIGURE 5.14: Equivalent 190-bus Mexican interconnected system.

correspondence of rows and columns is the same as in Table 5.22 and the highlighted elements correspond to the interaction indices of X_6 with respect to V_r for each AVR. As can be noted, the values of interaction indices relating V_r for each selected machine and X_6 for the WECS vary according to the topological location of each corresponding bus, i.e., the closer the location, the larger the value of the associated interaction index. Note that, although these can be seen as expected results, the electrical distance among controllers could not be easily detected or quantified especially if considering large-scale systems.

Figure 5.15 shows the plot of the dynamic interaction index relating V_r for each selected synchronous machine and X_6 along the entire simulation period. Note that, due to the used scale for the vertical axis in Figure 5.15, apparently the coupling

indices appear to be time-invariant, however, Figure 5.16 clearly shows that the index x_6/avr_{39} varies with time, although the variation is minimal. Similar dynamic behaviour applies for all other computed indices.

Lastly, the voltage magnitude of buses 1, 38 and 9 are plotted in Figure 5.17. Note that the same behaviour of Example 2 for the 14-bus system is observed, i. e., the most "coupled" signals are related to the associated interaction index with the largest absolute value.

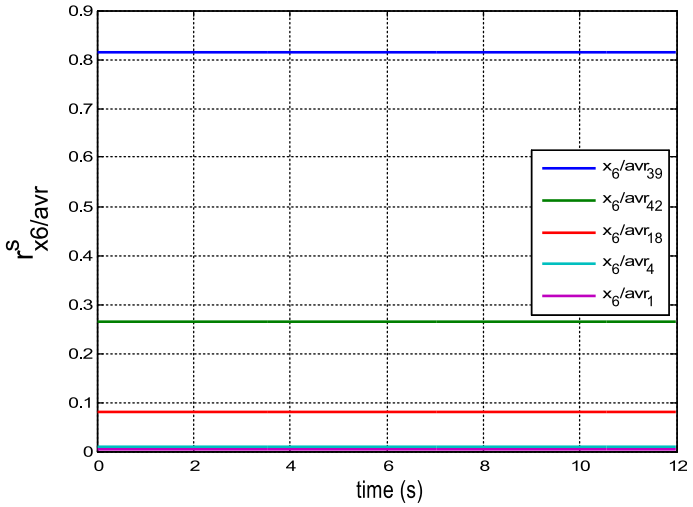

FIGURE 5.15: Dynamic interaction indices for V_r-X_6 for selected machines, 190-bus system, Example 1.

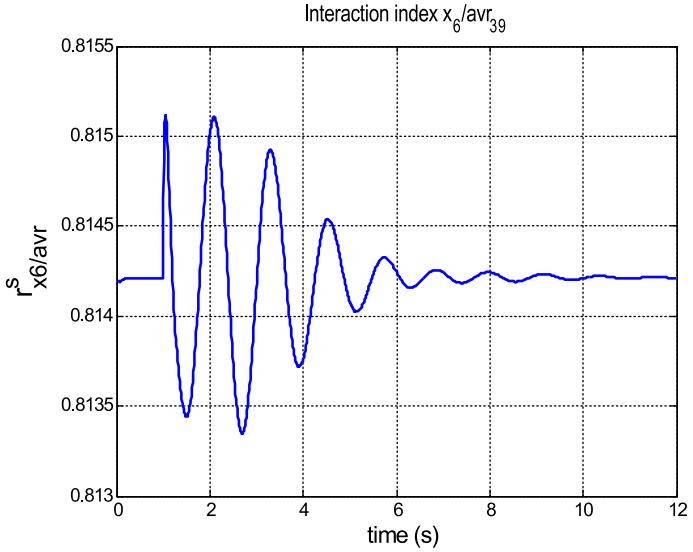

FIGURE 5.16: Dynamic interaction index x_6/avr_{39}, 190-bus system, Example 1.

TABLE 5.23: Dynamic interaction indices at time $t = 0.001$ s, 190-bus system, Example 1.

		AVR_{39}		AVR_{42}		AVR_{18}		AVR_4		AVR_1		$WECS$										
		1.0000	0.9998	0.3220	0.0000	0.0000	0.0000	0.0201	0.0000	0.0000	0.0120	0.0000	0.0030	0.0000	0.0000	0.0000	0.1188	0.1227	**0.8142**	0.8201	-0.0165
AVR_{39}			1.0000	0.3298	0.0000	0.0000	0.0000	0.0201	0.0000	0.0000	0.0120	0.0000	0.0030	0.0000	0.0000	0.0000	0.1188	0.1227	0.8141	0.8200	-0.0165
				1.0000	0.0496	0.0083	0.0083	0.0087	0.0007	0.0048	0.0005	0.0005	0.0013	-0.0322	-0.0004	0.0000	0.0048	0.0049	0.3013	0.3035	0.0325
					1.0000	0.9987	0.0540	0.0044	0.0083	0.0073	0.0044	0.0007	0.0000	0.0000	0.0000	0.0000	0.0280	0.0289	**0.2654**	0.2673	-0.0039
AVR_{42}					1.0000	0.0622	0.0000	0.0073	0.0000	0.0044	0.0044	0.0000	0.0011	0.0000	0.0000	0.0000	0.0280	0.0289	0.2651	0.2670	-0.0039
						1.0000	0.0004	0.0006	0.0000	0.0003	0.0003	0.0000	0.0001	-0.0009	0.0000	0.0000	0.0013	0.0013	0.0202	0.0204	0.0007
AVR_{18}						1.0000	0.9996	0.1732	0.0000	0.0442	0.0442	0.0000	0.0118	0.0000	0.0000	0.0000	0.0840	0.0868	**0.0805**	0.0811	-0.0116
							1.0000	0.1810	0.0000	0.0442	0.0442	0.0000	0.0118	0.0000	0.0000	0.0000	0.0840	0.0868	0.0805	0.0811	-0.0116
								1.0000	0.0083	0.0093	0.0093	0.0033	0.0028	-0.0045	-0.0001	0.0000	0.0128	0.0132	0.0356	0.0358	0.0028
AVR_4									1.0000	0.9987	0.1109	0.0000	0.0065	0.0000	0.0000	0.0000	0.0095	0.0098	**0.0082**	0.0082	-0.0013
										1.0000	0.1190	0.0000	0.0065	0.0000	0.0000	0.0000	0.0095	0.0098	0.0081	0.0082	-0.0013
											1.0000	0.0099	0.0029	-0.0027	0.0000	0.0000	0.0034	0.0035	0.0171	0.0172	0.0023
AVR_1												1.0000	0.1543	0.0000	0.0000	0.0000	0.0028	0.0029	**0.0040**	0.0041	-0.0004
												1.0000	0.1616	0.0000	0.0000	0.0000	0.0028	0.0029	0.0040	0.0041	-0.0004
													1.0000	-0.0007	0.0000	0.0000	0.0011	0.0012	0.0048	0.0048	0.0005
$WECS$														1.0000	0.0164	0.0000	0.8071	0.8334	-0.4177	-0.4207	-0.8434
															1.0000	0.0000	0.0094	0.0097	-0.0049	-0.0049	-0.0098
																1.0000	0.0000	0.0000	0.0000	0.0000	0.0000
																	1.0000	0.9679	-0.3626	-0.3652	-0.9574
																		1.0000	-0.3745	-0.3772	-0.9908
																			1.0000	0.9923	0.4796
																				1.0000	0.4831
																					1.0000

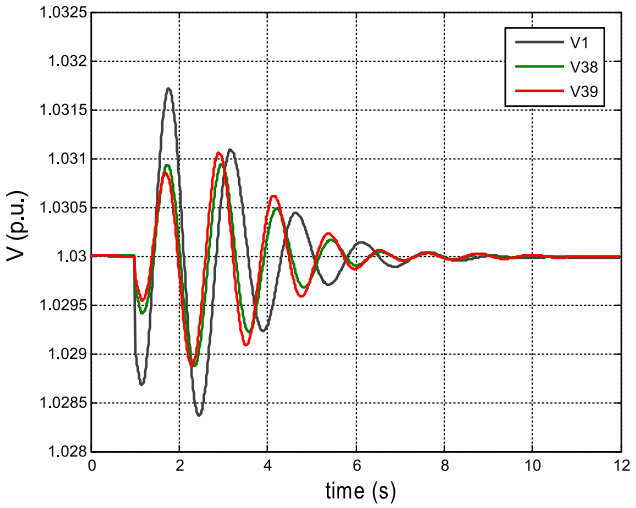

FIGURE 5.17: Voltage magnitudes for buses 1, 38 and 39, 190-bus system, Example 1.

190-bus system, Example 2. The purpose of this example is to show the application of the proposed approach in the dynamic framework for identifying groups of coherent generators in a power system. Coherent generators can be identified for having the same dynamic response in their swing angles in the presence of a certain disturbance in the system [Alsafih and Dunn, 2010]. Figure 5.18 depicts an example of this behaviour considering the oscillation of four generetors angles when subjected to a disturbance [Agrawal and Thukaram, 2011].

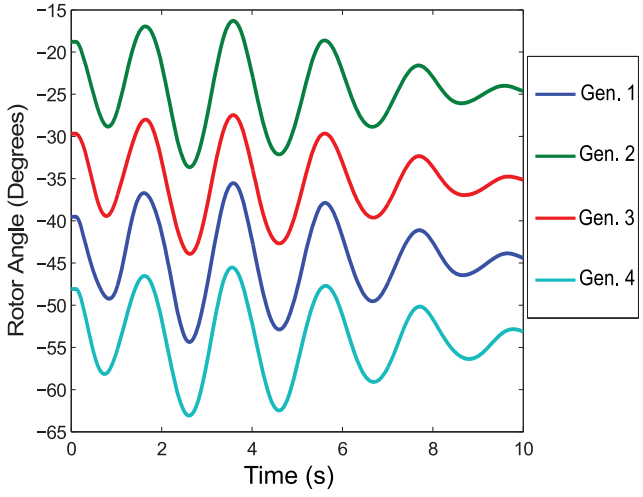

FIGURE 5.18: Example of a coherent group o generators.

To show the applicability of the author's proposal to identify coherent generators, the same Mexican 190-bus system of Example 1 is considered, but with the difference that all generators are defined as synchronous machines. A dynamic simulation is carried out considering a solid three-phase short circuit on Bus 75 occurring at time $t_f = 1$ s, which is liberated by the outage of the line connecting buses 75 and 84 at time $t_l = 1.15$ s. The time period of the simulation is given by $0 < T < 12$ s. By observing Figure 5.14, 6 clusters of generators are identified as being potentially coherent: Generators (3, 6), (8, 9), (13, 14), (32, 33) and (35, 36). Table 5.24 show the dynamic interaction index at the first simulation step obtained by taking into account the internal angles (δ) of each selected generator.

As indicated by the highlighted values of Table 5.24, the elements with largest absolute values are the associated with the angles of the pairs of possible coherent generators, however, those values are very small in magnitude and the association with the coherency between two generators could not be easily noted. With the idea of increasing the link among the angles of the generators, new dynamic interaction indices are computed by considering also the angular speed of each selected machine. As can be observed from the absolute value of the highlighted elements from Table 5.25, the new computed indices show in a more clear manner the high dynamic interaction level or coupling among the selected pairs of generators confirming the coherent behaviour between them.

TABLE 5.24: Dynamic interaction indices of δ at time $t = 0.001$ s for selected generators.

	δ_3	δ_6	δ_8	δ_9	δ_{13}	δ_{14}	δ_{32}	δ_{33}	δ_{35}	δ_{36}
δ_3	1.00000	**-0.00671**	-0.00027	-0.00069	-0.00020	-0.00011	-0.00002	-0.00004	-0.00008	-0.00005
δ_6		1.00000	-0.00006	-0.00031	-0.00003	0.00000	0.00004	0.00003	0.00002	0.00004
δ_8			1.00000	**-0.00391**	-0.00053	-0.00020	0.00002	0.00001	-0.00018	-0.00017
δ_9				1.00000	-0.00151	-0.00065	-0.00002	-0.00004	-0.00048	-0.00044
δ_{13}					1.00000	**-0.00325**	0.00002	0.00001	-0.00018	-0.00018
δ_{14}						1.00000	0.00002	0.00001	-0.00007	-0.00006
δ_{32}							1.00000	**-0.00804**	0.00000	-0.00001
δ_{33}								1.00000	-0.00002	-0.00003
δ_{35}									1.00000	**-0.01044**
δ_{36}										1.00000

Figure 5.19 show the plots of the internal angles corresponding to each pair of selected generators. As can be noted by visual inspection, the level of coherency

TABLE 5.25: Dynamic interaction indices of δ and ω at time $t = 0.001$ s for selected generators.

	δ_3	δ_6	δ_8	δ_9	δ_{13}	δ_{14}	δ_{32}	δ_{33}	δ_{35}	δ_{36}	ω_3	ω_6	ω_8	ω_9	ω_{13}	ω_{14}	ω_{32}	ω_{33}	ω_{35}	ω_{36}
δ_3	1.0000	**-0.4320**	-0.0137	-0.0073	-0.0109	-0.0334	-0.0065	0.0046	0.0023	0.0034	0.6640	-0.4266	-0.0220	-0.0184	-0.0282	-0.0465	-0.0162	-0.0091	0.0052	0.0055
δ_6		1.0000	-0.0093	-0.0204	-0.0060	-0.0106	-0.0022	0.0011	-0.0036	-0.0021	-0.1230	0.8464	-0.0100	-0.0169	-0.0097	-0.0138	-0.0073	-0.0069	-0.0102	-0.0078
δ_8			1.0000	**-0.2182**	-0.0326	-0.0230	-0.0016	0.0009	-0.0089	-0.0082	-0.0140	-0.0094	0.7554	-0.0933	-0.0366	-0.0298	-0.0051	-0.0045	-0.0102	-0.0090
δ_9				1.0000	-0.0789	-0.0655	-0.0044	0.0033	-0.0080	-0.0082	-0.0046	-0.0212	-0.2064	0.7684	-0.1097	-0.0928	-0.0106	-0.0052	-0.0060	-0.0068
δ_{13}					1.0000	**-0.2863**	-0.0011	0.0006	-0.0097	-0.0097	-0.0083	-0.0054	-0.0187	-0.0254	0.8018	-0.2461	-0.0034	-0.0029	-0.0065	-0.0062
δ_{14}						1.0000	-0.0011	-0.0003	-0.0149	-0.0127	-0.0516	-0.0138	-0.0158	-0.0386	-0.1192	0.7931	-0.0078	-0.0118	-0.0324	-0.0264
δ_{32}							1.0000	**-0.4787**	-0.0025	-0.0020	-0.0133	-0.0036	-0.0029	-0.0082	-0.0018	-0.0015	0.6161	-0.3600	-0.0082	-0.0066
δ_{33}								1.0000	0.0017	0.0014	0.0090	0.0020	0.0016	0.0056	0.0006	-0.0005	-0.5267	0.4304	0.0056	0.0045
δ_{35}									1.0000	**-0.4823**	-0.0001	-0.0046	-0.0133	-0.0133	-0.0184	-0.0214	-0.0064	-0.0039	0.6645	-0.3872
δ_{36}										1.0000	0.0008	-0.0031	-0.0107	-0.0101	-0.0161	-0.0179	-0.0052	-0.0032	-0.2930	0.7334
ω_3											1.0000	-0.0207	-0.0166	-0.0008	-0.0286	-0.0684	-0.0352	-0.0227	-0.0011	-0.0006
ω_6												1.0000	-0.0081	-0.0127	-0.0091	-0.0173	-0.0114	-0.0100	-0.0128	-0.0102
ω_8													1.0000	-0.0102	-0.0074	-0.0143	-0.0093	-0.0081	-0.0102	-0.0082
ω_9														1.0000	-0.0177	-0.0425	-0.0218	-0.0140	-0.0002	0.0000
ω_{13}															1.0000	-0.0080	-0.0075	-0.0086	-0.0178	-0.0143
ω_{14}																1.0000	-0.0104	-0.0158	-0.0425	-0.0343
ω_{32}																	1.0000	-0.0108	-0.0218	-0.0176
ω_{33}																		1.0000	-0.0140	-0.0113
ω_{35}																			1.0000	-0.0001
ω_{36}																				1.0000

between the generators is directly related to the magnitude of the corresponding coupling or interaction index; moreover, it can be observed that the highest absolute value of the interaction index between generators' angles is equal to 0.4823 and is associated with δ_{35} and δ_{36}. It results evident from Figure 5.19 that generators 35 and 36 are the most coherent pair. It can be noted also that the lower the absolute value of the interaction index, the lower the coherency between the associated generators. Moreover, note that the proposed approach can make the identification from the first step of the dynamic simulation.

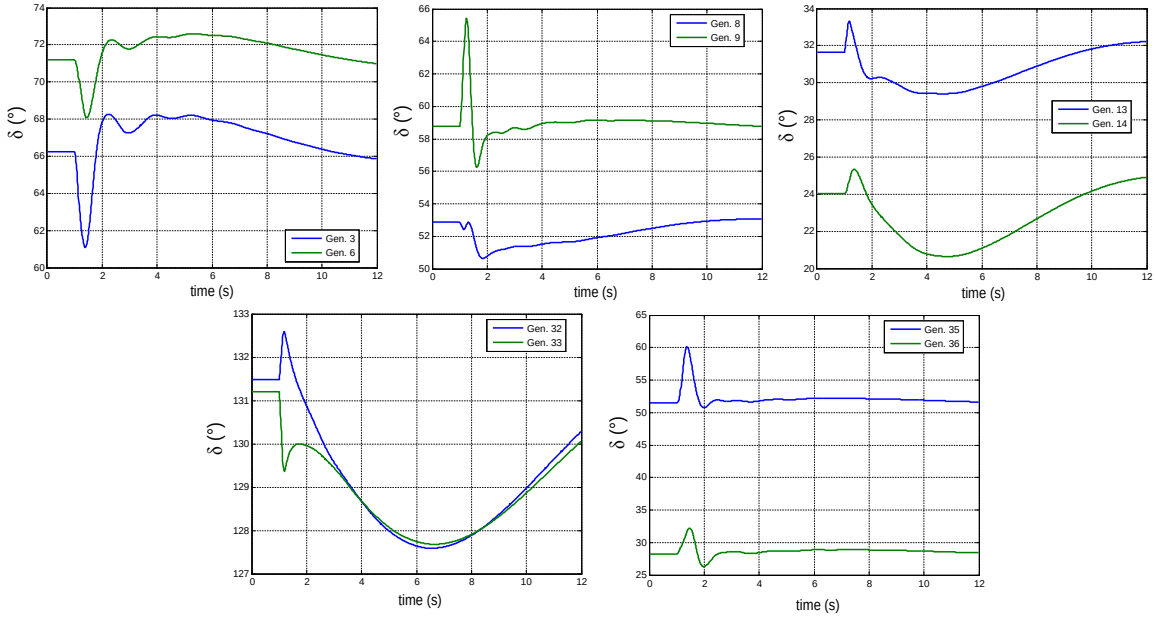

FIGURE 5.19: Selected generators' internal angles.

190-bus system, Example 3. This example is similar to Example 2 but now a solid three-phase short circuit is applied at Bus 86 at time $t = 1$ s, which is cleared out by tripping the line 86-182 at time $t = 1.7$ s . This disturbance causes an angular instability in the power system and the internal angles (δ) of synchronous machines oscillate in such a way that the set of generators divide into two coherent groups. This behaviour is depicted in Figure 5.20 where the angles of all machines are plotted for the first 10 seconds of the simulation.

Since coherency of generators is clearly affected by the disturbance, a change is expected on the indices computed in Example 2 and shown in Table 5.25. In order to apply the proposed interaction index to identify the coherent groups after

the disturbance, it is necessary to compute the same interaction indices a time-step after the disturbance is cleared. The matrix containing the interaction indices related to generators' angles is computed taking into account the generators' angular speeds as well and is shown in Tables 5.26 and 5.27. Although this matrix is symmetric, is full shown so the 2 groups of interaction can be observed. From Tables 5.26 and 5.27, the two groups of coherent generators can be clearly identified from the rows (or columns): the non-zero elements correspond to generators of one group and the zero values correspond to generators of the other coherent group. Hence, the generators related to increasing angles are 1-24, 35, 36 and 43-46, while the group of generators with decreasing angles are 25-34 and 37-43. The angles of those groups of generators are plotted separately and shown in Figure 5.21. Note that the identification of groups of coherent generators can be conducted in a single iteration step.

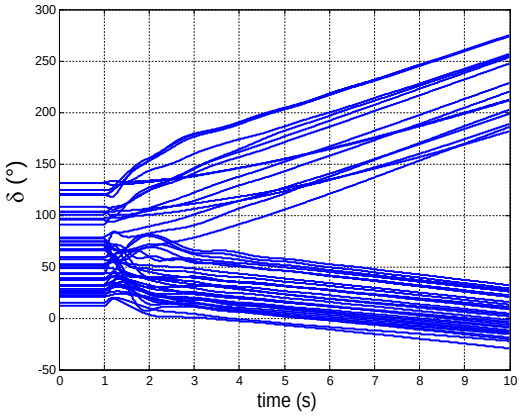

FIGURE 5.20: Internal angles of generators (190-bus system).

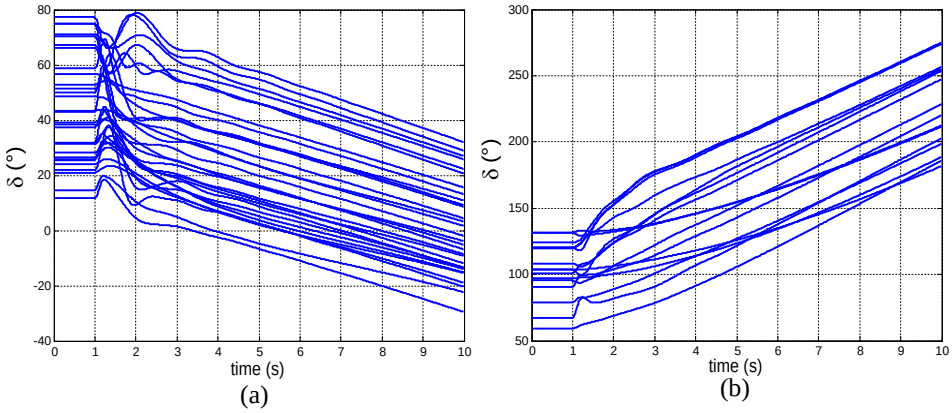

FIGURE 5.21: Internal angles of generators (a): 1-24, 35, 36, 43-46 and (b): 25-34, 37-42 (190-bus system).

TABLE 5.26: Interaction indices of δ at time $t = 1.171$ s for generators 24-46.

δ_{24}	δ_{25}	δ_{26}	δ_{27}	δ_{28}	δ_{29}	δ_{30}	δ_{31}	δ_{32}	δ_{33}	δ_{34}	δ_{35}	δ_{36}	δ_{37}	δ_{38}	δ_{39}	δ_{40}	δ_{41}	δ_{42}	δ_{43}	δ_{44}	δ_{45}	δ_{46}
0.0083	0	0	0	0	0	0	0	0	0	0	0.0049	0.0042	0	0	0	0	0	0	-0.0096	-0.0074	0.0134	-0.0009
0.0036	0	0	0	0	0	0	0	0	0	0	0.0019	0.0019	0	0	0	0	0	0	-0.0055	-0.0049	0.005	-0.0041
0.0074	0	0	0	0	0	0	0	0	0	0	0.0045	0.0037	0	0	0	0	0	0	-0.0107	-0.0096	0.0089	-0.0087
0.0257	0	0	0	0	0	0	0	0	0	0	0.0177	0.0135	0	0	0	0	0	0	-0.1203	-0.0689	0.0284	0.0029
0.0156	0	0	0	0	0	0	0	0	0	0	0.0118	0.0082	0	0	0	0	0	0	-0.0499	-0.0328	0.0154	-0.0385
0.0003	0	0	0	0	0	0	0	0	0	0	0.0001	0.0004	0	0	0	0	0	0	-0.0051	-0.0065	-0.0046	-0.0155
0.0055	0	0	0	0	0	0	0	0	0	0	0.0043	0.0028	0	0	0	0	0	0	-0.0245	-0.0229	-0.0115	-0.0077
0.0005	0	0	0	0	0	0	0	0	0	0	0.0012	0.0001	0	0	0	0	0	0	-0.0109	-0.0111	-0.0082	-0.0048
0.0182	0	0	0	0	0	0	0	0	0	0	0.0134	0.01	0	0	0	0	0	0	-0.026	-0.0215	0.0069	0.0012
-0.0024	0	0	0	0	0	0	0	0	0	0	-0.0004	-0.0014	0	0	0	0	0	0	-0.0338	-0.0455	-0.0424	-0.0181
-0.0027	0	0	0	0	0	0	0	0	0	0	-0.0019	-0.002	0	0	0	0	0	0	-0.0449	-0.0395	-0.0157	-0.0121
-0.0046	0	0	0	0	0	0	0	0	0	0	-0.0041	-0.0047	0	0	0	0	0	0	-0.0078	-0.0113	-0.0614	-0.0111
-0.0027	0	0	0	0	0	0	0	0	0	0	-0.0022	-0.0027	0	0	0	0	0	0	-0.0102	-0.0134	-0.0229	-0.0089
-0.0049	0	0	0	0	0	0	0	0	0	0	-0.004	-0.0039	0	0	0	0	0	0	-0.0058	-0.0088	-0.0203	-0.0082
0.0234	0	0	0	0	0	0	0	0	0	0	0.0094	0.0004	0	0	0	0	0	0	-0.0069	-0.0036	0.0154	0.0063
-0.0015	0	0	0	0	0	0	0	0	0	0	-0.0152	-0.0148	0	0	0	0	0	0	-0.0036	-0.0036	-0.0032	-0.0015
-0.0033	0	0	0	0	0	0	0	0	0	0	-0.0175	-0.017	0	0	0	0	0	0	-0.0036	-0.0039	-0.0046	-0.0022
0.0073	0	0	0	0	0	0	0	0	0	0	0.0049	0.004	0	0	0	0	0	0	-0.0972	-0.0575	0.0071	-0.0053
0.0436	0	0	0	0	0	0	0	0	0	0	0.0407	0.0144	0	0	0	0	0	0	-0.0037	0.0006	0.0227	0.0096
-0.13	0	0	0	0	0	0	0	0	0	0	-0.0443	-0.0372	0	0	0	0	0	0	-0.0073	-0.0106	-0.0211	-0.0107
-0.0734	0	0	0	0	0	0	0	0	0	0	-0.0547	-0.0502	0	0	0	0	0	0	-0.0025	-0.0037	-0.0086	-0.0049
-0.0579	0	0	0	0	0	0	0	0	0	0	-0.1216	-0.1079	0	0	0	0	0	0	-0.0015	-0.0013	0.0002	-0.0003
-0.0059	0	0	0	0	0	0	0	0	0	0	-0.0254	-0.0283	0	0	0	0	0	0	-0.0013	-0.0007	0.0026	0.0009
1	0	0	0	0	0	0	0	0	0	0	0.0114	-0.0028	0	0	0	0	0	0	-0.0015	0.0007	0.0112	0.0048
0	1	-0.0091	-0.0909	-0.0249	0.005	-0.029	0.0182	0.0101	0.0081	0.0122	0	0	0.0169	0.0067	0.0277	0.02	0.0048	-0.01	0	0	0	0
0	-0.0091	1	-0.1573	-0.051	0.0082	-0.0729	0.0378	0.0205	0.0165	0.0191	0	0	0.0318	0.0112	0.048	0.0398	0.0097	-0.0193	0	0	0	0
0	-0.0909	-0.1573	1	-0.077	-0.0006	-0.1215	0.03	0.0297	0.024	-0.0323	0	0	0.0235	-0.02	0.0068	0.0509	0.0113	-0.0329	0	0	0	0
0	-0.0249	-0.051	-0.077	1	-0.0188	-0.0297	-0.0307	-0.3733	-0.2829	-0.2237	0	0	-0.3858	-0.1974	-0.3872	-0.7	-0.2829	-0.0287	0	0	0	0
0	0.005	0.0082	-0.0006	-0.0188	1	-0.3216	-0.0109	0.0077	0.0062	0.0147	0	0	0.0159	0.0105	0.0268	0.0158	0.0042	-0.0071	0	0	0	0
0	-0.029	-0.0729	-0.1215	-0.0297	-0.3216	1	-0.3909	0.0105	0.0086	-0.0387	0	0	-0.0061	-0.0232	-0.0367	0.0154	0.0032	-0.0146	0	0	0	0
0	0.0182	0.0378	0.03	-0.0307	-0.0109	-0.3909	1	0.0129	0.0104	0.0404	0	0	0.0323	0.0252	0.0617	0.0282	0.0078	-0.0109	0	0	0	0
0	0.0101	0.0205	0.0297	-0.3733	0.0077	0.0105	0.0129	1	-0.2713	0.0888	0	0	0.1464	0.076	0.1553	0.2616	0.0897	0.0013	0	0	0	0
0	0.0081	0.0165	0.024	-0.2829	0.0062	0.0086	0.0104	-0.2713	1	0.0718	0	0	0.1186	0.0615	0.1255	0.2118	0.0731	0.0013	0	0	0	0
0	0.0122	0.0191	-0.0323	-0.2237	0.0147	-0.0387	0.0404	0.0888	0.0718	1	0	0	0.1059	0.0016	0.1351	0.1597	0.0323	-0.0816	0	0	0	0
0.0114	0	0	0	0	0	0	0	0	0	0	1	-0.4033	0	0	0	0	0	0	-0.001	0.0006	0.0087	0.0038
-0.0028	0	0	0	0	0	0	0	0	0	0	-0.4033	1	0	0	0	0	0	0	-0.0011	0	0.0058	0.0024
0	0.0169	0.0318	0.0235	-0.3858	0.0159	-0.0061	0.0323	0.1464	0.1186	0.1059	0	0	1	-0.03	0.1579	0.2819	0.092	-0.3452	0	0	0	0
0	0.0067	0.0112	-0.02	-0.1974	0.0105	-0.0232	0.0252	0.076	0.0615	0.0016	0	0	-0.03	1	-0.2148	0.1395	0.0404	-0.1528	0	0	0	0
0	0.0277	0.048	0.0068	-0.3872	0.0268	-0.0367	0.0617	0.1553	0.1255	0.1351	0	0	0.1579	-0.2148	1	0.3009	0.0872	-0.2788	0	0	0	0
0	0.02	0.0398	0.0509	-0.7	0.0158	0.0154	0.0282	0.2616	0.2118	0.1597	0	0	0.2819	0.1395	0.3009	1	-0.0405	-0.0067	0	0	0	0
0	0.0048	0.0097	0.0113	-0.2829	0.0042	0.0032	0.0078	0.0897	0.0731	0.0323	0	0	0.092	0.0404	0.0872	-0.0405	1	-0.0029	0	0	0	0
0	-0.01	-0.0193	-0.0329	-0.0287	-0.0071	-0.0146	-0.0109	0.0013	0.0013	-0.0816	0	0	-0.3452	-0.1528	-0.2788	-0.0067	-0.0029	1	0	0	0	0
-0.0015	0	0	0	0	0	0	0	0	0	0	-0.001	-0.0011	0	0	0	0	0	0	1	-0.0675	-0.0101	-0.013
0.0007	0	0	0	0	0	0	0	0	0	0	0.0006	0	0	0	0	0	0	0	-0.0675	1	-0.0097	-0.0104
0.0112	0	0	0	0	0	0	0	0	0	0	0.0087	0.0058	0	0	0	0	0	0	-0.0101	-0.0097	1	0.0024
0.0048	0	0	0	0	0	0	0	0	0	0	0.0038	0.0024	0	0	0	0	0	0	-0.013	-0.0104	0.0024	1

TABLE 5.27: Interaction indices of δ at time $t = 1.171$ s for generators 1-23.

δ_1	δ_2	δ_3	δ_4	δ_5	δ_6	δ_7	δ_8	δ_9	δ_{10}	δ_{11}	δ_{12}	δ_{13}	δ_{14}	δ_{15}	δ_{16}	δ_{17}	δ_{18}	δ_{19}	δ_{20}	δ_{21}	δ_{22}	δ_{23}
1	-0.1885	-0.0941	0.036	0.0226	-0.2366	-0.0036	-0.0015	0.0133	-0.0194	-0.009	-0.0069	-0.0074	-0.0072	0.0137	0.0016	0.0015	0.0074	0.0139	-0.009	0.0011	0.0023	0.0028
-0.1885	1	-0.1143	0.0116	0.0052	-0.1532	-0.0051	-0.0017	0.0025	-0.0127	-0.0049	-0.0027	-0.004	-0.0032	0.0054	0.0008	0.001	0.0012	0.0058	-0.0038	0.0017	0.0013	0.0014
-0.0941	-0.1143	1	0.0232	0.0092	-0.3722	-0.0088	-0.0039	0.0061	-0.0243	-0.0105	-0.0088	-0.0093	-0.0082	0.0109	0.0005	0.0003	0.0034	0.0127	-0.0101	-0.0001	0.0017	0.0023
0.036	0.0116	0.0232	1	0.022	-0.0167	-0.0435	-0.0203	0.0079	-0.0837	-0.0866	-0.0338	-0.0343	-0.0317	0.0369	-0.0006	-0.0021	-0.0872	0.0497	-0.0443	-0.01	0.0035	0.0074
0.0226	0.0052	0.0092	0.022	1	-0.0201	-0.0152	-0.0093	0.0138	-0.0442	-0.0399	-0.0256	-0.021	-0.0206	0.0234	-0.0014	-0.003	-0.0222	0.0316	-0.0272	-0.01	0.0011	0.0041
-0.2366	-0.1532	-0.3722	-0.0167	-0.0201	1	-0.0123	-0.0048	-0.0118	-0.0156	-0.0049	-0.0032	-0.0047	-0.0027	-0.0018	-0.001	-0.0008	-0.007	0.0012	-0.003	0.0003	0.0002	0.0003
-0.0036	-0.0051	-0.0088	-0.0435	-0.0152	-0.0123	1	-0.066	-0.1372	-0.0926	-0.0303	-0.037	-0.0441	-0.0305	-0.0078	-0.0126	-0.0133	-0.0199	0.0104	-0.0533	-0.0162	-0.0042	-0.0015
-0.0015	-0.0017	-0.0039	-0.0203	-0.0093	-0.0048	-0.066	1	-0.1684	-0.0476	-0.0148	-0.0196	-0.0218	-0.0148	-0.0059	-0.0068	-0.0074	-0.0084	0.0004	-0.0303	-0.0097	-0.0032	-0.0019
0.0133	0.0025	0.0061	0.0079	0.0138	-0.0118	-0.1372	-0.1684	1	-0.104	-0.0346	-0.0441	-0.0491	-0.0378	0.0144	-0.009	-0.0103	-0.005	0.0367	-0.0814	-0.0197	-0.0014	0.0029
-0.0194	-0.0127	-0.0243	-0.0837	-0.0442	-0.0156	-0.0926	-0.0476	-0.104	1	-0.0766	-0.0484	-0.0806	-0.048	-0.0259	-0.0175	-0.0181	-0.0332	-0.0033	-0.0466	-0.0145	-0.0059	-0.0038
-0.009	-0.0049	-0.0105	-0.0866	-0.0399	-0.0049	-0.0303	-0.0148	-0.0346	-0.0766	1	-0.0126	-0.0186	-0.0103	-0.0114	-0.0058	-0.006	-0.0568	-0.0071	-0.0111	-0.0042	-0.0026	-0.0023
-0.0069	-0.0027	-0.0088	-0.0338	-0.0256	-0.0032	-0.037	-0.0196	-0.0441	-0.0484	-0.0126	1	-0.0252	-0.0137	-0.0248	-0.0115	-0.012	-0.0101	-0.0146	-0.0127	-0.0065	-0.005	-0.0046
-0.0074	-0.004	-0.0093	-0.0343	-0.021	-0.0047	-0.0441	-0.0218	-0.0491	-0.0806	-0.0186	-0.0252	1	-0.2677	-0.0206	-0.0108	-0.0112	-0.0117	-0.0076	-0.0165	-0.0069	-0.004	-0.0032
-0.0072	-0.0032	-0.0082	-0.0317	-0.0206	-0.0027	-0.0305	-0.0148	-0.0378	-0.048	-0.0103	-0.0137	-0.2677	1	-0.0198	-0.0079	-0.008	-0.01	-0.013	-0.0079	-0.0036	-0.0035	-0.0035
0.0137	0.0054	0.0109	0.0369	0.0234	-0.0018	-0.0078	-0.0059	0.0144	-0.0259	-0.0114	-0.0248	-0.0206	-0.0198	1	-0.2779	-0.2867	0.0097	0.0498	-0.0353	-0.0269	-0.0259	-0.0055
0.0016	0.0008	0.0005	-0.0006	-0.0014	-0.001	-0.0126	-0.0068	-0.009	-0.0175	-0.0058	-0.0115	-0.0108	-0.0079	-0.2779	1	-0.1354	-0.0004	-0.0031	-0.0137	-0.0114	-0.0168	-0.0098
0.0015	0.001	0.0003	-0.0021	-0.003	-0.0008	-0.0133	-0.0074	-0.0103	-0.0181	-0.006	-0.012	-0.0112	-0.008	-0.2867	-0.1354	1	-0.0007	-0.007	-0.0138	-0.0121	-0.018	-0.0111
0.0074	0.0012	0.0034	-0.0872	-0.0222	-0.007	-0.0199	-0.0084	-0.005	-0.0332	-0.0568	-0.0101	-0.0117	-0.01	0.0097	-0.0004	-0.0007	1	0.0144	-0.0141	-0.0025	0.0011	0.0022
0.0139	0.0058	0.0127	0.0497	0.0316	0.0012	0.0104	0.0004	0.0367	-0.0033	-0.0071	-0.0146	-0.0076	-0.013	0.0498	-0.0031	-0.007	0.0144	1	-0.2004	-0.4409	-0.0641	-0.0302
-0.009	-0.0038	-0.0101	-0.0443	-0.0272	-0.003	-0.0533	-0.0303	-0.0814	-0.0466	-0.0111	-0.0127	-0.0165	-0.0079	-0.0353	-0.0137	-0.0138	-0.0141	-0.2004	1	-0.0404	-0.0339	-0.0375
0.0011	0.0017	-0.0001	-0.01	-0.01	0.0003	-0.0162	-0.0097	-0.0197	-0.0145	-0.0042	-0.0065	-0.0069	-0.0036	-0.0269	-0.0114	-0.0121	-0.0025	-0.4409	-0.0404	1	-0.0468	-0.0511
0.0023	0.0013	0.0017	0.0035	0.0011	0.0002	-0.0042	-0.0032	-0.0014	-0.0059	-0.0026	-0.005	-0.004	-0.0035	-0.0259	-0.0168	-0.018	0.0011	-0.0641	-0.0339	-0.0468	1	-0.05
0.0028	0.0014	0.0023	0.0074	0.0041	0.0003	-0.0015	-0.0019	0.0029	-0.0038	-0.0023	-0.0046	-0.0032	-0.0035	-0.0055	-0.0098	-0.0111	0.0022	-0.0302	-0.0375	-0.0511	-0.05	1
0.0083	0.0036	0.0074	0.0257	0.0156	0.0003	0.0055	0.0005	0.0182	-0.0024	-0.0027	-0.0046	-0.0027	-0.0049	0.0234	-0.0015	-0.0033	0.0073	0.0436	-0.13	-0.0734	-0.0579	-0.0059
0	0	0	0	0	0	0	0	0	0	0	0	0	0	0	0	0	0	0	0	0	0	0
0	0	0	0	0	0	0	0	0	0	0	0	0	0	0	0	0	0	0	0	0	0	0
0	0	0	0	0	0	0	0	0	0	0	0	0	0	0	0	0	0	0	0	0	0	0
0	0	0	0	0	0	0	0	0	0	0	0	0	0	0	0	0	0	0	0	0	0	0
0	0	0	0	0	0	0	0	0	0	0	0	0	0	0	0	0	0	0	0	0	0	0
0	0	0	0	0	0	0	0	0	0	0	0	0	0	0	0	0	0	0	0	0	0	0
0	0	0	0	0	0	0	0	0	0	0	0	0	0	0	0	0	0	0	0	0	0	0
0	0	0	0	0	0	0	0	0	0	0	0	0	0	0	0	0	0	0	0	0	0	0
0	0	0	0	0	0	0	0	0	0	0	0	0	0	0	0	0	0	0	0	0	0	0
0	0	0	0	0	0	0	0	0	0	0	0	0	0	0	0	0	0	0	0	0	0	0
0.0049	0.0019	0.0045	0.0177	0.0118	0.0001	0.0043	0.0012	0.0134	-0.0004	-0.0019	-0.0041	-0.0022	-0.004	0.0094	-0.0152	-0.0175	0.0049	0.0407	-0.0443	-0.0547	-0.1216	-0.0254
0.0042	0.0019	0.0037	0.0135	0.0082	0.0004	0.0028	0.0001	0.01	-0.0014	-0.002	-0.0047	-0.0027	-0.0039	0.0004	-0.0148	-0.017	0.004	0.0144	-0.0372	-0.0502	-0.1079	-0.0283
0	0	0	0	0	0	0	0	0	0	0	0	0	0	0	0	0	0	0	0	0	0	0
0	0	0	0	0	0	0	0	0	0	0	0	0	0	0	0	0	0	0	0	0	0	0
0	0	0	0	0	0	0	0	0	0	0	0	0	0	0	0	0	0	0	0	0	0	0
0	0	0	0	0	0	0	0	0	0	0	0	0	0	0	0	0	0	0	0	0	0	0
0	0	0	0	0	0	0	0	0	0	0	0	0	0	0	0	0	0	0	0	0	0	0
0	0	0	0	0	0	0	0	0	0	0	0	0	0	0	0	0	0	0	0	0	0	0
-0.0096	-0.0055	-0.0107	-0.1203	-0.0499	-0.0051	-0.0245	-0.0109	-0.026	-0.0338	-0.0449	-0.0078	-0.0102	-0.0058	-0.0069	-0.0036	-0.0036	-0.0972	-0.0037	-0.0073	-0.0025	-0.0015	-0.0013
-0.0074	-0.0049	-0.0096	-0.0689	-0.0328	-0.0065	-0.0229	-0.0111	-0.0215	-0.0455	-0.0395	-0.0113	-0.0134	-0.0088	-0.0036	-0.0036	-0.0039	-0.0575	0.0006	-0.0106	-0.0037	-0.0013	-0.0007
0.0134	0.005	0.0089	0.0284	0.0154	-0.0046	-0.0115	-0.0082	0.0069	-0.0424	-0.0157	-0.0614	-0.0229	-0.0203	0.0154	-0.0032	-0.0046	0.0071	0.0227	-0.0211	-0.0086	0.0002	0.0026
-0.0009	-0.0041	-0.0087	0.0029	-0.0385	-0.0155	-0.0077	-0.0048	0.0012	-0.0181	-0.0121	-0.0111	-0.0089	-0.0082	0.0063	-0.0015	-0.0022	-0.0053	0.0096	-0.0107	-0.0049	-0.0003	0.0009

5.4.2 Sensitivity-based approach

The sensitivity-based dynamic interaction assessment approach described in Section 4.2.2 is tested on the IEEE 6-machine, 30-bus test system. The system is modified according to [Alsac and Stott, 1974] such that all machines generate active power. The dynamic simulation is performed in a time period of $0 < T < 25$ s, with a sudden 30% load increase at bus 30 at time $t = 1$ s.

The proposed method is applied to compute the dynamic sensitivities of bus voltage magnitudes with respect to the frequency. In addition, two simulation cases are considered: Case 1, without including the inertia emulation controller model, and Case 2 in which the controller model is included. Figure 5.22 shows the dynamic behaviour of the frequency value resulting from the two simulation scenarios.

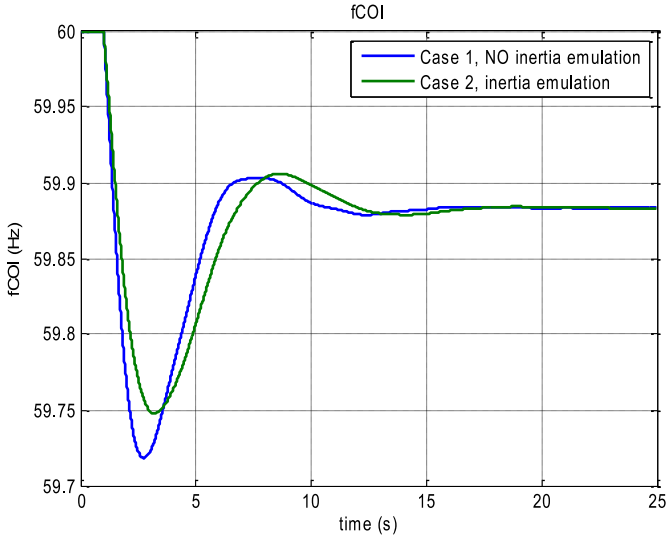

FIGURE 5.22: Dynamic behaviour of the frequency of the system for Case 1 and Case 2 .

The objective is to assess the sensitivity between two variables that have a non-explicit relation by means of (4.29). Then, the sensitivity index (4.30) of the voltage magnitudes with respect to the system's frequency is obtained for each bus of the system considering both simulation cases. These values are reported in Table 5.28 in ascending order.

The bus voltage magnitudes corresponding to the smallest and the largest index values are plotted and shown in Figure 5.23 for each simulation case. Note from

TABLE 5.28: Bus voltages corresponding to the largest and smallest index shifts from Case 1 to Case 2.

Case 1		Case 2	
Bus #	Sensitivity Index $I_{i,j}$ (p.u)	Bus #	Sensitivity Index $I_{i,j}$ (p.u)
1	0.3282	19	0.275
4	0.3482	4	0.2985
19	0.3905	16	0.3047
16	0.5353	21	0.3102
21	0.6104	18	0.3207
18	0.66	20	0.339
20	0.757	1	0.3457
14	0.8149	22	0.3528
22	0.8316	14	0.3556
13	1.0753	13	0.4481
15	1.1507	10	0.4715
10	1.1596	15	0.4804
11	1.1814	11	0.4805
17	1.206	12	0.4971
12	1.2753	24	0.5003
9	1.2793	7	0.5017
7	1.2843	6	0.5023
6	1.2864	30	0.5028
30	1.2945	9	0.5035
24	1.2979	17	0.5041
5	1.3109	29	0.5077
8	1.3143	5	0.5089
29	1.3163	25	0.5095
3	1.3214	8	0.5109
2	1.3281	3	0.5124
25	1.3319	28	0.5133
28	1.3326	2	0.5137
27	1.3397	27	0.5141
26	1.68	26	0.6142
23	1.8797	23	0.6833

Table 5.28 that by including an inertia controller model in the wind farm the most and least sensitive bus voltages can change. In fact, it can be observed that almost the complete sensitivity index ranking changes. In Figure 5.23, is clearly shown that

the sensitivity index magnitude is directly related to the amplitude of the voltage oscillations and to the number of the oscillations occurring in the waveform.

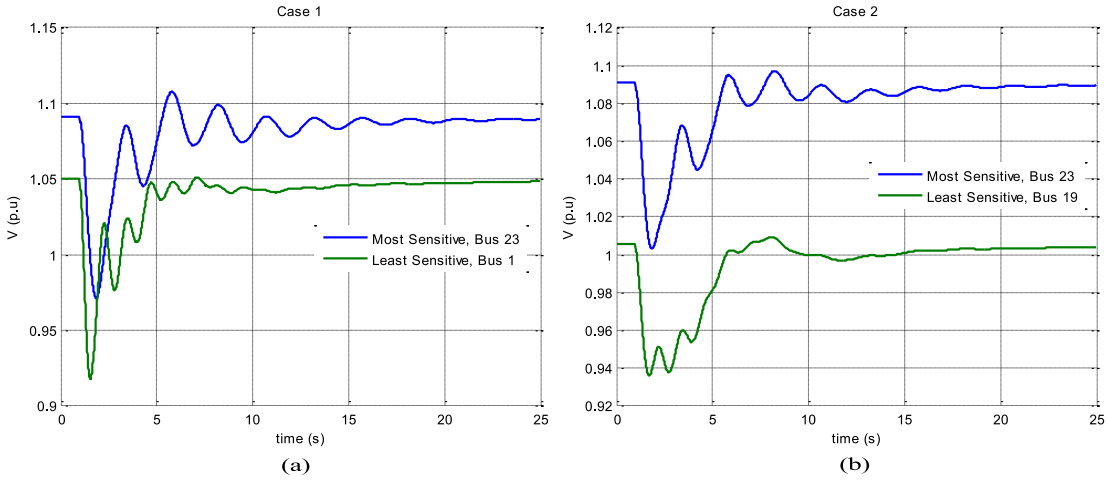

FIGURE 5.23: Bus voltages corresponding to the largest (a) and smallest (b) sensitivity index values.

In addition to identifying the most and the least sensitive bus voltage for a given simulation case, the voltage-frequency sensitivity index can be used to identify bus voltage magnitudes having the most and least changes in their dynamics between two simulation scenarios. This can be done by subtracting the values of the indices corresponding to both cases. Hence, for the k-th bus,

$$\Delta I_{i,j} = I_{i,j}^{c1} - I_{i,j}^{c2}, \tag{5.3}$$

where $\Delta I_{i,j}$ is the sensitivity index shift and superscripts $c1$ and $c2$ denote simulation cases 1 and 2, respectively.

The two bus voltages that experience the least and most amount of change in their dynamics according to (5.3) are plotted in Figure 5.24. The sensitivity index shift functions as an indicator of the amount of dynamic variation of the bus voltages. This can be observed from Figure 5.24 that bus 23 presents the larger voltage magnitude variation from Case 1 to Case 2 during the transient period. In fact, the dynamic behaviour of bus voltage magnitudes can be seen to improve when including the inertia emulation controller model in the wind farm; this is consistent

with the sensitivity indices listed in Table 5.28 which decrease in the case of including the inertia emulation controller (Case 2).

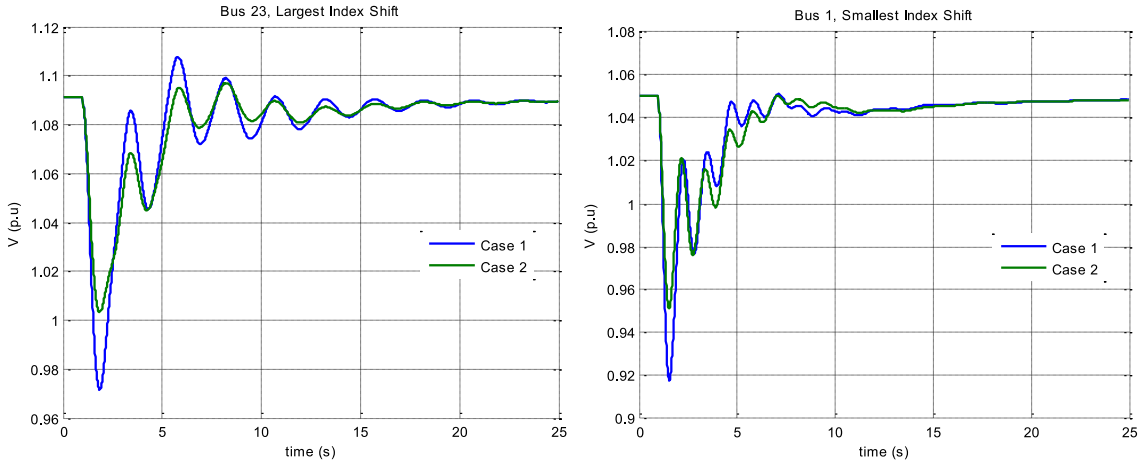

FIGURE 5.24: Bus voltages corresponding to the largest (a) and smallest (b) index shifts from Case 1 to Case 2.

5.5 Conclusions

In this chapter the proposed approaches for the assessment of interaction of control devices in power systems has been tested by means of numerical simulations in order to demonstrate their suitability and applicability, both in the steady-state and transient stability operation frameworks. In addition, the proposed power flow models of AIC and SVCs are validated and tested.

Several real-life and benchmark systems were analysed in order to show the usefulness of the proposals to identify and quantify the interaction level among control devices in power systems.

Chapter 6

General Conclusions and Suggestions for Future Research Work

6.1 General Conclusions.

The interaction phenomena among control devices in power systems has been addressed taking into consideration two stages: Steady-state analysis and dynamic analysis. Regarding the steady-state operation framework, power flow models of FACTS devices, Area Interchange Control (AIC) and Automatic Frequency Control (AFC) models have been considered and implemented, along with the power network model, into a Matlab-based digital program capable of solving large-scale power systems. In this context, a method to identify and quantify the interactions among control devices has been proposed. This method is based on the numerical analysis of the Jacobian matrix obtained during the Newton-based power flow solution process. In this case, a reduced-order matrix is first obtained from the full Jacobian matrix and a numerical index is then computed by means of geometric numerical projections of the column vectors of the reduced matrix. This index is obtained for each control device in the system and is capable to identify, if any, the control devices that interact in such way that an ill-conditioned numerical problem occurs during the iterative solution process. This adverse interaction can be originated by a poor control

coordination, redundant control schemes, infeasible control configurations, etc. In addition to the identification of potentially adverse interactions, the proposed index can also provide information about if the system is operating near to an unstable mode. Moreover, the sign of the index indicates if the variables associated with the detected control devices change in the same or opposite directions. This proposed approach is numerically simpler and equally reliable than the existing methods for steady-state control interaction analysis. The effectiveness and applicability of the proposal are demonstrated by means of numerical simulation using a small 5-bus power system and a modified version of the IEEE 118-bus benchmark system.

A new Area Interchange Control (AIC) model has been proposed in this work suitable for Newton-based power flow studies. Unlike other existing models, only one additional equation per controlled area is added to the set of power flow mismatch equations, regardless of the number of regulating generators at each area, in order to regulate the interchange of active power between specified areas of the network. The way in which the proposed model has been implemented in the formulation of the power flow problem retains Newton's quadratic convergence. In addition, a suitable approach for handling the violation of the maximum amount of power that can be transferred through tie-lines is also proposed. Furthermore, a novel Static VAR Compensator (SVC) model suitable for a Newton-based power flow method based on an augmented Jacobian matrix is proposed. An important characteristic that distinguishes our SVC model from other previous proposals is that only one control mismatch equation per SVC is aggregated in the formulation to represent the SVC's control action, without compromising the quadratic convergence characteristic of the Newton method. This approach permits the direct application of the proposed model to compute a control sensitivity matrix $\mathbf{J_C}$ for identifying control conflicts among SVC devices.

In the context of the dynamic power system analysis, the adopted time framework in this research work is encompassed in the transient stability phenomenon. The device models considered include the well-known two-axis synchronous machine model, as well as the most common machine controls, i. e. Automatic Voltage Regulators (AVRs), turbine-governor groups, and Power System Stabilizers (PSSs). Additionally, in order to consider the recent developments in renewable energy integration to power systems, models of Type-4 Wind Energy Conversion Systems (WECSs) and their related back-to-back power converters are

included in the power system dynamic formulation. Also, the inertia emulation capability of wind-based generation is granted. All these models are numerically solved together in a unified way along with the network model, and implemented into a digital Matlab-based digital program. Similarly to the steady-state analysis, a novel approach is proposed in order to assess the interaction level among the different controllers considered in the dynamic framework. The geometry-based approach employed in the steady-state analysis of the power system is also applied on a reduced matrix obtained from the Jacobian matrix at the end of each integration step of the dynamic solution method. As a result, an interaction index is obtained for each control device to be analysed. One of the applications of the proposal is to detect tuning issues among control devices of generators. Another important application of this proposal is the identification of coherent groups of synchronous generators or isolated areas in the system. Unlike other similar methods, the proposal can be carried out in a single integration step of the dynamic simulation. Finally a sensitivity-based approach is proposed in order to quantify the dynamic relation that a pair of state variables have during the dynamic simulation. By the latter approach it is possible to quantify the dynamic variation that any pair of state variables have in a transient period. These proposals are tested using benchmark as well as real-life power systems.

6.2 Suggestions for Future Research Work

The proposed approaches have been proved to be simple but effective solutions for identifying control devices causing conflicts due to adverse interactions, both in the steady-state and dynamic operation frameworks. Moreover, a quantification of the interaction level can be obtained. However, given the complexity of the interaction phenomena arising as a consequence of the diverse control devices embedded in modern power systems and the different time scales at which these operate, the applications of the proposed methods can be extended to address problems out of the focus of this thesis. Hence, some interesting suggestions for future research work can be derived:

- The dynamic analysis framework could be expanded to long term dynamics, where another type of controllers operate, e. g. Automatic Generation Control (AGC).
- An interaction assessment method could be developed in future research efforts in order to be included into on-line applications such as state estimators.
- The interaction phenomena must be further investigated considering high-frequency controls, as there are currently a limited number of tools for analysis.
- The newly-introduced technologies such as large-scale photovoltaic generation systems and energy storage systems, as well as their related controls, must be accounted in future research works.
- The proposed interaction assessment method could be applied to perform a selective modal analysis from a small-signal stability viewpoint.

Appendix A

Steady-state data of test systems.

The data of the test power systems used in power-flow simulations in this research work are given in this appendix. The MVA base is 100 MVA and the base frequency is 60 Hz for all systems.

A.1 5-bus system

TABLE A.1: Transmission lines.

Sending Bus	Receiving Bus	R (p.u.)	X_L (p.u.)	B_{total} (p.u.)
north	south	0.02	0.06	0.06
north	lake	0.08	0.24	0.05
south	lake	0.06	0.18	0.04
south	main	0.06	0.18	0.04
south	elm	0.04	0.12	0.03
lake	main	0.01	0.03	0.02
main	elm	0.08	0.24	0.05

TABLE A.2: Conventional Loads.

Bus	P_{LOAD} (MW)	Q_{LOAD} (MVAR)
south	20	10
lake	45	15
main	40	5
elm	60	10

Table A.3: Generators (PV).

Bus	V_i (p.u.)	P_G (MW)	Q_{Gmax} (MVARs)	Q_{Gmin} (MVARs)
south	1.0	40	-300	300

Table A.4: Generators (regulators).

Bus	V_i (p.u.)	P_{G_set} (MW)	Q_{G_set} (MVAR)	P_R (p.u.)	R (p.u.)	a_Q	b_Q
North	1.06	130.12	90.82	1.0	0.04	1.0	1.0

A.2 118-bus system

Table A.5: Transmission lines.

Sending Bus	Receiving Bus	Sending Area	Receiving Area	R (p.u.)	X_L (p.u.)	B_{total} (p.u.)
1	2	1	1	0.0303	0.0999	0.0254
1	3	1	1	0.0129	0.0424	0.01082
4	5	1	1	0.00176	0.00798	0.0021
3	5	1	1	0.0241	0.108	0.0284
5	6	1	1	0.0119	0.054	0.01426
6	7	1	1	0.00459	0.0208	0.0055
8	9	1	1	0.00244	0.0305	1.162
9	10	1	1	0.00258	0.0322	1.23
4	11	1	1	0.0209	0.0688	0.01748
5	11	1	1	0.0203	0.0682	0.01738
11	12	1	1	0.00595	0.0196	0.00502
2	12	1	1	0.0187	0.0616	0.01572
3	12	1	1	0.0484	0.16	0.0406
7	12	1	1	0.00862	0.034	0.00874
11	13	1	2	0.02225	0.0731	0.01876
12	14	1	2	0.0215	0.0707	0.01816
13	15	2	2	0.0744	0.2444	0.06268
14	15	2	2	0.0595	0.195	0.0502
12	16	1	2	0.0212	0.0834	0.0214
15	17	2	2	0.0132	0.0437	0.0444
16	17	2	2	0.0454	0.1801	0.0466
17	18	2	2	0.0123	0.0505	0.01298
18	19	2	2	0.01119	0.0493	0.01142
19	20	2	2	0.0252	0.117	0.0298
15	19	2	2	0.012	0.0394	0.0101
20	21	2	2	0.0183	0.0849	0.0216
21	22	2	2	0.0209	0.097	0.0246
22	23	2	4	0.0342	0.159	0.0404
23	24	4	4	0.0135	0.0492	0.0498
23	25	4	4	0.0156	0.08	0.0864
25	27	4	4	0.0318	0.163	0.1764
27	28	4	4	0.01913	0.0855	0.0216
28	29	4	4	0.0237	0.0943	0.0238
8	30	1	2	0.00431	0.0504	0.514
26	30	4	2	0.00799	0.086	0.908
17	31	2	2	0.0474	0.1563	0.0399
29	31	4	3	0.0108	0.0331	0.0083
23	32	4	4	0.0317	0.1153	0.1173
31	32	2	4	0.0298	0.0985	0.0251
27	32	4	4	0.0229	0.0755	0.01926
15	33	2	3	0.038	0.1244	0.03194
19	34	2	3	0.0752	0.247	0.0632
35	36	3	3	0.00224	0.0102	0.00268
35	37	3	3	0.011	0.0497	0.01318
33	37	3	3	0.0415	0.142	0.0366
34	36	3	3	0.00871	0.0268	0.00568
34	37	3	3	0.00256	0.0094	0.00984
37	39	3	3	0.0321	0.106	0.027
37	40	3	3	0.0593	0.168	0.042
30	38	2	3	0.00464	0.054	0.422
39	40	3	3	0.0184	0.0605	0.01552
40	41	3	3	0.0145	0.0487	0.01222

40	42	3	3	0.0555	0.183	0.0466
41	42	3	3	0.041	0.135	0.0344
43	44	3	3	0.0608	0.2454	0.06068
34	43	3	3	0.0413	0.1681	0.04226
44	45	3	6	0.0224	0.0901	0.0224
45	46	6	6	0.04	0.1356	0.0332
46	47	6	6	0.038	0.127	0.0316
46	48	6	6	0.0601	0.189	0.0472
47	49	6	6	0.0191	0.0625	0.01604
42	49	3	6	0.0715	0.323	0.086
42	49	3	6	0.0715	0.323	0.086
45	49	6	6	0.0684	0.186	0.0444
48	49	6	6	0.0179	0.0505	0.01258
49	50	6	9	0.0267	0.0752	0.01874
49	51	6	6	0.0486	0.137	0.0342
51	52	6	6	0.0203	0.0588	0.01396
52	53	6	9	0.0405	0.1635	0.04058
53	54	9	9	0.0263	0.122	0.031
49	54	6	9	0.073	0.289	0.0738
49	54	6	9	0.0869	0.291	0.073
54	55	9	9	0.0169	0.0707	0.0202
54	56	9	9	0.00275	0.00955	0.00732
55	56	9	9	0.00488	0.0151	0.00374
56	57	9	9	0.0343	0.0966	0.0242
50	57	9	9	0.0474	0.134	0.0332
56	58	9	9	0.0343	0.0966	0.0242
51	58	6	9	0.0255	0.0719	0.01788
54	59	9	9	0.0503	0.2293	0.0598
56	59	9	9	0.0825	0.251	0.0569
56	59	9	9	0.0803	0.239	0.0536
55	59	9	9	0.04739	0.2158	0.05646
59	60	9	9	0.0317	0.145	0.0376
59	61	9	9	0.0328	0.15	0.0388
60	61	9	9	0.00264	0.0135	0.01456
60	62	9	9	0.0123	0.0561	0.01468
61	62	9	9	0.00824	0.0376	0.0098
63	64	9	9	0.00172	0.02	0.216
38	65	3	6	0.00901	0.0986	1.046
64	65	9	6	0.00269	0.0302	0.38
49	66	6	6	0.018	0.0919	0.0248
49	66	6	6	0.018	0.0919	0.0248
62	66	9	6	0.0482	0.218	0.0578
62	67	9	6	0.0258	0.117	0.031
66	67	6	6	0.0224	0.1015	0.02682
65	68	6	6	0.00138	0.016	0.638
47	69	6	6	0.0844	0.2778	0.07092
49	69	6	6	0.0985	0.324	0.0828
69	70	6	4	0.03	0.127	0.122
24	70	4	4	0.00221	0.4115	0.10198
70	71	4	4	0.00882	0.0355	0.00878
24	72	4	4	0.0488	0.196	0.0488
71	72	4	4	0.0446	0.18	0.04444
71	73	4	4	0.00866	0.0454	0.01178
70	74	4	5	0.0401	0.1323	0.03368
70	75	5	5	0.0428	0.141	0.036
69	75	6	5	0.0405	0.122	0.124
74	75	5	5	0.0123	0.0406	0.01034
76	77	5	5	0.0444	0.148	0.0368
69	77	6	5	0.0309	0.101	0.1038
75	77	5	5	0.0601	0.1999	0.04978
77	78	5	5	0.00376	0.0124	0.01264
78	79	5	8	0.00546	0.0244	0.00648
77	80	5	8	0.017	0.0485	0.0472
77	80	5	8	0.0294	0.105	0.0228
79	80	8	8	0.0156	0.0704	0.0187
68	81	6	8	0.00175	0.0202	0.808
77	82	5	5	0.0298	0.0853	0.08174
82	83	5	5	0.0112	0.03665	0.03796
83	84	5	5	0.0625	0.132	0.0258
83	85	5	5	0.043	0.148	0.0348
84	85	5	5	0.0302	0.0641	0.01234
85	86	5	5	0.035	0.123	0.0276
86	87	5	5	0.02828	0.2074	0.0445
85	88	5	5	0.02	0.102	0.0276

85	89	5	8	0.0239	0.173	0.047
88	89	5	8	0.0139	0.0712	0.01934
89	90	8	8	0.0518	0.188	0.0528
89	90	8	8	0.0238	0.0997	0.106
90	91	8	8	0.0254	0.0836	0.0214
89	92	8	8	0.0099	0.0505	0.0548
89	92	8	8	0.0393	0.1581	0.0414
91	92	8	8	0.0387	0.1272	0.03268
92	93	8	8	0.0258	0.0848	0.0218
92	94	8	8	0.0481	0.158	0.0406
93	94	8	8	0.0223	0.0732	0.01876
94	95	8	8	0.0132	0.0434	0.0111
80	96	8	8	0.0356	0.182	0.0494
82	96	5	8	0.0162	0.053	0.0544
94	96	8	8	0.0269	0.0869	0.023
80	97	8	8	0.0183	0.0934	0.0254
80	98	8	8	0.0238	0.108	0.0286
80	99	8	8	0.0454	0.206	0.0546
92	100	8	7	0.0648	0.295	0.0472
94	100	8	7	0.0178	0.058	0.0604
95	96	8	8	0.0171	0.0547	0.01474
96	97	8	8	0.0173	0.0885	0.024
98	100	8	7	0.0397	0.179	0.0476
99	100	8	7	0.018	0.0813	0.0216
100	101	7	7	0.0277	0.1262	0.0328
92	102	8	7	0.0123	0.0559	0.01464
101	102	7	7	0.0246	0.112	0.0294
100	103	7	7	0.016	0.0525	0.0536
100	104	7	7	0.0451	0.204	0.0541
103	104	7	7	0.0466	0.1584	0.0407
103	105	7	7	0.0535	0.1625	0.0408
100	106	7	7	0.0605	0.229	0.062
104	105	7	7	0.00994	0.0378	0.00986
105	106	7	7	0.014	0.0547	0.01434
105	107	7	7	0.053	0.183	0.0472
105	108	7	7	0.0261	0.0703	0.01844
106	107	7	7	0.053	0.183	0.0472
108	109	7	7	0.0105	0.0288	0.0076
103	110	7	7	0.03906	0.1813	0.0461
109	110	7	7	0.0278	0.0762	0.0202
110	111	7	7	0.022	0.0755	0.02
110	112	7	7	0.0247	0.064	0.062
17	113	2	2	0.00913	0.0301	0.00768
32	113	4	2	0.0615	0.203	0.0518
32	114	4	4	0.0135	0.0612	0.01628
27	115	4	4	0.0164	0.0741	0.01972
114	115	4	4	0.0023	0.0104	0.00276
68	116	6	6	0.00034	0.00405	0.164
12	117	1	1	0.0329	0.14	0.0358
75	118	5	5	0.0145	0.0481	0.01198
76	118	5	5	0.0164	0.0544	0.01356

TABLE A.6: Transformers.

Sending Bus	Receiving Bus	Sending Area	Receiving Area	R_p (p.u.)	X_p (p.u.)	R_s (p.u.)	X_s (p.u.)	G_0 (p.u.)	B_0 (p.u.)	T_v (p.u.)	T_i (p.u.)	U_v (°)	U_i (°)
8	5	1	1	0	0	0	0.0267	0	0	0.985	1	0	0
26	25	4	4	0	0	0	0.0382	0	0	0.96	1	0	0
30	17	2	2	0	0	0	0.0388	0	0	0.96	1	0	0
38	37	3	3	0	0	0	0.0375	0	0	0.935	1	0	0
63	59	9	9	0	0	0	0.0386	0	0	0.96	1	0	0
64	61	9	9	0	0	0	0.0268	0	0	0.985	1	0	0
65	66	6	6	0	0	0	0.037	0	0	0.935	1	0	0
68	69	6	6	0	0	0	0.037	0	0	0.935	1	0	0
81	80	8	8	0	0	0	0.037	0	0	0.935	1	0	0

TABLE A.7: Conventional Loads.

Bus	P_{LOAD} (MW)	Q_{LOAD} (MVAR)	Bus	P_{LOAD} (MW)	Q_{LOAD} (MVAR)
1	51	27	58	12	3
2	20	9	59	277	113
3	39	10	60	78	3
4	30	12	62	77	14
7	19	2	66	39	18
11	70	23	67	28	7
12	47	10	70	66	20
13	34	16	74	68	27
14	14	1	75	47	11
15	90	30	76	68	36
16	25	10	77	61	28
17	11	3	78	71	26
19	45	25	79	39	32
20	18	3	80	130	26
21	14	8	82	54	27
22	10	5	83	20	10
23	7	3	84	11	7
27	62	13	85	24	15
28	17	7	86	21	10
29	24	4	88	48	10
31	43	27	90	78	42
32	59	23	92	65	10
33	23	9	93	12	7
35	33	9	94	30	16
36	31	17	95	42	31
39	27	11	96	38	15
40	20	23	97	15	9
41	37	10	98	34	8
42	37	23	100	37	18
43	18	7	101	22	15
44	16	8	102	5	3
45	53	22	103	23	16
46	28	10	104	38	25
47	34	0	105	31	26
48	20	11	106	43	16
49	87	30	107	28	12
50	17	4	108	2	1
51	17	8	109	8	3
52	18	5	110	39	30
53	23	11	112	25	13
54	113	32	114	8	3
55	63	22	115	22	7
56	84	18	117	20	8
57	12	3	118	33	15

Table A.8: Voltage-Dependent Loads.

Bus	P_{Lset} (MW)	Q_{Lset} (MVARs)	K_p	K_q	p_p	p_c	p_z	q_p	q_c	q_z	V_{LB} (p.u.)
6	52	22	0.04	0	0.2	0.3	0.5	0.2	0.3	0.5	1
18	60	34	0.04	0	0.2	0.3	0.5	0.2	0.3	0.5	1
34	59	26	0.04	0	0.2	0.3	0.5	0.2	0.3	0.5	1

Table A.9: Generators (PV).

Bus	V_i (p.u.)	P_G (MW)	Q_{Gmax} (MVARs)	Q_{Gmin} (MVARs)
1	0.955	0	15	-5
4	0.998	-9	300	-300
8	1.015	-28	300	-300
10	1.05	450	200	-147
12	0.99	85	120	-35
15	0.97	0	30	-10
19	0.962	0	24	-8
24	0.992	-13	300	-300
26	1.015	314	1000	-1000
27	0.968	-9	300	-300
31	0.967	7	300	-300
32	0.963	0	42	-14
36	0.98	0	24	-8
40	0.97	-46	300	-300
42	0.985	-59	300	-300
46	1.005	19	100	-100
49	1.025	204	210	-85
54	0.955	48	300	-300
55	0.952	0	23	-8
56	0.954	0	15	-8
59	0.985	155	180	-60
62	0.998	0	20	-20
65	1.005	391	200	-67
66	1.05	392	200	-67
70	0.984	0	32	-10
72	0.98	-12	100	-100
73	0.991	-6	100	-100
74	0.958	0	9	-6
76	0.943	0	23	-8
77	1.006	0	70	-20
80	1.04	477	280	-165
85	0.985	0	23	-8
89	1.005	607	300	-210
90	0.985	-85	300	-300
92	0.99	0	9	-3
99	1.01	-42	100	-100
100	1.017	252	155	-50
103	1.01	40	40	-15
104	0.971	0	23	-8
105	0.965	0	23	-8
107	0.952	-22	200	-200
110	0.973	0	23	-8
112	0.975	-43	1000	-100
113	0.993	-6	200	-100
116	1.005	-184	1000	-1000

Table A.10: Generators (Regulators).

Bus	V_i (p.u.)	P_{G_set} (MW)	Q_{G_set} (MVAR)	P_R (p.u.)	R (p.u.)	a_Q	b_Q	Q_{Gmax} (MVARs)	Q_{Gmin} (MVARs)
69	1.035	548.51	-101.38	1	0.04	1	1	8000	-8000
6	0.99	0	15.926	1	0.04	1	1	50	-13
18	0.973	0	19.5028	1	0.04	1	1	50	-16
25	1.05	220	57.2213	1	0.04	1	1	140	-47
34	0.984	0	-8	1	0.04	1	1	24	-8
61	0.995	160	-40.3871	1	0.04	1	1	300	-100
87	1.015	4	11.0216	1	0.04	1	1	1000	-100
91	0.98	-10	-14.8017	1	0.04	1	1	100	-100
111	0.98	36	-1.84382	1	0.04	1	1	1000	-100

Table A.11: Shunt Fixed VAR Compensators.

Bus	G_{shunt} (p.u.)	B_{shunt} (p.u.)
5	0	-0.4
34	0	0.14
37	0	-0.25
44	0	0.1
45	0	0.1
46	0	0.1
74	0	0.12
79	0	0.2
82	0	0.2
83	0	0.1
105	0	0.2
107	0	0.06
110	0	0.06

A.3 166-bus system

Table A.12: Transmission lines.

Sending Bus	Receiving Bus	R (p.u.)	X_L (p.u.)	B_{total} (p.u.)	Sending Bus	Receiving Bus	R (p.u.)	X_L (p.u.)	B_{total} (p.u.)
APD230	CPT230	0.00481	0.03367	0.06656	LGO69.0	LMS69.0	0.00756	0.04185	0.00078
APD230	CTY230	0.00052	0.00364	0.00716	LGO69.0	TJI69.0	0.00588	0.03255	0.00062
AMO69.0	INA69.0	0.00144	0.00696	0.00006	LMS69.0	TJI69.0	0.0121	0.06693	0.00126
BAO69.0	ONG69.0	0.07548	0.15247	0.00244	MSN69.0	PTN69.0	0.07548	0.15247	0.00244
CEC69.0	CIP69.0	0.02452	0.0844	0.00166	MTR69.0	LMS69.0	0.02533	0.12931	0.00266
SDE69.0	GER69.0	0.01681	0.09296	0.00176	MTR69.0	TJI69.0	0.01781	0.08334	0.00154
SDE69.0	TTJ69.0	0.01563	0.08646	0.00164	MTR230	TTJ230	0.00145	0.00975	0.01846
CHA161	CPU161	0.00928	0.05373	0.05006	MXC69.0	RII69.0	0.00792	0.03173	0.00244
CHA161	HGO161	0.01408	0.0904	0.03754	MXI161	RZC161	0.01871	0.10995	0.05462
CES69.0	MTR69.0	0.00631	0.03047	0.00032	MXI230	OZA230	0.00113	0.00918	0.01792

CIP115	EPCH115	0.02912	0.10428	0.0129	MXI230	SIC230	0.00283	0.01846	0.03672
CIP230	TTJ230	0.01252	0.08674	0.15224	MXI230	STB230	0.00098	0.0064	0.01274
CIP69.0	EDA69.0	0.02319	0.12289	0.00254	NZI161	RIN161	0.00196	0.01074	0.00616
CIP69.0	GLL69.0	0.04823	0.09751	0.00154	OZA230	ROA230	0.0021	0.01695	0.03308
CIP69.0	MND69.0	0.02939	0.05942	0.00094	PAP230	TJI230	0.00245	0.02058	0.04026
CNA69.0	TTJ69.0	0.02841	0.15717	0.00298	PAP230	TTJ230	0.00136	0.01145	0.02236
CPD230	CPT230	0.00038	0.00264	0.00456	PAP69.0	CNA69.0	0.02976	0.14365	0.00156
CPD230	ROA230	0.00577	0.04528	0.09324	PNM69.0	LMS69.0	0.02297	0.12583	0.0024
CPT230	SIC230	0.0017	0.01111	0.02208	PNM69.0	TTJ69.0	0.0289	0.1599	0.00302
CPU161	MXI161	0.00957	0.05781	0.02714	POP69.0	PTN69.0	0.06996	0.14145	0.00222
CPU161	MXI161	0.00957	0.05781	0.02714	POP69.0	TTJ69.0	0.05803	0.11732	0.00184
CRO161	MXI161	0.00284	0.00991	0.00498	RII69.0	UND69.0	0.02272	0.1097	0.0012
CRO161	RIN161	0.00108	0.00591	0.00338	ROA230	RUM230	0.00303	0.02442	0.04764
CTY161	MXI161	0.00228	0.01282	0.00698	ROA230	WIA230	0.00195	0.01559	0.03064
CTY161	NZI161	0.00193	0.01098	0.0061	ROA230	TJI230	0.01465	0.11774	0.22978
CTY230	TEK230	0.00187	0.01226	0.02438	RUM230	TJI230	0.01172	0.0942	0.18438
EDA69.0	BAO69.0	0.10064	0.20329	0.00326	RUM69.0	PBO69.0	0.09055	0.28886	0.00292
EDA69.0	FAM69.0	0.00677	0.01316	0.00022	RUM69.0	PBC69.0	0.02046	0.06529	0.00066
EDA69.0	JAT69.0	0.17058	0.34487	0.00544	SAF115	EPE115	0.0561	0.19834	0.01248
EDA69.0	SAZ69.0	0.05716	0.11557	0.00182	SAZ115	CIP115	0.01944	0.10548	0.007
EDA69.0	VLP69.0	0.21971	0.38614	0.00524	SAZ69.0	TTJ69.0	0.32948	0.66611	0.01054
EPCH115	PCH115	0.02543	0.09104	0.01128	SIM115	SQN115	0.01953	0.11519	0.013
EPCH115	SVE115	0.03654	0.13085	0.01618	STB230	TEK230	0.00339	0.02217	0.04408
EPE115	PTE115	0.09782	0.20956	0.01142	PB169.0	CNA69.0	0.01082	0.5223	0.00056
EPE115	TRI115	0.0408	0.14426	0.00908	PB169.0	MXC69.0	0.00591	0.02611	0.00056
FAM69.0	GLL69.0	0.02136	0.04152	0.0007	TCT69.0	FICT69.0	0.05346	0.28118	0.00656
FLO69.0	FLO13.8	0	0.6488	0	TCT69.0	FICT69.0	0.07575	0.36567	0.008
FLO69.0	MTR69.0	0.05723	0.14514	0.00234	TRA69.0	TCT69.0	0.05284	0.10673	0.0017
FLO69.0	VPM69.0	0.16761	0.29457	0.004	WIA230	MXI230	0.00069	0.0055	0.01882
GER69.0	MXC69.0	0.01018	0.05174	0.00106	TJI230	MTR230	0.00252	0.01978	0.04044
GER69.0	PAP69.0	0.0298	0.16038	0.00282	TJI230	TTJ230	0.00375	0.03018	0.0589
GLL69.0	CEC69.0	0.01014	0.01087	0.00026	TJI69.0	AMO69.0	0.011	0.05311	0.00058
HGO161	RZC161	0.00209	0.01148	0.0066	TJI69.0	INA69.0	0.011	0.05311	0.00058
HMO69.0	INA69.0	0.01497	0.07226	0.00078	TTJ69.0	MTR69.0	0.04533	0.23995	0.00476
HMO69.0	LMS69.0	0.00941	0.04979	0.00102	VLP69.0	VPM69.0	0.13909	0.28125	0.00444
HMO69.0	PAP69.0	0.0176	0.09234	0.00162	PBO69.0	PBU69.0	0.00609	0.01945	0.0002
HMO69.0	PAP69.0	0.0176	0.09234	0.00162	PBU69.0	PBD69.0	0.05339	0.17189	0.00174
HMO69.0	RII69.0	0.01208	0.05833	0.00064	PBD69.0	PBT69.0	0.0183	0.05837	0.00058
INA69.0	MTX69.0	0.01694	0.05405	0.00054	PBT69.0	RUM69.0	0.00883	0.02819	0.00028
INA69.0	UND69.0	0.01713	0.08271	0.0009	PBC69.0	PBQ69.0	0.00286	0.0091	0.00008
JAT69.0	MSN69.0	0.03376	0.06826	0.00108	PBQ69.0	RUM69.0	0.0218	0.06953	0.0007
KON115	SQN115	0.12161	0.25536	0.02886	ROA230	IV230	0.0017	0.0137	0.0272
KON115	SVE115	0.01488	0.0533	0.00658	TJI230	ML230	0.0014	0.0109	0.0734
KON115	TRI115	0.04262	0.15893	0.0181	IV500	ML500	0.00077	0.02014	1.47832

Table A.13: Transformers.

Sending Bus	Receiving Bus	R_p (p.u.)	X_p (p.u.)	R_s (p.u.)	X_s (p.u.)	G_0 (p.u.)	B_0 (p.u.)	T_v (p.u.)	T_i (p.u.)	U_v (°)	U_i (°)
APD230	APD13.8	0	0	0.04045	0.49209	0	0	1	1	0	0
APD230	APD13.8	0	0	0.04045	0.49209	0	0	1	1	0	0
CHA161	CHA34.5	0	0	0.03755	0.7502	0	0	1	1	0	0
CIP230	CIP115	0	0	0.00932	0.18616	0	0	1	1	0	0
CIP230	CIP115	0	0	0	0.06237	0	0	1	1	0	0
CIP230	CIP69.0	0	0	0.002	0.05806	0	0	1	1	0	0
CIP69.0	CIP13.8	0	0	0.02189	0.4334	0	0	1	1	0	0
CNA69.0	CNA13.8	0	0	0.0324	0.64719	0	0	1	1	0	0
CNA69.0	CNA13.8	0	0	0.03236	0.64639	0	0	1	1	0	0
CPD230	CPD-U1	0	0	0.0029	0.07485	0	0	1	1	0	0
CPD230	CPD-U2	0	0	0.0029	0.07485	0	0	1	1	0	0
CPT230	CPT-U1	0	0	0.00577	0.04528	0	0	1	1	0	0
CPT230	CPT-U2	0	0	0.0029	0.07485	0	0	1	1	0	0
CPU161	CPU-U1	0	0	0.00976	0.1724	0	0	1	1	0	0
CPU161	CPU-U2	0	0	0.00976	0.17167	0	0	1	1	0	0
CPU161	CPU-U3	0	0	0.00976	0.17703	0	0	1	1	0	0
CPU161	CPU-U4	0	0	0.00976	0.17631	0	0	1	1	0	0
CPU161	CPU-U5	0	0	0.01	0.29554	0	0	1	1	0	0
CRO161	CRO15.0	0	0	0.01666	0.36787	0	0	1	1	0	0
CRO161	CRO15.0	0	0	0.01666	0.3501	0	0	1	1	0	0
CRO161	CRO34.5	0	0	0.01428	0.26414	0	0	1	1	0	0
CRO161	CRO34.5	0	0	0.01428	0.27829	0	0	1	1	0	0
CTY161	CTY15.0	0	0	0.01433	0.5	0	0	1	1	0	0
CTY161	CTY34.5	0	0	0.01	0.43563	0	0	1	1	0	0
CTY230	CTY13.8	0	0	0.04045	0.49209	0	0	1	1	0	0
CTY230	CTY13.8	0	0	0.04045	0.49209	0	0	1	1	0	0
CTY230	CTY161	0	0	0.002	0.11498	0	0	1	1	0	0
EDA69.0	EDA13.8	0	0	0.01723	0.34407	0	0	1	1	0	0
EDA69.0	EDA13.8	0	0	0.01723	0.34407	0	0	1	1	0	0
GER69.0	GER13.8	0	0	0.03572	0.7135	0	0	1	1	0	0
GER69.0	GER13.8	0	0	0.0366	0.73108	0	0	1	1	0	0
GLL69.0	GLL13.8	0	0	0.02656	0.53045	0	0	1	1	0	0
GLL69.0	GLL13.8	0	0	0.02656	0.53045	0	0	1	1	0	0
HGO161	HGO15.0	0	0	0.02	0.4972	0	0	1	1	0	0
HGO161	HGO15.0	0	0	0.02	0.4972	0	0	1	1	0	0
HMO69.0	HMO13.8	0	0	0.01427	0.2851	0	0	1	1	0	0
HMO69.0	HMO13.8	0	0	0.01427	0.2851	0	0	1	1	0	0
INA69.0	INA13.8	0	0	0.01906	0.38074	0	0	1	1	0	0
INA69.0	INA13.8	0	0	0.01906	0.38074	0	0	1	1	0	0
JAT69.0	JAT13.8	0	0	0	0.488	0	0	1	1	0	0
LGO69.0	LGO13.8	0	0	0.0197	0.39536	0	0	1	1	0	0
LGO69.0	LGO13.8	0	0	0.0197	0.39536	0	0	1	1	0	0
LMS69.0	LMS13.8	0	0	0.0255	0.50953	0	0	1	1	0	0
LMS69.0	LMS13.8	0	0	0.02051	0.40983	0	0	1	1	0	0
LMS69.0	LMS15.0	0	0	0.01736	0.33825	0	0	1	1	0	0
MSN69.0	MSN13.8	0	0	0	0.06036	0	0	1	1	0	0

MSN69.0	MSN13.8	0	0	0	0.06036	0	0	1	1	0	0
MTR69.0	MTR13.8	0	0	0.0366	0.53448	0	0	1	1	0	0
MTR69.0	MTR13.8	0	0	0.0366	0.53448	0	0	1	1	0	0
MTR69.0	MTR13.8	0	0	0.2051	0.40983	0	0	1	1	0	0
MTR230	MTR69.0	0	0	0	0.05226	0	0	1	1	0	0
MXC69.0	MXC13.8	0	0	0.02165	0.43252	0	0	1	1	0	0
MXC69.0	MXC13.8	0	0	0.01726	0.3448	0	0	1	1	0	0
MXI161	MXI34.5	0	0	0.01066	0.29713	0	0	1	1	0	0
MXI161	MXI34.5	0	0	0.01066	0.27739	0	0	1	1	0	0
MXI161	MXI34.5	0	0	0.01066	0.27712	0	0	1	1	0	0
MXI230	MXI13.8	0	0	0.01	0.49209	0	0	1	1	0	0
MXI230	MXI161	0	0	0.002	0.05356	0	0	1	1	0	0
MXI230	MXI161	0	0	0.002	0.05356	0	0	1	1	0	0
MXI230	MXI161	0	0	0.002	0.05356	0	0	1	1	0	0
MXI-U1	MXI34.5	0	0	0	0.22309	0	0	1	1	0	0
MXI-U2	MXI34.5	0	0	0	0.22571	0	0	1	1	0	0
MXI-U3	MXI34.5	0	0	0	0.1115	0	0	1	1	0	0
NZI161	NZI15.0	0	0	0.02	0.41376	0	0	1	1	0	0
NZI161	NZI15.0	0	0	0.02	0.41426	0	0	1	1	0	0
ONG69.0	ONG13.8	0	0	0	0.392	0	0	1	1	0	0
OZA230	OZA13.8	0	0	0.04045	0.49209	0	0	1	1	0	0
OZA230	OZA13.8	0	0	0.04045	0.49209	0	0	1	1	0	0
PAP230	PAP69.0	0	0	0	0.05226	0	0	1	1	0	0
PTN69.0	PTN13.8	0	0	0	0.7304	0	0	1	1	0	0
PNM69.0	PNM13.8	0	0	0.02723	0.54401	0	0	1	1	0	0
POP69.0	POP13.8	0	0	0.05016	0.002	0	0	1	1	0	0
RII69.0	RII13.8	0	0	0.02165	0.43252	0	0	1	1	0	0
RII69.0	RII13.8	0	0	0.01811	0.36181	0	0	1	1	0	0
RIN161	RIN15.0	0	0	0.02	0.41552	0	0	1	1	0	0
RIN161	RIN15.0	0	0	0.02	0.41982	0	0	1	1	0	0
RUM230	RUM69.0	0	0	0.00183	0.05517	0	0	1	1	0	0
RZC161	RZC34.5	0	0	0.0225	0.39385	0	0	1	1	0	0
RZC161	RZC34.5	0	0	0.0225	0.43291	0	0	1	1	0	0
RZC161	RZC34.5	0	0	0.0275	0.42411	0	0	1	1	0	0
RZC161	RZC34.5	0	0	0.0225	0.43291	0	0	1	1	0	0
SAF115	SAF13.8	0	0	0.05558	0.1101	0	0	1	1	0	0
SAF115	SAF13.8	0	0	0.06154	0.2293	0	0	1	1	0	0
SAZ115	SAZ69.0	0	0	0	0.38477	0	0	1	1	0	0
SAZ69.0	SAZ13.8	0	0	0	0.536	0	0	1	1	0	0
SIM115	SIM34.5	0	0	0.02504	0.50017	0	0	1	1	0	0
SQN115	SQN34.5	0	0	0.05008	0.0003	0	0	1	1	0	0
SQN115	SQN34.5	0	0	0.03659	0.73103	0	0	1	1	0	0
STB230	STB13.8	0	0	0.04045	0.49209	0	0	1	1	0	0
SVE115	SVE34.5	0	0	0.05008	0.0003	0	0	1	1	0	0
TCT69.0	TCT13.8	0	0	0.05075	0.0136	0	0	1	1	0	0
TCT69.0	TCT13.8	0	0	0.05075	0.0136	0	0	1	1	0	0
TCT69.0	TCT13.8	0	0	0.05075	0.0136	0	0	1	1	0	0
TEK230	TEK13.8	0	0	0.04	0.49	0	0	1	1	0	0
TEK230	TEK13.8	0	0	0.04	0.49	0	0	1	1	0	0

TEK230	TEK34.5	0	0	0.01692	0.33798	0	0	1	1	0	0
WIA230	WIA13.8	0	0	0	0.4833	0	0	1	1	0	0
TJI230	TJI69.0	0	0	0.002	0.05226	0	0	1	1	0	0
TJI230	TJI69.0	0	0	0.002	0.05146	0	0	1	1	0	0
TJI230	FICT69.0	0	0	0	0.08	0	0	1	1	0	0
TJI69.0	TJI13.8	0	0	0.07832	0.5644	0	0	1	1	0	0
TRI115	TRI13.8	0	0	0.05533	0.1053	0	0	1	1	0	0
TTJ230	PJZ-U1	0	0	0.00185	0.06179	0	0	1	1	0	0
TTJ230	PJZ-U2	0	0	0.00185	0.06179	0	0	1	1	0	0
TTJ230	TTJ69.0	0	0	0.008	0.26868	0	0	1	1	0	0
TTJ230	TTJ69.0	0	0	0.008	0.27088	0	0	1	1	0	0
TTJ230	TTJ-U1	0	0	0.004	0.14381	0	0	1	1	0	0
TTJ230	TTJ-U2	0	0	0.004	0.14575	0	0	1	1	0	0
TTJ230	TTJ-U3	0	0	0.004	0.14633	0	0	1	1	0	0
TTJ230	TTJ-U4	0	0	0.00347	0.135	0	0	1	1	0	0
TTJ-U5	TTJ69.0	0	0	0	0.19476	0	0	1	1	0	0
TTJ-U6	TTJ69.0	0	0	0	0.19476	0	0	1	1	0	0
CIP-U1	CIP69.0	0	0	0	0.19476	0	0	1	1	0	0
CIP-U2	CIP69.0	0	0	0	0.19476	0	0	1	1	0	0
UND69.0	UND13.8	0	0	0.01964	0.39232	0	0	1	1	0	0
UND69.0	UND13.8	0	0	0.01964	0.39232	0	0	1	1	0	0
VLP69.0	VLP13.8	0	0	0	0.89066	0	0	1	1	0	0
VPM69.0	VPM13.8	0	0	0	0.648	0	0	1	1	0	0
PBO69.0	PBO4.16	0	0	0	0.0304	0	0	1	1	0	0
PBU69.0	PBU4.16	0	0	0	0.0304	0	0	1	1	0	0
PBD69.0	PBD4.16	0	0	0	0.0304	0	0	1	1	0	0
PBT69.0	PBT4.16	0	0	0	0.0224	0	0	1	1	0	0
PBC69.0	PBC4.16	0	0	0	0.53	0	0	1	1	0	0
PBQ69.0	PBQ4.16	0	0	0	0.53	0	0	1	1	0	0
IV500	IV230	0	0	0.0003	0.02394	0	0	1	1	0	0
IV500	IV-U1	0	0	0	0.001	0	0	1	1	0	0
ML500	ML-U1	0	0	0	0.001	0	0	1	1	0	0
ML500	ML230	0	0	0.00012	0.01261	0	0	1	1	0	0

TABLE A.14: Generators (regulators).

Bus	V_i (p.u.)	P_{G_set} (MW)	Q_{G_set} (MVAR)	P_R (p.u.)	R (p.u.)	a_Q	b_Q
PJZ-U1	1.00	-114.878	9.55995	1.0	0.04	1.0	1.0

TABLE A.15: Generators (PV).

Bus	V_i (p.u.)	P_G (MW)	Q_{Gmax} (MVARs)	Q_{Gmin} (MVARs)
CIP-U1	1	27.5	9	-9
CIP-U2	1	27.5	9	-9
CPD-U1	1	109.9	40	-30
CPD-U2	1	109.9	40	-30
CPT-U1	1	109.9	40	-30
CPT-U2	1	109.9	40	-30
CPU-U1	1	37.5	12	-10
CPU-U2	1	37.5	12	-10
CPU-U3	1	37.5	12	-10
CPU-U4	1	37.5	12	-10
CPU-U5	1	20	12	-10
MXI-U1	1	26	8	-8
MXI-U2	1	18	6	-6
MXI-U3	1	18	6	-6
PJZ-U2	1	159.9	60	-50
TTJ-U1	1	74.99	30	-25
TTJ-U2	1	74.99	30	-25
TTJ-U3	1	74.99	30	-25
TTJ-U4	1	74.99	30	-25
TTJ-U5	1	30	10	-10
TTJ-U6	1	30	10	-10
IV-U1	1	380	500	-500
ML-U1	1	380	500	-500

TABLE A.16: Shunt Fixed VAR Compensators.

Bus	G_{shunt} (p.u.)	B_{shunt} (p.u.)
CHA34.5	0	0.12
TEK34.5	0	0.12
HGO15.0	0	0.12
APD13.8	0	0.12
UND13.8	0	0.1
TEK13.8	0	0.12
STB13.8	0	0.08
RZC34.5	0	0
RIN15.0	0	0.12
RII13.8	0	0.08
PNM13.8	0	0.1
OZA13.8	0	0.12
NZI15.0	0	0.12
MXI13.8	0	0.08
MXC13.8	0	0.08
LMS13.8	0	0.12
INA13.8	0	0.12
HMO13.8	0	0.12
GER13.8	0	0.1
CTY13.8	0	0.12
CTY34.5	0	0
CRO34.5	0	0
CRO15.0	0	0.12
CNA13.8	0	0.1

Table A.17: Conventional Loads.

Bus	P_{LOAD} (MW)	Q_{LOAD} (MVAR)	Bus	P_{LOAD} (MW)	Q_{LOAD} (MVAR)
AMO69.0	2.49	0.8184	ONG13.8	2.49	0.8184
APD13.8	39.01	12.822	OZA13.8	32.37	10.6395
BAO69.0	0.83	0.2728	PB169.0	1.66	0.5456
CEC69.0	8.3	2.7281	PBD4.16	4.98	1.6368
CES69.0	2.49	0.8184	PBO4.16	4.98	1.6368
CHA34.5	19.09	6.2746	PBT4.16	4.98	1.6368
CIP13.8	4.98	1.6368	PBU4.16	4.98	1.6368
CNA13.8	16.6	5.4562	PCH115	1.66	0.5456
CPU161	4.98	1.6368	PNM13.8	14.94	4.9105
CRO15.0	38.18	12.5492	POP13.8	12.45	4.0921
CRO34.5	33.2	10.9123	PTE115	3.32	1.0912
CTY13.8	23.24	7.6386	PTN13.8	2.49	0.8184
CTY15.0	5.81	1.9097	RII13.8	24.07	7.9114
CTY34.5	19.09	6.2746	RIN15.0	19.92	6.5474
EDA13.8	15.77	5.1833	RZC34.5	48.14	15.8229
EDA69.0	0.83	0.2728	SAF13.8	4.98	1.6368
EPE115	2.49	0.8184	SAZ13.8	3.32	1.0912
FAM69.0	2.49	0.8184	SDE69.0	2.49	0.8184
FLO13.8	4.15	1.364	SIC230	34.86	11.4579
GER13.8	20.75	6.8202	SIM34.5	1.66	0.5456
GLL13.8	16.6	5.4562	SQN34.5	4.98	1.6368
HGO15.0	31.54	10.3667	STB13.8	12.45	4.0921
HMO13.8	27.39	9.0027	SVE34.5	1.66	0.5456
INA13.8	32.37	10.6395	TCT13.8	14.94	4.9105
JAT13.8	1.66	0.5456	TEK13.8	27.39	9.0027
LGO13.8	14.11	4.6377	TEK34.5	28.22	9.2755
LMS13.8	21.58	7.093	TJI13.8	5.81	1.9097
LMS15.0	4.15	1.364	TRA69.0	1.66	0.5456
MND69.0	4.98	1.6368	TRI13.8	2.49	0.8184
MSN13.8	0.83	0.2728	UND13.8	14.11	4.6377
MTR13.8	16.6	5.4562	VLP13.8	2.49	0.8184
MTX69.0	0.83	0.2728	VPM13.8	1.66	0.5456
MXC13.8	21.58	7.093	WIA13.8	6.64	2.1825
MXI13.8	14.94	4.9105	IV500	257.3	84.5704
MXI34.5	49.8	16.3685	ML500	705.5	231.8866
NZI15.0	34.03	11.1851			

A.4 14-bus system

Table A.18: Transmission Lines.

Sending Bus	Receiving Bus	R (p.u.)	X_L (p.u.)	B_{total} (p.u.)
1	2	0.01938	0.05917	0.0528
1	5	0.05403	0.22304	0.0492
2	3	0.04699	0.19797	0.0438
2	4	0.05811	0.17632	0.034
2	5	0.05695	0.17388	0.0346
3	4	0.06701	0.17103	0.0128
4	5	0.01335	0.04211	0
6	11	0.09498	0.1989	0
6	12	0.12291	0.25581	0
6	13	0.06615	0.13027	0
7	8	0	0.17615	0
7	9	0	0.11001	0
9	10	0.03181	0.0845	0
9	14	0.12711	0.27038	0
10	11	0.08205	0.19207	0
12	13	0.22092	0.19988	0
13	14	0.17093	0.34802	0

Table A.19: Transformers.

Sending Bus	Receiving Bus	R_p (p.u.)	X_p (p.u.)	R_s (p.u.)	X_s (p.u.)	G_0 (p.u.)	B_0 (p.u.)	T_v (p.u.)	T_i (p.u.)	U_v (°)	U_i (°)
4	7	0	0	0	0.20912	0	0	0.978	1	0	0
4	9	0	0	0	0.55618	0	0	0.969	1	0	0
5	6	0	0	0	0.25202	0	0	0.932	1	0	0

Table A.20: Conventional Loads.

Bus	P_{LOAD} (MW)	Q_{LOAD} (MVAR)
1	0	0
2	21.7	12.7
3	94.2	19
4	47.8	-3.9
5	7.6	1.6
6	11.2	7.5
7	0	0
8	0	0
9	29.5	16.6
10	9	5.8
11	3.5	1.8
12	6.1	1.6
13	13.5	5.8
14	14.9	5

Table A.21: Generators (PV).

Bus	V_i (p.u.)	P_G (MW)	Q_{Gmax} (MVARs)	Q_{Gmin} (MVARs)
2	1.045	40	800	-800
3	1.010	0	800	-800
6	1.070	0	800	-800
8	1.090	0	800	-800

Table A.22: Generators (regulators).

Bus	V_i (p.u.)	P_{G_set} (MW)	Q_{G_set} (MVAR)	P_R (p.u.)	R (p.u.)	a_Q	b_Q
1	1.06	232.393272	-16.5493	1	0.04	1	1

Table A.23: Shunt Fixed VAR Compensators.

Bus	G_{shunt} (p.u.)	B_{shunt} (p.u.)
9	0	0.19

A.5 190-bus system

Table A.24: Transmission lines.

Sending Bus	Receiving Bus	R (p.u.)	X_L (p.u.)	B_{total} (p.u.)	Sending Bus	Receiving Bus	R (p.u.)	X_L (p.u.)	B_{total} (p.u.)
48	49	0.00067	0.00859	0.9714	113	102	0.00089	0.01132	1.286
49	50	0.00052	0.00633	0.7192	103	102	0.0004	0.0042	0.128
50	52	0.00091	0.01127	2.96352	59	103	0.0006	0.0065	0.1993
52	51	0.00001	-0.00338	0	110	115	0.00377	0.05243	1.48916
49	56	0.0043	0.0532	1.6678	114	115	0.00168	0.02145	0.60924
49	56	0.0043	0.0532	1.6678	118	114	0.00048	0.0062	0.17538
57	53	0.0029	0.0354	1.0954	118	124	0.00393	0.05013	1.41666
57	53	0.0029	0.0354	1.0954	118	189	0.00131	0.01688	0.47382
57	56	0.00001	-0.00832	0	118	120	0.00392	0.05027	1.4166
51	55	0.0041	0.0552	1.444	114	120	0.0044	0.0569	1.5841
51	55	0.0041	0.0552	1.444	120	115	0.00344	0.04409	1.24548
53	55	0.00001	-0.01297	0	121	115	0.00196	0.02502	0.71074
53	69	0.00209	0.0287	2.843	127	121	0.00234	0.02979	0.84612
70	83	0.00617	0.03805	0.28754	116	117	0.0015	0.00965	0.313
69	64	0.00001	-0.01349	0	116	190	0.00173	0.01161	0.35164
53	73	0.0076	0.1062	0.6574	114	189	0.00094	0.01192	0.33844
53	73	0.0076	0.1062	0.6574	189	124	0.00377	0.0429	1.21842
71	73	0.00001	-0.0249	0	118	127	0.0043	0.0549	1.55158
71	74	0.00001	-0.0124	0	119	117	0.00086	0.0058	0.1758
71	64	0.00075	0.092	0.2688	127	122	0.0173	0.11609	0.21978
74	59	0.00249	0.0317	0.90026	119	122	0.02464	0.1653	0.31298
59	92	0.00064	0.0078	0.2284	127	130	0.00153	0.02076	0.5869

59	92	0.00064	0.0078	0.2284	130	89	0.00308	0.03938	1.11308
64	78	0.0017	0.023	0.591	128	126	0.0056	0.0372	0.28064
64	78	0.0017	0.023	0.591	128	123	0.0035	0.02325	0.04384
75	89	0.0041	0.053	1.5312	123	126	0.01092	0.07254	0.13682
75	86	0.004	0.0526	1.5176	126	125	0.00755	0.05022	0.37884
75	86	0.004	0.0526	1.5176	125	129	0.01036	0.06882	0.5192
75	84	0.0028	0.0345	1.008	128	131	0.0134	0.0785	0.1427
75	77	0.00138	0.01764	0.5009	128	132	0.00699	0.0411	0.0747
77	78	0.0048	0.0577	1.596	131	129	0.1302	0.08646	0.65248
77	78	0.0048	0.0577	1.596	133	132	0.01315	0.08822	0.16704
89	78	0.00075	0.00905	1.0858	117	190	0.00346	0.02322	0.17584
87	80	0.03149	0.11127	0.46454	136	134	0.0298	0.2023	0.3888
80	76	0.00069	0.00464	0.0088	134	135	0.00001	-0.0668	0
80	81	0.00966	0.06417	0.12102	135	138	0.0257	0.17354	0.33686
81	68	0.0168	0.1116	0.21048	138	137	0.0018	0.01207	0.09144
68	65	0.007	0.0465	0.0967	158	141	0.00593	0.07556	2.14576
68	72	0.01758	0.11794	0.2233	138	140	0.00161	0.01096	0.08508
68	88	0.0126	0.0837	0.15786	139	140	0.00189	0.01279	0.02482
68	96	0.01512	0.10044	0.18942	157	155	0.0032	0.05293	0.10022
97	96	0.0072	0.0567	0.4608	137	139	0.0035	0.0233	0.0408
97	76	0.00678	0.04551	0.34462	139	188	0.0146	0.0973	0.1834
82	76	0.01245	0.0836	0.15824	188	187	0.00001	-0.0668	0
85	83	0.0056	0.0372	0.28064	137	142	0.02044	0.13578	1.02428
83	54	0.00805	0.04965	0.37512	143	148	0.00276	0.01857	0.56264
82	81	0.0049	0.03255	0.06136	143	144	0.02411	0.16065	0.3049
82	68	0.0154	0.10235	0.19296	148	153	0.00401	0.02693	0.05098
84	64	0.00417	0.05129	1.4984	142	143	0.00471	0.03158	0.2393
84	71	0.00398	0.05084	1.4369	146	153	0.0063	0.04225	0.32
182	86	0.00155	0.02335	2.0544	148	149	0.00235	0.01579	0.0299
182	185	0.00458	0.0584	1.6584	149	153	0.00235	0.01579	0.0299
185	184	0.00198	0.02527	0.7175	146	151	0.00498	0.03023	0.23068
184	182	0.0073	0.093	0.66	151	150	0.00102	0.0068	0.05124
184	182	0.0073	0.093	0.66	151	152	0.00789	0.05229	0.10422
78	92	0.00035	0.0044	0.5286	152	150	0.00318	0.02136	0.04044
89	98	0.0005	0.00615	0.7374	157	154	0.00899	0.06036	0.11428
90	109	0.0105	0.06975	0.13154	154	155	0.0011	0.00743	0.01406
90	131	0.0213	0.1263	0.2354	154	187	0.0146	0.0993	0.1925
88	96	0.00146	0.00878	0.0735	157	160	0.00168	0.01116	0.0842
88	79	0.0046	0.0347	0.0702	158	159	0.00045	0.00572	0.16244
91	79	0.0022	0.0165	0.0334	185	183	0.00073	0.0093	0.26398
91	90	0.0021	0.01345	0.10524	158	183	0.0056	0.00715	0.20306
93	96	0.0043	0.0344	0.0691	169	158	0.00169	0.0207	2.4192
93	62	0.0015	0.012	0.027	170	144	0.01324	0.16869	0.52368
93	95	0.0037	0.0305	0.0735	170	168	0.00104	0.00697	0.05274
93	94	0.0013	0.0104	0.023	163	169	0.00186	0.02288	2.67456
94	96	0.003	0.0242	0.054	164	161	0.0021	0.0189	0.1055
96	131	0.0308	0.1771	0.3586	161	167	0.00518	0.03441	0.25956
98	102	0.0002	0.00265	0.32	167	168	0.01554	0.10323	0.1947
100	96	0.00125	0.0102	0.092	168	160	0.0259	0.17205	0.32448

100	109	0.0025	0.0194	0.04	164	171	0.0119	0.07905	0.59636
100	101	0.00196	0.01302	0.02456	164	161	0.00291	0.0195	0.03692
101	109	0.00154	0.01023	0.0193	172	173	0.0049	0.01792	0.0444
67	107	0.00854	0.05673	0.42796	172	174	0.0785	0.28669	0.07122
107	106	0.00854	0.05673	0.42796	173	174	0.0761	0.3091	0.076
107	108	0.00147	0.01874	0.23272	181	174	0.01298	0.434	0.1116
106	72	0.01805	0.11135	0.21034	178	176	0.005	0.02949	0.03182
106	60	0.00374	0.02508	0.18988	177	175	0.00166	0.01114	0.0844
62	60	0.0016	0.0123	0.0257	174	178	0.03655	0.14195	0.152
61	60	0.0015	0.0114	0.02302	186	177	0.03192	0.21204	0.39992
95	60	0.0029	0.0219	0.045	185	159	0.00056	0.00715	0.20306
65	72	0.00226	0.01392	0.10516	160	186	0.00335	0.00645	0.0144
106	104	0.00917	0.05985	0.11306	165	166	0.00108	0.0139	3.5526
104	109	0.00364	0.02418	0.0456	165	163	0.00006	0.00071	0.0203
63	109	0.00194	0.01478	0.0298	159	166	0.0014	0.01779	2.0304
63	61	0.0008	0.0065	0.013	185	159	0.00301	0.03837	1.0898
63	60	0.0043	0.033	0.0674	179	186	0.0045	0.0085	0.194
110	113	0.00229	0.02921	3.31676	53	47	0.00001	0.001	0
110	111	0.00112	0.0143	0.40614					

TABLE A.25: Transformers.

Sending Bus	Receiving Bus	R_p (p.u.)	X_p (p.u.)	R_s (p.u.)	X_s (p.u.)	G_0 (p.u.)	B_0 (p.u.)	T_v (p.u.)	T_i (p.u.)	U_v (°)	U_i (°)
48	2	0	0	0.0001	0.0057	0	0	1	1	0	0
49	1	0	0	0.0001	0.0065	0	0	1	1	0	0
50	3	0	0	0.0001	0.0042	0	0	1	1	0	0
50	6	0	0	0.0001	0.0157	0	0	1	1	0	0
56	58	0	0	0.0001	0.0291	0	0	1	1	0	0
53	54	0	0	0.0001	0.0275	0	0	0.975	1	0	0
59	60	0	0	0.0001	0.0145	0	0	0.97	1	0	0
64	65	0	0	0.0001	0.0291	0	0	1.025	1	0	0
64	66	0	0	0.0001	0.017	0	0	0.97	1	0	0
75	76	0	0	0.0001	0.0095	0	0	1	1	0	0
77	4	0	0	0.0001	0.0082	0	0	1	1	0	0
84	85	0	0	0.0001	0.0275	0	0	0.96	1	0	0
86	87	0	0	0.0001	0.0137	0	0	0.98	1	0	0
80	43	0	0	0.0001	0.0726	0	0	1	1	0	0
81	44	0	0	0.0001	0.077	0	0	1	1	0	0
83	46	0	0	0.0001	0.0462	0	0	1	1	0	0
84	5	0	0	0.0001	0.016	0	0	1	1	0	0
86	18	0	0	0.0001	0.0164	0	0	1	1	0	0
78	88	0	0	0.0001	0.0275	0	0	0.97	1	0	0
89	90	0	0	0.0001	0.0065	0	0	0.98	1	0	0
89	7	0	0	0.0001	0.0164	0	0	1	1	0	0
90	8	0	0	0.0001	0.0331	0	0	1	1	0	0
90	9	0	0	0.0001	0.0098	0	0	1	1	0	0
92	93	0	0	0.0001	0.0111	0	0	0.97	1	0	0
96	10	0	0	0.0001	0.0131	0	0	1	1	0	0
97	11	0	0	0.0001	0.0505	0	0	1	1	0	0
105	12	0	0	0.0001	0.0426	0	0	1	1	0	0
104	105	0	0	0.0001	0.087	0	0	1	1	0	0

98	100	0	0	0.0001	0.0111	0	0	0.98	1	0	0
100	99	0	0	0.0001	0.0435	0	0	1	1	0	0
99	13	0	0	0.0001	0.0389	0	0	1	1	0	0
99	14	0	0	0.0001	0.0999	0	0	1	1	0	0
102	109	0	0	0.0001	0.0062	0	0	0.98	1	0	0
108	45	0	0	0.0001	0.0084	0	0	1	1	0	0
71	72	0	0	0.0001	0.0291	0	0	0.98	1	0	0
110	15	0	0	0.0001	0.011	0	0	1	1	0	0
111	16	0	0	0.0001	0.0326	0	0	1	1	0	0
110	112	0	0	0.0001	0.017	0	0	1	1	0	0
112	17	0	0	0.0001	0.0172	0	0	1	1	0	0
114	116	0	0	0.0001	0.011	0	0	1	1	0	0
121	122	0	0	0.0001	0.019	0	0	0.98	1	0	0
122	23	0	0	0.0001	0.062	0	0	1	1	0	0
118	119	0	0	0.0001	0.011	0	0	1	1	0	0
189	190	0	0	0.0001	0.019	0	0	1	1	0	0
127	128	0	0	0.0001	0.011	0	0	0.98	1	0	0
130	131	0	0	0.0001	0.019	0	0	0.98	1	0	0
128	19	0	0	0.0001	0.0101	0	0	1	1	0	0
133	21	0	0	0.0001	0.0628	0	0	1	1	0	0
117	22	0	0	0.0001	0.0344	0	0	1	1	0	0
129	24	0	0	0.0001	0.0163	0	0	1	1	0	0
124	125	0	0	0.0001	0.011	0	0	1	1	0	0
131	20	0	0	0.0001	0.0661	0	0	1	1	0	0
136	25	0	0	0.0001	0.0325	0	0	1	1	0	0
141	140	0	0	0.0001	0.019	0	0	1	1	0	0
138	27	0	0	0.0001	0.0314	0	0	1	1	0	0
137	26	0	0	0.0001	0.052	0	0	1	1	0	0
151	31	0	0	0.0001	0.0314	0	0	1	1	0	0
146	147	0	0	0.0001	0.0173	0	0	0.98	1	0	0
143	145	0	0	0.0001	0.0385	0	0	1	1	0	0
145	29	0	0	0.0001	0.1089	0	0	1	1	0	0
143	30	0	0	0.0001	0.0314	0	0	1	1	0	0
158	156	0	0	0.0001	0.0339	0	0	0.98	1	0	0
169	170	0	0	0.0001	0.021	0	0	0.98	1	0	0
158	157	0	0	0.0001	0.021	0	0	0.97	1	0	0
181	180	0	0	0.0001	0.051	0	0	0.99	1	0	0
171	172	0	0	0.0001	0.0231	0	0	1	1	0	0
28	174	0	0	0.0001	0.041	0	0	1	1	0	0
177	178	0	0	0.0001	0.0268	0	0	0.98	1	0	0
176	41	0	0	0.0001	0.1145	0	0	1	1	0	0
162	42	0	0	0.0001	0.15	0	0	1	1	0	0
161	162	0	0	0.0001	0.0516	0	0	1	1	0	0
175	40	0	0	0.0001	0.0316	0	0	1	1	0	0
175	176	0	0	0.0001	0.046	0	0	1	1	0	0
164	37	0	0	0.0001	0.0198	0	0	1	1	0	0
163	38	0	0	0.0001	0.015	0	0	1	1	0	0
165	39	0	0	0.0001	0.0082	0	0	1	1	0	0
163	164	0	0	0.0001	0.021	0	0	1	1	0	0
180	32	0	0	0.0001	0.028	0	0	1	1	0	0
180	33	0	0	0.0001	0.028	0	0	1	1	0	0
185	186	0	0	0.0001	0.0104	0	0	0.97	1	0	0
186	34	0	0	0.0001	0.0282	0	0	1	1	0	0
120	35	0	0	0.0001	0.0108	0	0	1	1	0	0
120	36	0	0	0.0001	0.0163	0	0	1	1	0	0

TABLE A.26: Generators (PV).

Bus	V_i (p.u.)	P_G (MW)	Q_G (MW)	Q_{Gmax} (MVARs)	Q_{Gmin} (MVARs)
1	1.03	1500	166.46	8000	-8000
2	1.03	900	61.67	8000	-8000
3	1.03	1000	231.5	8000	-8000
4	1.03	1330	253.14	8000	-8000
5	1.03	650	110.05	8000	-8000
6	1.03	400	68.54	8000	-8000
7	1.0159	500	196.71	8000	-8000
8	1.03	200	62.11	8000	-8000
9	1.03	900	225.75	8000	-8000
10	1.01	450	244.19	8000	-8000
11	1.03	100	35.1	8000	-8000
12	0.986	150	100.12	8000	-8000
13	1.02	100	50.05	8000	-8000
14	1.02	50	19.97	8000	-8000
15	1.03	920	172.91	8000	-8000
16	1.03	200	66.23	8000	-8000
17	1.03	190	75.89	8000	-8000
18	1.03	500	184.9	8000	-8000
19	1.018	450	214.97	8000	-8000
20	1.03	150	73.9	8000	-8000
21	1.03	100	34.29	8000	-8000
22	1	240	68.01	8000	-8000
23	1.0101	170	48.05	8000	-8000
24	1.03	600	206.77	8000	-8000
25	1.04	180	21.2	8000	-8000
26	1.03	140	26.18	8000	-8000
27	1.03	300	31.89	8000	-8000
28	1.04	31	25.75	8000	-8000
29	1.03	91	29.53	8000	-8000
30	1.03	290	92.64	8000	-8000
31	1.03	300	125.3	8000	-8000
32	1.01	247.5	54.15	8000	-8000
33	1.01	247.5	54.15	8000	-8000
34	1.03	308	-30.56	8000	-8000
35	1.03	900	127.75	8000	-8000
37	1.03	638	56.53	8000	-8000
38	1.03	638	49.92	8000	-8000
39	1.03	1100	78.71	8000	-8000
40	1.01	290	47.33	8000	-8000
41	1.01	60	6.54	8000	-8000
42	1.02	30	13.63	8000	-8000
43	1.03	110	26.76	8000	-8000
44	1.01	200	26.05	8000	-8000
45	1.03	500	154.16	8000	-8000
46	1.02	230	117.5	8000	-8000

Table A.27: Generators (regulators).

Bus	V_i (p.u.)	P_{G_set} (MW)	Q_{G_set} (MVAR)	P_R (p.u.)	R (p.u.)	a_Q	b_Q
36	1.03	300.543	40.6295	1	0.04	1	1

Table A.28: Conventional Loads.

Bus	P_{LOAD} (MW)	Q_{LOAD} (MVAR)	Bus	P_{LOAD} (MW)	Q_{LOAD} (MVAR)
47	0	-96.63	125	480	140
48	133	43	126	285	83
49	128	42	128	167	49
50	381	125	129	465	155
51	624	205	131	527	154
58	265	87	132	251	73
61	85	28	135	155	51
62	105	34.4	137	223	74
63	169	56	138	58	19
65	89	29	139	98	32
66	400	131	140	59	19
67	265	87	142	171	54
68	100	33	143	39	13
70	234	77	145	80	26
71	162	55	147	100	34
72	158	52	148	125	41
77	80	27	149	50	17
79	81	27	150	181	64
80	180	59	151	18	6
81	142	47	152	166	55
83	504	166	153	75	25
84	60	20	154	97	32
86	190	62	155	72	24
87	455	149	156	158	53
89	30	10	160	152	51
91	202	67	162	139	46
93	562	185	163	50	17
94	167	55	164	50	17
95	71	23	165	68	32
96	741	270	167	65	21
100	392	129	168	147	48
101	80	26	170	57	19
103	620	204	172	25	8
105	290	95	173	91	30
106	217	72	174	25	8
108	38	13	175	140	46
109	584	192	176	38	13
111	556	74	178	112	37
112	207	60	179	110	37
113	268	88	180	455	152
116	296	86	182	66	22
117	296	86	183	212	71
119	296	86	184	62	20
120	297	87	186	80	26
122	421	123	190	296	86
123	197	57			

TABLE A.29: Shunt Fixed VAR Compensators.

Bus	G_{shunt} (p.u.)	B_{shunt} (p.u.)	Bus	G_{shunt} (p.u.)	B_{shunt} (p.u.)
49	0	-2	121	0	-0.5
51	0	-0.35	127	0	-1
59	0	-0.7	150	0	0.6
64	0	-0.62	158	0	-1.25
65	0	1.5	159	0	-1
71	0	-0.62	160	0	0.2
75	0	-1	163	0	-1.5
77	0	-1.5	165	0	-1.24
86	0	-2.48	166	0	-1
89	0	-0.5	169	0	-1.5
110	0	-2.25	180	0	0.6
114	0	-1.37	182	0	-2
118	0	-0.62	185	0	-0.5

A.6 30-bus system

TABLE A.30: Transmission Lines.

Sending Bus	Receiving Bus	R (p.u.)	X_L (p.u.)	B_{total} (p.u.)	Sending Bus	Receiving Bus	R (p.u.)	X_L (p.u.)	B_{total} (p.u.)
1	2	0.0192	0.0575	0.0528	18	19	0.0639	0.1292	0
1	3	0.0452	0.1652	0.0408	19	20	0.034	0.068	0
2	4	0.057	0.1737	0.0368	10	20	0.0936	0.209	0
3	4	0.0132	0.0379	0.0084	10	17	0.0324	0.0845	0
2	5	0.0472	0.1983	0.0418	10	21	0.0348	0.0749	0
2	6	0.0581	0.1763	0.0374	10	22	0.0727	0.1499	0
4	6	0.0119	0.0414	0.009	21	22	0.0116	0.0236	0
5	7	0.046	0.116	0.0204	15	23	0.1	0.202	0
6	7	0.0267	0.082	0.017	22	24	0.115	0.179	0
6	8	0.012	0.042	0.009	23	24	0.132	0.27	0
9	11	0	0.208	0	24	25	0.1885	0.3292	0
9	10	0	0.11	0	25	26	0.2544	0.38	0
12	13	0	0.14	0	25	27	0.1093	0.2087	0
12	14	0.1231	0.2559	0	27	29	0.2198	0.4153	0
12	15	0.0662	0.1304	0	27	30	0.3202	0.6027	0
12	16	0.0945	0.1987	0	29	30	0.2399	0.4533	0
14	15	0.221	0.1997	0	8	28	0.0636	0.2	0.0428
16	17	0.0524	0.1923	0	6	28	0.0169	0.0599	0.013
15	18	0.1073	0.2185	0					

TABLE A.31: Transformers.

Sending Bus	Receiving Bus	R_p (p.u.)	X_p (p.u.)	R_s (p.u.)	X_s (p.u.)	G_0 (p.u.)	B_0 (p.u.)	T_v (p.u.)	T_i (p.u.)	U_v (°)	U_i (°)
6	9	0	0	0	0.208	0	0	0.978	1	0	0
6	10	0	0	0	0.556	0	0	0.969	1	0	0
4	12	0	0	0	0.256	0	0	0.932	1	0	0
28	27	0	0	0	0.396	0	0	0.968	1	0	0

TABLE A.32: Conventional Loads.

Bus	P_{LOAD} (MW)	Q_{LOAD} (MVAR)	Bus	P_{LOAD} (MW)	Q_{LOAD} (MVAR)
2	21.7	12.7	17	9	5.8
3	2.4	1.2	18	3.2	0.9
4	7.6	1.6	19	9.5	3.4
5	94.2	19	20	2.2	0.7
7	22.8	10.9	21	17.5	11.2
8	30	30	23	3.2	1.6
10	5.8	2	24	8.7	6.7
12	11.2	7.5	26	3.5	2.3
14	6.2	1.6	29	2.4	0.9
15	8.2	2.5	30	10.6	1.9
16	3.5	1.8			

TABLE A.33: Generators (PV).

Bus	V_i (p.u.)	P_G (MW)	Q_{Gmax} (MVARs)	Q_{Gmin} (MVARs)
2	1.0338	57.56	800	-800
5	1.0058	24.56	800	-800
8	1.023	35	800	-800
11	1.0913	17.93	800	-800
13	1.0883	16.91	800	-800

TABLE A.34: Generators (regulators).

Bus	V_i (p.u.)	P_{G_set} (MW)	Q_{G_set} (MVAR)	P_R (p.u.)	R (p.u.)	a_Q	b_Q
1	1.05	138.5561	0.3468976	1	0.04	1	1

TABLE A.35: Shunt Fixed VAR Compensators.

Bus	G_{shunt} (p.u.)	B_{shunt} (p.u.)
10	0	0.19
24	0	0.043

Appendix B

Dynamic data of test systems.

The dynamic data of the test power systems used in this research work are given in this appendix. The base frequency is 60 Hz for all systems. The mechanical parameters used in WECS where applicable are given in Table B.1 [Xin et al., 2013]. The parameters of the back-to-back power converters are given in Table B.2 [Wu et al., 2008].

TABLE B.1: Mechanical parameters of WECSs.

ρ (kg/m^3)	1.225	R_q (Ω)	0.00821
C_f	0.9	p	26
r (m)	34	ψ (Wb)	6.5029
L_d (H)	0.00157	H_C (W*s/VA)	5.5
L_q (H)	0.00157	B (N*m*s)	0.002
R_d (Ω)	0.00821	v_w (m/s)	9

TABLE B.2: Parameters of Back-to-Back converters.

C_c (F)	0.0188	K_{p4}	0.2
X_c (p.u.)	0.05	K_{i4} (s)	5
V_{dc} (V)	1200	K_{p5}	0.1
K_{p1}	150	K_{i5} (s)	10
K_{i1} (s)	200	K_{p6}	0.3
K_{p2}	4	K_{i6} (s)	0.02
K_{i2} (s)	5	K_{p7}	0.1
K_{p3}	4	K_{i7} (s)	5
K_{i3} (s)	5		

B.1 14-bus system

Table B.3: Synchronous machines.

Bus	X_d (p.u.)	$X_d^{'}$ (p.u.)	X_q (p.u.)	$X_q^{'}$ (p.u.)	$T_{d0}^{'}$ (s)	$T_{q0}^{'}$ (s)	H ($\frac{\text{MW*s}}{\text{MVA}}$)	D (p.u.)
1	0.8979	0.2995	0.646	0.646	7.4	1.00E-09	5.148	2
2	1.05	0.185	0.98	0.36	6.1	0.3	6.54	2
3	1.05	0.185	0.98	0.36	6.1	0.3	6.54	2
6	1.25	0.232	1.22	0.715	4.75	1.5	5.06	2
8	1.25	0.232	1.22	0.715	4.75	1.5	5.06	2

Table B.4: AVRs.

Bus	Vr_{max} (p.u)	Vr_{min} (p.u)	K_a	T_a (s)	K_f	T_f (s)	T_e (s)	A_e	B_e (1/p.u.)
1	7.32	0	200	0.02	0.0012	1	0.19	0.0006	0.9
2	4.38	0	20	0.02	0.001	1	1.98	0.0006	0.9
3	4.38	0	20	0.02	0.001	1	1.98	0.0006	0.9
6	6.81	1.395	20	0.02	0.001	1	0.7	0.0006	0.9
8	6.81	1.395	20	0.02	0.001	1	0.7	0.0006	0.9

Table B.5: Turbine-Governors.

Bus	R (p.u.)	T_{GV} (s)	T_{ch} (s)	T_{rh} (s)	T_{co} (s)	F_{hp}	F_{ip}	F_{lp}	P_{GV}^{max} (p.u.)	P_{GV}^{min} (p.u.)
1	0.04	0.1	0.1	4.0	0.3	0.3	0.4	0.3	1.2	0.1
2	0.04	0.1	0.1	4.0	0.3	0.3	0.4	0.3	1.2	0.1

B.2 190-bus system

Table B.6: Synchronous machines.

Bus	X_d (p.u.)	$X_d^{'}$ (p.u.)	X_q (p.u.)	$X_q^{'}$ (p.u.)	$T_{d0}^{'}$ (s)	$T_{q0}^{'}$ (s)	H ($\frac{\text{MW*s}}{\text{MVA}}$)	D (p.u.)
1	0.045612924	0.015837821	0.025340513	0.015837821	7.4	0.4	73.08455	1.583782072
2	0.078534031	0.02513089	0.045026178	0.02513089	5.2	0.4	41.065	2.617801047
3	0.062385321	0.019082569	0.034862385	0.019082569	5.53	0.4	52.974	2.752293578
4	0.094373402	0.013938619	0.093350384	0.013938619	5.2	0.47	53.958	0.767263427
5	0.210666667	0.0428	0.198666667	0.0428	6.5	0.7	44.025	0.133333333
6	0.196	0.05	0.108	0.05	6	0.4	16.15	3.2
7	0.239564962	0.038212816	0.227807172	0.038212816	5.5	0.6	21.0924	0.587889477

8	0.5	0.09	0.6	0.09	5	0.6	12.6	2
9	0.159611993	0.025455614	0.151675485	0.025455614	5.5	0.6	31.6386	0.881834215
10	0.311503417	0.035876993	0.282460137	0.035876993	5.7	0.7	16.64688	1.708428246
11	0.5	0.183	0.5	0.183	5	0.6	6.3	2
12	0.5	0.1947	0.5	0.1947	5	0.5	4.8	2
13	0.5	0.08	0.5	0.08	5	0.5	7.5	2
14	0.5	0.3314	0.5	0.3314	5	0.5	3.2	2
15	0.072222222	0.022777778	0.045	0.022777778	5.88	0.4	36.18	3.333333333
16	0.418766067	0.057840617	0.401028278	0.057840617	5.06	0.6	12.6036	0.257069409
17	0.25	0.0875	0.15	0.0875	5.5	0.4	11.744	5
18	0.228197674	0.040697674	0.225290698	0.040697674	5.5	0.4	21.7408	0.581395349
19	0.119	0.0191	0.114	0.0191	5.5	0.6	42.18	4
20	0.5	0.1706	0.5	0.1706	5	0.5	4.14	2
21	0.5	0.035	0.5	0.035	5	0.5	4.17	2
22	0.5	0.066	0.5	0.066	5	0.5	11.06	1
23	0.5	0.09	0.5	0.09	5	0.5	12.6	1
24	0.20971867	0.033887468	0.12915601	0.033887468	5.5	0.47	28.6994	0.511508951
25	0.479129924	0.076425632	0.455614345	0.076425632	5.5	0.6	10.5462	0.293944738
26	0.945744681	0.178723404	0.923404255	0.178723404	6.5	0.96	12.7088	2.127659574
27	0.532058493	0.066085489	0.433070866	0.066085489	5.75	0.46	11.23696	1.124859393
28	0.5	0.1704	0.5	0.1704	5	0.5	1.17	2
29	0.5	0.1704	0.5	0.1704	5	0.5	6.21	2
30	0.9	0.0825	0.875	0.0825	4.8	0.5	5.6	2
31	0.512528474	0.036731207	0.498291572	0.036731207	4.8	0.5	12.36224	1.138952164
32	0.602272727	0.065454545	0.568181818	0.065454545	6	0.5	10.56	3.409090909
33	0.595789474	0.105263158	0.561052632	0.105263158	3.75	0.4	14.9055	3.157894737
34	0.497467072	0.061803445	0.470111449	0.061803445	5.25	0.442	25.97784	4.052684904
35	0.159611993	0.025455614	0.151675485	0.025455614	5.5	0.6	31.6386	0.881834215
36	0.212082262	0.027634961	0.20437018	0.027634961	4	0.52	25.2072	0.514138817
37	0.183715461	0.030276308	0.161669606	0.030276308	6.2	0.5	21.0924	0.587889477
38	0.183715461	0.030276308	0.161669606	0.030276308	6.2	0.5	21.0924	0.587889477
39	0.094373402	0.013938619	0.093350384	0.013938619	5.2	0.47	53.958	1.023017903
40	0.465317919	0.076300578	0.456647399	0.076300578	5.5	1	12.2138	0.289017341
41	1.136363636	0.289772727	1.136363636	0.289772727	5	0.5	3.52	4.545454545
42	2.5	0.735294118	1.911764706	0.735294118	4.7	0.4	1.0132	2.941176471
43	0.5	0.18	0.5	0.18	5	0.5	6.3	2
44	0.210344828	0.074137931	0.15862069	0.074137931	5	0.4	9.396	6.896551724
45	0.130909091	0.034363636	0.085909091	0.034363636	7.08	0.4	28.71	1.363636364
46	0.628177966	0.104449153	0.612288136	0.104449153	5.79	0.96	19.14432	3.177966102

For the 190-bus Mexican system, all AVRs share most of the parameters, except for K_a and T_a. Table B.7 shows the parameters in common while K_a and T_a are shown in Table B.8 for each generator.

TABLE B.7: Data in common for the AVRs.

Bus	Vr_{max} (p.u)	Vr_{min} (p.u)	K_f	T_f (s)	T_e (s)	A_e	B_e (1/p.u.)
1-46	10	1	0.1	1	0.46	0.33	1.2

TABLE B.8: AVRs' data.

Bus	K_f	T_f (s)	Bus	K_f	T_f (s)
1	150	0.03	24	100	0.05
2	100	0.05	25	100	0.05
3	100	0.05	26	100	0.05
4	100	0.05	27	100	0.05
5	100	0.05	28	100	0.05
6	175	0.03	29	100	0.05
7	100	0.05	30	100	0.05
8	100	0.05	31	100	0.05
9	100	0.05	32	100	0.05
10	100	0.05	33	100	0.05
11	200	0.05	34	100	0.05
12	100	0.05	35	100	0.05
13	150	0.05	36	100	0.05
14	150	0.05	37	100	0.05
15	100	0.05	38	75	0.04
16	75	0.04	39	100	0.05
17	100	0.05	40	100	0.05
18	150	0.04	41	200	0.05
19	100	0.05	42	100	0.05
20	200	0.05	43	200	0.05
21	100	0.05	44	100	0.05
22	100	0.05	45	100	0.04
23	100	0.05	46	100	0.05

In the case of the turbine-governor group of each generator, they share the same parameters shown in Table B.9.

TABLE B.9: Turbine-governor data for all generators.

Bus	R (p.u.)	T_{GV} (s)	T_{ch} (s)	T_{rh} (s)	T_{co} (s)	F_{hp}	F_{ip}	F_{lp}	P_{GV}^{max} (p.u.)	P_{GV}^{min} (p.u.)
1-46	0.04	0.1	0.1	4.0	0.3	0.3	0.4	0.3	1.2	0.1

B.3 30-bus system

Table B.10: Synchronous machines.

Bus	X_d (p.u.)	$X_d^{'}$ (p.u.)	X_q (p.u.)	$X_q^{'}$ (p.u.)	$T_{d0}^{'}$ (s)	$T_{q0}^{'}$ (s)	H ($\frac{\text{MW*s}}{\text{MVA}}$)	D (p.u.)
1	0.8979	0.2995	0.646	0.646	7.4	1.00E-09	5.148	2
2	1.0500	0.1850	0.9800	0.3600	6.1	0.3	6.54	2
5	1.05	0.185	0.98	0.36	6.1	0.3	6.54	2
8	1.25	0.232	1.22	0.715	4.75	1.5	5.06	2
11	1.25	0.232	1.22	0.715	4.75	1.5	5.06	2
13	1.25	0.232	1.22	0.715	4.75	1.5	5.06	2

Table B.11: AVRs.

Bus	Vr_{max} (p.u)	Vr_{min} (p.u)	K_a	T_a (s)	K_f	T_f (s)	T_e (s)	A_e	B_e (1/p.u.)
1	7.32	0	175	0.05	0.0012	1	0.19	0.0006	0.9
5	4.38	0	30	0.05	0.001	1	1.98	0.0006	0.9
8	6.81	1.395	30	0.05	0.001	1	0.7	0.0006	0.9
11	6.81	1.395	30	0.05	0.001	1	0.7	0.0006	0.9
13	6.81	1.395	30	0.05	0.001	1	0.7	0.0006	0.9

Table B.12: Turbine-governor data for all generators.

Bus	R (p.u.)	T_{GV} (s)	T_{ch} (s)	T_{rh} (s)	T_{co} (s)	F_{hp}	F_{ip}	F_{lp}	P_{GV}^{max} (p.u.)	P_{GV}^{min} (p.u.)
1, 5, 8, 11, 13	0.04	0.1	0.1	4.0	0.3	0.3	0.4	0.3	1.2	0.1

Table B.13: PSSs' data for all generators.

Bus	K_w	T_w (s)	T_1 (s)	T_2 (s)	T_3 (s)	T_4 (s)	V_s^{max} (p.u.)	V_s^{min} (p.u.)
1, 5, 8, 11, 13	15.0	10.0	0.38	0.02	0.38	0.02	0.1	-0.1

Bibliography

[Aboytes and Arroyo, 1986] Aboytes, F. and Arroyo, G. (1986). Security assessment in the operation of longitudinal power systems. *IEEE Transactions on Power Systems*, 1(2):225–232.

[Acha et al., 2004] Acha, E., Fuerte-Esquivel, C., Ambriz-Pérez, H., and Angeles-Camacho, C. (2004). *FACTS: Modelling and Simulation in Power Networks*. Wiley.

[Agrawal and Thukaram, 2011] Agrawal, R. and Thukaram, D. (2011). Identification of coherent synchronous generators in a multi-machine power system using support vector clustering. In *Power and Energy Systems (ICPS), 2011 International Conference on*, pages 1–6.

[Aik, 2007] Aik, D. L. H. (2007). Voltage and power interactions on multi-infeed hvdc systems. Technical Report DL/07/01, The Power Systems and High Voltage Laboratories (EEH).

[Alsac and Stott, 1974] Alsac, O. and Stott, B. (1974). Optimal load flow with steady-state security. *IEEE Transactions on Power Apparatus and Systems*, PAS-93(3):745–751.

[Alsafih and Dunn, 2010] Alsafih, H. A. and Dunn, R. (2010). Determination of coherent clusters in a multi-machine power system based on wide-area signal measurements. In *IEEE PES General Meeting*, pages 1–8.

[Ambriz-Perez et al., 2000] Ambriz-Perez, H., Acha, E., and Fuerte-Esquivel, C. R. (2000). Advanced svc models for newton-raphson load flow and newton optimal power flow studies. *IEEE Transactions on Power Systems*, 15(1):129–136.

[Bahrman, 2006] Bahrman, M. P. (2006). Overview of hvdc transmission. In *2006 IEEE PES Power Systems Conference and Exposition*, pages 18–23.

[Bati, 2010] Bati, A. F. (2010). Optimal interaction between pss and facts devices in damping power systems oscillations. In *2010 7th International Multi-Conference on Systems Signals and Devices (SSD)*, pages 1–6.

[Boole, 2009] Boole, G. (2009). *A Treatise on the Calculus of Finite Differences*. Macmillan, Cambridge, 1860 reprinted edition.

[Britton, 1969] Britton, J. P. (1969). Improved area interchange control for newton's method load flows. *IEEE Transactions on Power Apparatus and Systems*, PAS-88(10):1577–1581.

[Canizares and Faur, 1999] Canizares, C. A. and Faur, Z. T. (1999). Analysis of svc and tcsc controllers in voltage collapse. *IEEE Transactions on Power Systems*, 14(1):158–165.

[dos Santos et al., 2004] dos Santos, M. J., Pereira, J. L. R., Filho, J. A. P., de Oliveira, E. J., and da Silva, I. C. (2004). A new approach for area interchange control modeling. *IEEE Transactions on Power Systems*, 19(3):1271–1276.

[Elgerd, 1981] Elgerd, O. (1981). Control of electric power systems. *IEEE Control Systems Magazine*, 1(2):4–16.

[Fabozzi and Cutsem, 2011] Fabozzi, D. and Cutsem, T. V. (2011). On angle references in long-term time-domain simulations. *IEEE Transactions on Power Systems*, 26(1):483–484.

[Filho et al., 2009] Filho, J. A. P., Martins, N., and Falcao, D. M. (2009). Identifying power flow control infeasibilities in large-scale power system models. *IEEE Transactions on Power Systems*, 24(1):86–95.

[Freund et al., 2004] Freund, J., Miller, I., and Miller, M. (2004). *John E. Freund's Mathematical Statistics: With Applications*. Pearson/Prentice Hall.

[Fuerte-Esquivel, 1997] Fuerte-Esquivel, C. R. (1997). *Steady State Modelling and Analysis of Flexible AC Transmission Systems*. PhD thesis, The University of Glasgow, Glasgow.

[Fuerte-Esquivel and Acha, 1996] Fuerte-Esquivel, C. R. and Acha, E. (1996). Newton-raphson algorithm for the reliable solution of large power networks with embedded facts devices. *IEE Proceedings - Generation, Transmission and Distribution*, 143(5):447–454.

[Gao et al., 1992] Gao, B., Morison, G. K., and Kundur, P. (1992). Voltage stability evaluation using modal analysis. *IEEE Transactions on Power Systems*, 7(4):1529–1542.

[Gonzalez-Longatt, 2012] Gonzalez-Longatt, F. M. (2012). Effects of the synthetic inertia from wind power on the total system inertia: simulation study. In *2012 2nd International Symposium on Environment Friendly Energies and Applications (EFEA)*, pages 389–395.

[Hamdan and Elabdalla, 1988] Hamdan, A. and Elabdalla, A. (1988). Geometric measures of modal controllability and observability of power system models. *Electric Power Systems Research*, 15(2):147 – 155.

[Kim et al., 2011] Kim, H. J., Nam, T., Hur, K., Chang, B., Chow, J. H., and Entriken, R. (2011). Dynamic interactions among multiple facts controllers - a survey. In *2011 IEEE Power and Energy Society General Meeting*, pages 1–8.

[Kothari and Nagrath, 2003] Kothari, D. and Nagrath, I. (2003). *Modern Power System Analysis*. Tata McGraw-Hill Publishing Company.

[Krause et al., 2002] Krause, P., Wasynczuk, O., and Sudhoff, S. (2002). *Analysis of electric machinery and drive systems*. IEEE Press.

[Kundur et al., 1994] Kundur, P., Balu, N., and Lauby, M. (1994). *Power system stability and control*. McGraw-Hill.

[Kundur et al., 1989] Kundur, P., Klein, M., Rogers, G. J., and Zywno, M. S. (1989). Application of power system stabilizers for enhancement of overall system stability. *IEEE Transactions on Power Systems*, 4(2):614–626.

[Mathur and Varma, 2002] Mathur, R. M. and Varma, R. K. (2002). *Thyristor-Based FACTS Controllers for Electrical Transmission Systems*. IEEE Press Series on Power Engineering. Wiley-IEEE Press.

[Messina et al., 2002] Messina, A. R., Hernández, H., Barocio, E., Ochoa, M., and Arroyo, J. (2002). Coordinated application of facts controllers to damp out inter-area oscillations. *Electric Power Systems Research*, 62:43–53.

[Milano, 2010] Milano, F. (2010). *Power System Modelling and Scripting*. Springer Berlin Heidelberg.

[Mithulananthan et al., 2002] Mithulananthan, N., Canizares, C. A., and Reeve, J. (2002). Tuning, performance and interactions of pss and facts controllers. In *Power Engineering Society Summer Meeting, 2002 IEEE*, volume 2, pages 981–987.

[Morren et al., 2006] Morren, J., Pierik, J., and de Haan, S. W. (2006). Inertial response of variable speed wind turbines. *Electric Power Systems Research*, 76(11):980 – 987.

[Najafi and Kazemi, 2006] Najafi, M. and Kazemi, A. (2006). Coordination of pss and facts damping controllers in large power systems for dynamic stability improvement. In *2006 International Conference on Power System Technology*, pages 1–6.

[Nouh and Mohamed, 2014] Nouh, A. and Mohamed, F. (2014). Wind energy conversion systems: Classifications and trends in application. In *Renewable Energy Congress (IREC), 2014 5th International*, pages 1–6.

[Okamura et al., 1975] Okamura, M., O-ura, Y., Hayashi, S., Uemura, K., and Ishiguro, F. (1975). A new power flow model and solution method – including load and generator characteristics and effects of system control devices. *IEEE Transactions on Power Apparatus and Systems*, 94(3):1042–1050.

[Parniani and Iravani, 1995] Parniani, M. and Iravani, M. R. (1995). Voltage control stability and dynamic interaction phenomena of static var compensators. *IEEE Transactions on Power Systems*, 10(3):1592–1597.

[Pilotto et al., 2000] Pilotto, L. A. S., Alves, J. E. R., and Watanabe, E. H. (2000). High frequency eigenanalysis of hvdc and facts assisted power systems. In *Power Engineering Society Summer Meeting, 2000. IEEE*, volume 2, pages 823–829.

[Pilotto et al., 1995] Pilotto, L. A. S., Ping, W. W., and Szechtman, M. (1995). Converter control interactions on multi-infeed hvdc systems. In *CIGRE International Colloquium on HVDC and FACTS*, pages 1–8.

[Rafian et al., 1987] Rafian, M., Sterling, M. J. H., and Irving, M. R. (1987). Real-time power system simulation. *IEEE Proceedings C - Generation, Transmission and Distribution*, 134(3):206–223.

[Rahmann et al., 2015] Rahmann, C., Jara, J., and Salles, M. B. C. (2015). Effects of inertia emulation in modern wind parks on isolated power systems. In *2015 IEEE Power Energy Society General Meeting*, pages 1–5.

[CIGRE Task Force, 2000] CIGRE Task Force (2000). Impact of interactions among power system controls. Technical Report 16-02-38, Power Systems Engineering Research Center.

[CIGRE Working Group, 1999] CIGRE Working Group (1999). Coordination of controls of multiple facts / hvdc links in the same system. Technical Report 149, Power Systems Engineering Research Center.

[E. H. Camm et al., 2009] E. H. Camm et al. (2009). Characteristics of wind turbine generators for wind power plants. In *2009 IEEE Power Energy Society General Meeting*, pages 1–5.

[EPRI Report, 1998] EPRI Report (1998). Analysis of control interactions on facts-assisted power systems. Technical Report TR-109969, The Electric Power System Research Institute (EPRI).

[IEEE Committee, 1973] IEEE Committee (1973). Dynamic models for steam and hydro turbines in power system studies. *Power Apparatus and Systems, IEEE Transactions on*, PAS-92(6):1904–1915.

[IEEE Committee, 1981] IEEE Committee (1981). Excitation system models for power system stability studies. *Power Apparatus and Systems, IEEE Transactions on*, PAS-100(2):494–509.

[IEEE Committee, 1992] IEEE Committee (1992). Reader's guide to subsynchronous resonance. *IEEE Transactions on Power Systems*, 7(1):150–157.

[IEEE Committee, 2006] IEEE Committee (2006). Ieee recommended practice for excitation system models for power system stability studies. *IEEE Std 421.5-2005 (Revision of IEEE Std 421.5-1992)*, pages 1–93.

[Rodgers et al., 1984] Rodgers, J. L., Nicewander, W. A., and Toothaker, L. (1984). Linearly independent, orthogonal, and uncorrelated variables. *The American Statistician*, 38(2):133–134.

[Rogers and Overbye, 2009] Rogers, K. M. and Overbye, T. J. (2009). Power flow control with distributed flexible ac transmission system (d-facts) devices. In *North American Power Symposium (NAPS), 2009*, pages 1–6.

[Sauer and Pai, 1998] Sauer, P. and Pai, M. (1998). *Power System Dynamics and Stability*. Prentice Hall.

[Stagg and El-Abiad, 1968] Stagg, G. and El-Abiad, A. (1968). *Computer methods in power system analysis*. McGraw-Hill series in electronic systems. McGraw-Hill.

[Stewart, 2011] Stewart, J. (2011). *Multivariable Calculus*. Cengage Learning.

[Stott, 1974] Stott, B. (1974). Review of load-flow calculation methods. *Proceedings of the IEEE*, 62(7):916–929.

[Tiegna et al., 2012] Tiegna, H., Amara, Y., Barakat, G., and Dakyo, B. (2012). Overview of high power wind turbine generators. In *2012 International Conference on Renewable Energy Research and Applications (ICRERA)*, pages 1–6.

[van Cutsem and Bo$\upsilon\rho\nu\acute{\alpha}\varsigma$, 1998] van Cutsem, T. and Bo$\upsilon\rho\nu\acute{\alpha}\varsigma$, K. (1998). *Voltage Stability of Electric Power Systems*. Kluwer international series in engineering and computer science. Springer.

[Wu et al., 2008] Wu, F., Zhang, X., and Ju, P. (2008). Modeling and control of the wind turbine with the direct drive permanent magnet generator integrated to power grid. In *Third International Conference on Electric Utility Deregulation and Restructuring and Power Technologies, 2008*, pages 57–60.

[Xin et al., 2013] Xin, W., Mingfeng, C., Li, Q., Lulu, C., and Bin, Q. (2013). Control of direct-drive permanent-magnet wind power system grid-connected

using back-to-back pwm converter. In *Third International Conference on Intelligent System Design and Engineering Applications (ISDEA), 2013*, pages 478–481.

[Xu et al., 1998] Xu, X., Mathur, R. M., Jiang, J., Rogers, G. J., and Kundur, P. (1998). Modeling of generators and their controls in power system simulations using singular perturbations. *IEEE Transactions on Power Systems*, 13(1):109–114.

[Zhang et al., 2006] Zhang, L., Zhang, P. X., Wang, H. F., Chen, Z., Du, W., Cao, Y. J., and Chen, S. J. (2006). Interaction assessment of facts control by rga for the effective design of facts damping controllers. *IEE Proceedings - Generation, Transmission and Distribution*, 153(5):610–616.

[Zhu et al., 2006] Zhu, J., Abur, A., Rice, M. J., Heydt, G. T., and Meliopolus, S. (2006). Enhanced state estimators. Technical Report 06-45, Power Systems Engineering Research Center.

[Zou et al., 2005] Zou, Z. Y., Jiang, Q. Y., Cao, Y. J., and Wang, H. F. (2005). Normal form analysis of interactions among multiple svc controllers in power systems. *IEE Proceedings - Generation, Transmission and Distribution*, 152(4):469–474.